AN ELECTRICAL ANALOGY FOR ANALYSIS OF FLOW THROUGH CASCADES

FRANK R. FAHLAND
AND
LARRY L. HAWKINS

AN ELECTRICAL ANALOGY
FOR
ANALYSIS OF FLOW THROUGH CASCADES

* * * *

Frank R. Fahland

and

Larry L. Hawkins

AN ELECTRICAL ANALOGY

FOR

ANALYSIS OF FLOW THROUGH CASCADES

by

Frank R. Fahland
Lieutenant, United States Navy

and

Larry L. Hawkins
Lieutenant, United States Navy

Submitted in partial fulfillment of
the requirements for the degree of

MASTER OF SCIENCE
IN
MECHANICAL ENGINEERING

United States Naval Postgraduate School
Monterey, California

1 9 5 8

AN ELECTRICAL ANALOGY
FOR
ANALYSIS OF FLOW THROUGH CASCADES

by

Frank R. Fahland

and

Larry L. Hawkins

This work is accepted as fulfilling
the thesis requirements for the degree of
MASTER OF SCIENCE
IN
MECHANICAL ENGINEERING

from the
United States Naval Postgraduate School

SUMMARY

A method of analysis of arbitrary cascades under conditions of ideal fluid flow is described. The method is based on conformal transformation, achieved experimentally through an electrical analogy. Tests were conducted to permit comparison of results obtained by this method with those of a previous analytical solution and with NACA two dimensional cascade tests. Results indicate that the quick and inexpensive procedure of this method is applicable to engineering problems of cascade analysis.

This work was conducted at the U. S. Naval Postgraduate School, Monterey, California.

TABLE OF CONTENTS

TABLE OF CONTENTS Cont.

TABLE OF CONTENTS Cont.

TABLE OF CONTENTS Cont.

1. INTRODUCTION

One of the first steps in the aerodynamic design of an axial flow turbomachine is the design of cascades which produce desired deflections of the fluid as it passes through the machine. Fundamental to the solution of this problem is the determination of the two dimensional flow of an ideal fluid across cascades of compressor and turbine blades. An ideal fluid is here assumed to mean one that is homogeneous, continuous, incompressible, and inviscid.

The development of a method which predicts the two dimensional flow of an ideal fluid across any arbitrary cascade was the objective of this investigation. One measure of cascade performance is the fluid turning angle. More basic parameters are the cascade coefficient K defined in Section 5.1 and the relative zero lift angle β_{L_0} defined in Section 5.1 and illustrated in Fig. 17. Of primary interest was the effect of changes in cascade solidity and blade stagger on these indicators of cascade performance, but a preliminary test of the ability of this method to predict velocity distribution around the airfoils in cascade is also included.

Considerable ingenuity has been exerted in previous work done on this problem, and many mathematical analyses exist of the two dimensional potential flow past infinite cascades of airfoils. Some provide exact solutions for special shapes such as straight blades of zero thickness. See Refs. 1 and 2. Some provide approximate solutions for particular airfoil shapes and

cascade arrangements. See Refs. 3 and 4. Finally in regard to the general problem of arbitrary airfoils in cascade, there have been several attempts at a mathematical solution. These usually involve iteration methods. See Refs. 5, 6, 7, and 8. The labor involved in the application of these methods is great; and, for some applications, even modern high speed computers prove inadequate. Particular difficulty is encountered with blades of high camber and cascades of high stagger angles. Hence the engineering application of these methods is limited.

Theoretically, the method here investigated is based upon the conformal transformation of an arbitrary cascade into a circle. This is accomplished experimentally, using electrical conducting paper. The flow of an ideal fluid is analytically known about a circle. Through LaPlace's equation the flow can be determined about the cascade.

To compare the results obtained by this analog method with those of a previous analytical study, the airfoil in cascade which had been analyzed by Mutterperl and reported in Ref. 7 was investigated. To determine the effect of solidity and stagger upon turning angle, a blade more closely approximating those currectly used in the gas turbine industry was desired. The NACA 65-(15)10 airfoil section was chosen for this reason and because its use permitted comparison with NACA two dimensional cascade tests reported in Ref. 9.

This work was conducted at the U. S. Naval Postgraduate School, Monterey, California during the 1957 - 1958 school year.

The authors wish to express their appreciation to Professor M. H. Vavra and Professor T. H. Gawain of the U. S. Naval Post-

graduate School. This thesis project was conceived by Professor Vavra and is an outgrowth of previous investigative work performed by Professors Vavra and Gawain. The association with Professor Gawain who guided and assisted in the work of this investigation was most rewarding.

2. TABLE OF SYMBOLS

a	radius of circle in the picture plane, feet
b	distance from origin of sources and sinks in picture plane, feet
c	chord length, inches or feet
c_l	airfoil section coefficient of lift
f	dimensionless transformation parameter, defined by equation 3.27
i	current, amperes
i	indicates imaginary part in complex number notation
l	characteristic distance used in conformal transformation, feet
m	source strength in picture plane, feet squared per second
q	dynamic head, pounds per square foot
r	radius vector length in picture plane, feet
s	tangential spacing between blades, inches or feet
w	complex velocity potential function
x	real axis, real plane
y	imaginary axis, real plane
z	complex coordinate, real plane
E	potential, volts
I	total current function, defined in Appendix A
K	cascade coefficient, defined in Section 5.1
R	total resistance, ohms
S	pressure coefficient = $\left(\frac{V_2}{V_1}\right)^2$
V	velocity, feet per second

α angle of fluid flow, degrees

α_a absolute angle of attack

α_m angle of mean velocity

α_{L_o} angle of zero lift

α_1 cascade entrance angle

α_2 cascade exit angle

α_i ideal approach angle

β cascade stagger angle, degrees

β_{L_o} relative angle of zero lift, degrees

γ $\log_e \frac{b}{a}$

ζ complex coordinate in the picture plane

η imaginary axis, picture plane

θ angular coordinate, picture plane, degrees

ν specific resistance, ohms

ξ real axis, picture plane

ρ resistivity, ohm-inches

ρ density, slugs per cubic foot

σ solidity = $\frac{c}{s}$

τ 'aspect ratio', defined by equation 3.13

φ velocity potential function

ψ velocity stream function

Γ circulation, feet squared per second

Θ turning angle, degrees

Λ vortex strength, feet squared per second

$\mathcal{E}$ percent potential

$\mathcal{I}$ percent current quantity

Subscripts:

1	upstream of blade row
2	downstream of blade row
a	axial direction
i	ideal
m	mean
s	stagnation
t	tangential direction
L	leading edge
T	trailing edge

Superscripts:

*	indicates maximum value

3. ANALYSIS

3.1 IDEAL FLUID FLOW

If, in a two dimensional steady flow, there exists a velocity point function such that

$$\bar{V} = \bar{V}(\bar{r}) = \bar{V}(x, y) \tag{3.1}$$

the necessary and sufficient condition for this to be potential flow is that

$$\nabla \times \bar{V} = 0 \tag{3.2}$$

which means that

$$\bar{V} = \nabla \varphi \tag{3.3}$$

But, if further, the density of this flow be constant, continuity requires that

$$\nabla \cdot \bar{V} = 0 \tag{3.4}$$

If both 3.3 and 3.4 are satisfied; then the potential is a plane harmonic function such that

$$\nabla^2 \varphi = 0 \tag{3.5}$$

which is LaPlace's equation.

Correspondingly in this theoretical, two dimensional fluid flow there is a stream function for which

$$\nabla^2 \psi = 0 \tag{3.6}$$

Trajectories of constant φ are orthogonal to trajectories of constant ψ.

Analagous to this theoretical, two dimensional fluid flow is the flow of a steady current in a thin, flat sheet of uniform conductivity. Details of the analogy are contained in Appendix A. On the sheet the electric potential E, analagous to φ, can be represented by

$$\nabla^2 E = 0 \qquad 3.7$$

Similarly, introduction of a total current function I results in

$$\nabla^2 I = 0 \qquad 3.8$$

Trajectories of constant E are orthogonal to trajectories of constant I.

3.2 CONFORMAL TRANSFORMATION

Various flows of an ideal fluid are analytically known about certain simple domains such as a circle. LaPlace's equation, which characterizes such a perfect fluid flow, remains invariant for any conformal transformation. Hence, if an arbitrary shape can be conformally transformed into a suitable circle, the flow of an ideal fluid about the arbitrary shape can be determined.

The theory of conformal transformation with the aid of an electric tank is discussed in Ref. 10. In general the whole region between two arbitrarily specified closed curves is not transformable into the whole region between two other arbitrarily specified closed curves. Transformation can be accomplished,

however, if there exists a function, in the picture plane, of the real plane complex variable z such that for every assigned value of the variable the function has a definite value or system of values and also a definite derivative.

The arbitrary shape transformed in this investigation consists of an infinite cascade of equally spaced compressor blades of the same shape and orientation.

Imagine a conducting sheet of uniform conductivity, infinite in extent in two dimensions, Fig. 1, in which the blades are areas of infinite resistance (cutouts from the sheet). With a potential E* imposed on a line parallel to the axis of the cascade and located infinitely far ahead of the cascade and a zero potential imposed on a similar line located infinitely far behind the cascade, corresponding points on each of the blades have equal potential. Immediately in front of the cascade a line connecting points of equal potential exhibits a shape that is strongly influenced by the geometry of the cascade; but with increasing separation from the cascade the influence diminishes rapidly, and at finite distances ahead of and behind the cascade these lines of constant potential are virtually straight and parallel to the axis of the cascade. Hence, the conditions at infinity may be closely approximated by imposing a voltage on the sheet through straight bus bars parallel to the axis of the cascade and a finite distance away.

No generality is lost if a single strip of width s which includes the space between two blade cutouts is considered, provided that the boundaries or edges of the strip are lines of constant I. Let the boundaries be chosen to coincide with portions

of the blade profiles as shown in Fig. 2.

For the strip of conducting sheet

$$R^*i^*=E^* \qquad 3.9$$

For points on this strip (from Appendix A)

$$E + i\nu I = f(z) \qquad 3.10$$

Dividing both sides of 3.10 by 3.9

$$f_1(z) = \frac{E}{E^*} + i\,\frac{\nu I}{R^* i^*} = \mathcal{E} + i\,\mathcal{A} \qquad 3.11$$

$\mathcal{A}$ will be constant along the edge of the strip and $\mathcal{E}$ will vary from one on the front bus bar to zero on the after bus bar. Any point on the strip can be located by coordinates x, y; but $\mathcal{E}$ and $\mathcal{A}$ are continuous functions on the strip and are definite at any point. Optionally, then, any point may be designated by its coordinates or by the values of $\mathcal{E}$ and $\mathcal{A}$ which characterize it. In symbols:

$$\mathcal{E} = \mathcal{E}(x,y) \qquad x = x(\mathcal{E},\mathcal{A})$$

and conversely 3.12

$$\mathcal{A} = \mathcal{A}(x,y) \qquad y = y(\mathcal{E},\mathcal{A})$$

On the front part of the profile cut-out $\mathcal{E}$ will reach a maximum value at a point 1, and on the trailing part a minimum value at a point 2. Fig. 3 shows a typical plot of percent potential $\mathcal{E}$ vs. percent chord. The quantity $\mathcal{E}_1 - \mathcal{E}_2$ is one of the parameters used to accomplish transformation.

In the region near the bus bars where lines of constant $\mathcal{E}$ are straight and parallel to the cascade, imagine two lines of

constant $\mathcal{E}$; $\mathcal{E}_a$ and $\mathcal{E}_b$ such that $\mathcal{E}_a - \mathcal{E}_b = \mathcal{E}_1 - \mathcal{E}_2$. See Fig. 4. Imagine that the width of the conducting strip, s, is divided into n_1 equal parts, each measuring $\frac{s}{n_1}$. This same increment of length is used to measure along the distance l between $\mathcal{E}_a$ and $\mathcal{E}_b$, dividing this distance into $n_2 = \frac{l}{s/n_1}$ parts. Lines of constant $\mathcal{E}$ drawn at these stations are separated by equal distances and represent equal increments $\Delta\mathcal{E}$. For convenience it is assumed in Fig. 4 that n_1 and n_2 are integers. Lines of constant $\mathcal{E}$ and constant $\mathcal{A}$ drawn at these measured stations form an orthogonal grid of $n_1 n_2$ squares over this portion of the strip.

A similar conceptual procedure is valid at any position in the strip. Lines of constant $\mathcal{E}$ may be drawn such that $\mathcal{E}_i - \mathcal{E}_j = \mathcal{E}_1 - \mathcal{E}_2$. Let the distance between them, as measured along a line of constant 1, be divided into n_2 segments of equal potential drop, $\Delta\mathcal{E}$. The distance between the edges of the strip, as measured along a line of constant $\mathcal{E}$, can then be divided into n_1 segments. A grid of orthogonal curvilinear coordinates results and the region consists of the same number $n_1 n_2$ of curvilinear squares as before.

Let there be a parameter τ such that

$$\tau = \frac{\mathcal{E}_1 - \mathcal{E}_2}{s\left(-\frac{\partial \mathcal{E}}{\partial x}\right)_\infty} \qquad 3.13$$

In the regions of the bus bars $\mathcal{E}$ varies linearly with 1; so

$$\left(-\frac{\partial \mathcal{E}}{\partial x}\right)_\infty = \frac{\mathcal{E}_a - \mathcal{E}_b}{l} \qquad 3.14$$

τ then reduces to the ratio $\frac{l}{s}$ which might be considered an 'aspect ratio' for the gridded section. It represents the ra-

tio of the number of squares along the strip to the number of squares across the strip. The quantity represents a unique and invariant characteristic of the geometry, and must be maintained in mapping to achieve conformal transformation.

Consider the denominator of the quantity τ. From the analogy developed in Appendix A, at any point,

$$\nu i_x = -\frac{\partial E}{\partial x} \qquad 3.15$$

In the region near the bus bars where i_x is constant across the width of the strip

$$\nu i_x = \frac{E_a - E_b}{\ell} \qquad 3.16$$

Multiplying both sides by s, the width of the strip,

$$\nu i_x s = (E_a - E_b)\left(\frac{s}{\ell}\right) \qquad 3.17$$

$i_x s$ is the total current flowing in the strip between bus bars. The right side of the equation might be labeled the specific voltage drop of the strip. It represents the voltage drop between two equipotential lines which form a square with lines of constant I that are s distance apart. Equations 3.15, 3.16, and 3.17 may be used in non-dimensional form if each is divided by equation 3.9.

Now consider the ζ or picture plane of Fig. 4 with sources of equal strength m on the negative, real axis at -b and $-\frac{a^2}{b}$ and sinks of the same strength on the positive, real axis at +b and $+\frac{a^2}{b}$. These sources and sinks create a complex function in the ζ plane. See Appendix B:

$$w = \frac{m}{2\pi}\left[\ln\frac{b+\zeta}{b-\zeta} + \ln\frac{a^2/b+\zeta}{a^2/b-\zeta}\right] = \varphi + i\psi \qquad 3.18$$

Any point in the picture plane can be located by coordinates η, ξ or by the values of φ and ψ which characterize the point. Symbolically,

$$\varphi = \varphi(\xi,\eta) \qquad \xi = \xi(\varphi,\psi)$$

and conversely 3.19

$$\psi = \psi(\xi,\eta) \qquad \eta = \eta(\varphi,\psi)$$

The circle $|\zeta| = a$ is a line of constant ψ. Sought is the conformal transformation of the strip of the real plane external to the blade cut-out onto the area of the picture plane outside the circle so that the cascade blade outline becomes the circumference of the circle. φ is a minimum at a point 1 and a maximum at a point 2. The difference in potential $\varphi_2 - \varphi_1$ is

$$\varphi_2 - \varphi_1 = \frac{m}{\pi}\ln\frac{\cosh\gamma+1}{\cosh\gamma-1} \qquad 3.20$$

$$\frac{1}{\pi}\ln\frac{\cosh\gamma+1}{\cosh\gamma-1} = \frac{\varphi_2-\varphi_1}{m} \qquad 3.21$$

See Appendix B. It will be shown that the right side of eq. 3.21 is the corresponding form of τ for the picture plane.

With reference to the strength term m in the denominator of eq. 3.21, recall that in two dimensional, unidirectional flow of an ideal fluid the uniform quantity rate of flow between streamlines h distance apart is Vh, Fig. 5. Correspondingly for a point source from which flow emanates, a uniform quantity rate of flow crosses any simply connected curve enclosing the source. The velocity at any point is the gradient of φ, that is $V = \frac{\partial\varphi}{\partial r}$.

The change of φ between two φ countours which, with two streamlines h distance apart, form a curvilinear square is $\frac{\partial \varphi}{\partial r} h$. This quantity might be dubbed the specific φ drop, analogous to specific voltage drop, but for fluid flow considerations it is designated a quantity rate of flow, here represented by m.

To achieve conformal transformation between the z and ζ planes, the following condition is imposed

$$\varphi = K_1 - K_2 \mathcal{E} \qquad 3.22$$

where K_1 and K_2 are arbitrary constants.

It follows that $\varphi_2 - \varphi_1 = K_2 (\mathcal{E}_1 - \mathcal{E}_2)$. 3.23

Further, let $m = K_2 s \left(-\frac{\partial \mathcal{E}}{\partial x}\right)_\infty$. 3.24

Then $$\frac{\varphi_2 - \varphi_1}{m} = \frac{K_2 (\mathcal{E}_1 - \mathcal{E}_2)}{K_2 s \left(-\frac{\partial \mathcal{E}}{\partial x}\right)_\infty} \qquad 3.25$$

The consequence of equal τ in the real and picture planes is this: for any area in the real plane bounded by lines of constant $\mathcal{E}$ and $\mathcal{I}$ there is an area in the picture plane bounded by corresponding lines of constant φ and ψ. The 'aspect ratios' of the areas are the same. See Fig. 4.

For every point $\mathcal{E}$, $\mathcal{I}$ in the real plane there is a corresponding point φ, ψ in the picture plane. $\frac{\Delta \mathcal{E}}{\Delta \mathcal{I}}$ can be measured in the real plane, and a corresponding $\frac{\Delta \varphi}{\Delta \psi}$ can be calculated in the picture plane. These conditions are sufficient to establish the existence of a function of a complex variable which relates the two planes conformally. An analytical expression of this function is not determined nor required.

Definition of τ in the ζ plane uniquely determines the location of the sources and sinks. Eq. 3.21 is solved giving

$$\cosh\gamma = \frac{e^{\pi\tau}+1}{e^{\pi\tau}-1} \qquad 3.26$$

Further, the periodicity of the mapping function is such that each strip of width s in the infinite cascade is mapped onto this same area in the picture plane; so the result is truly a map of the infinite cascade. Fig. 6 indicates the location of corresponding points on the two planes.

Reference to eqs. 3.23, 3.24 and 3.25 indicates that only three quantities need be measured in the real plane to accomplish the transformation. These are $\mathcal{E}_1-\mathcal{E}_2$, $\left(-\frac{\partial\mathcal{E}}{\partial x}\right)_\infty$, s. Other measurable quantities might perhaps be used, but the above listed parameters seem to be the ones most naturally, conveniently, and accurately obtainable. They are sufficient to achieve transformation.

The position of a point on the blade profile such as P in Fig. 6 may be expressed in terms of the measured value of $\mathcal{E}$ which characterizes it. Similarly the position of a point on the circle such as P' in Fig. 6 may be expressed in terms of the calculated value of φ which characterizes it. Points P on the blade and P' on the circle which correspond have identical values of the parameter f, where f is defined by the expression

$$\frac{\mathcal{E}_1-\mathcal{E}}{\mathcal{E}_1-\mathcal{E}_2} = f = \frac{\varphi-\varphi_1}{\varphi_2-\varphi_1} \qquad 3.27$$

Each such point P' on the circle also has an angular coordinate θ as shown in Fig. 7. The coordinate θ is related to

the parameter f by the expression

$$\theta = \cos^{-1}\left[\cosh\gamma\,\frac{e^{\pi\tau(2f-1)}-1}{e^{\pi\tau(2f-1)}+1}\right] \qquad 3.28$$

This formula is derived in Appendix B.

3.3 THE FLOW RELATIONS

Once the transformation has been completed the flow in the picture plane can be modified to correspond to various desired flow conditions in the real plane. This involves variation in the direction of the mean flow and variation in the circulation around the blade to satisfy the Kutta condition.

The direction of the mean flow may be changed by superposition of a set of vortices Λ at the singularities in the picture plane as shown in Fig. 7. The circulation around the airfoil can be modified by superposition of a second set of vortices $\frac{\Gamma}{2}$ as indicated in the same figure.

The Kutta condition states that the rear stagnation point of the fluid flow about an airfoil with a sharp trailing edge occurs at the sharp trailing edge. Therefore the rear stagnation point in the picture plane must occur at the point on the circle which corresponds to the trailing edge. This determines the strength of the circulation that must be imposed.

At the desired angle of attack and with the Kutta condition satisfied, the velocity V_3 at every point on the circle may be calculated. Since the conformal transformation has established the correspondence between points on the blade in the real plane and on the circle in the picture plane, the velocity V_2 at each

point on the blade is obtainable by means of the relation

$$V_z = \frac{V_\zeta}{\left|\frac{dz}{d\zeta}\right|} \qquad 3.29$$

It may further be shown that $\frac{dz}{d\zeta} = \frac{\frac{df}{d\zeta}}{\frac{df}{dz}} = \frac{\frac{\Delta\mathcal{E}}{\Delta z}}{\frac{d\varphi}{d\zeta}} \left(\frac{\varphi_2 - \varphi_1}{\mathcal{E}_1 - \mathcal{E}_2}\right)$ 3.30

where $\frac{\Delta\mathcal{E}}{\Delta z}$ is measured along the blade profile. See Appendix B. It should be noted that when transformation has been accomplished velocities of corresponding points on the blade and circle are related by the factor $\left|\frac{dz}{d\zeta}\right|$, which is a constant at any given point and is not a function of angle of attack or circulation imposed upon the circle in the picture plane.

The detailed analytical development of the ideal fluid flow in the picture plane is contained in Appendix C. What follows here is a descriptive summary of the procedure. The sources m placed in the picture plane to accomplish the conformal transformation create a 'straight through' fluid flow. This flow causes the front and rear stagnation points to occur on the circle at the ends of a diameter which lies along the real axis. See points 1 and 2 in Fig. 7.

To develop an angle of attack of the fluid with the zero direction of the real axis, vortices of strength Λ are imposed upon the four point sources. For positive approach angles, counter-clockwise vortices of equal strength are placed at the source at $\zeta = -b$ and at the sink at $\zeta = \frac{a^2}{b}$. Clockwise vortices of the same strength are placed at the other source and sink. The mean approach angle then becomes:

$$\alpha_m = \tan^{-1}\frac{\Lambda}{m} \qquad 3.31$$

The front and rear stagnation points still occur at the ends of a diameter of the circle but the diameter makes an angle with the real axis

$$\theta_s = \tan^{-1}(\tan\alpha_m \tanh\gamma) \qquad 3.32$$

The flow is undeflected as it passes around the circle; so no net circulation or lift is present.

To produce deflection and lift, vortices each of strength $\frac{\Gamma}{2}$ and of the same direction are placed at the source and sink inside the circle. The strength and the direction of these vortices are those required to satisfy the Kutta condition; i.e. the rear stagnation point must be brought to the location on the circle which corresponds through mapping to the trailing edge of the airfoil. Vortices of the opposite direction must be placed at the source and sink outside the circle to insure that the stagnation streamline remains a circle of radius a.

With sources and sinks m, and with vortices Λ and $\frac{\Gamma}{2}$ in place, the picture plane is complete. The velocity at any point on the circle is

$$\left(V_\zeta\right)_{|\zeta|=a} = V_\theta = -\frac{2m}{\pi a}\left(\frac{\cosh\gamma\sin\theta}{\cosh 2\gamma - \sin 2\theta}\right) + \frac{2\Lambda}{\pi a}\left(\frac{\sinh\gamma\cos\theta}{\cosh 2\gamma - \sin 2\theta}\right) - \frac{\Gamma}{2\pi a}\left(\frac{\sinh 2\gamma}{\cosh 2\gamma - \sin 2\theta}\right) \qquad 3.33$$

m is determined by $m = s(V_a) = s\left(-\frac{\partial\varepsilon}{\partial x}\right)_\infty$ 3.34

$\frac{\Lambda}{m}$ is determined by eq. 3.31 once α_m is arbitrarily chosen. To satisfy the Kutta condition, let $\theta = \theta_T$ and $V_\theta = 0$. The value of θ_T is determined by substituting the value of f_T in eq. 3.28. Solving eq. 3.33 then gives

$$\frac{\Gamma}{2m} = \tan\alpha_m \frac{\cos\theta_T}{\cosh\gamma} - \frac{\sin\theta_T}{\sinh\gamma} \qquad 3.35$$

The picture plane is thus completely determined. See Fig. 7.

For subsequent work, formulas for particular quantities relating to the flow direction are developed. The cascade entrance angle is

$$\alpha_1 = \tan^{-1}\left[\tan\alpha_m + \frac{\Gamma}{2m}\right] \qquad 3.36$$

The cascade leaving angle is

$$\alpha_2 = \tan^{-1}\left[\tan\alpha_m - \frac{\Gamma}{2m}\right] \qquad 3.37$$

The turning angle of the fluid as it passes through the cascade is

$$\Theta = \alpha_1 - \alpha_2 \qquad 3.38$$

Of aerodynamic interest is the ideal angle of attack. When the front stagnation point occurs at the point of the circle corresponding to the leading edge of the airfoil

$$\alpha_i = \alpha_1 = \tan^{-1}\left[\frac{\sin\Theta_T - \sin\Theta_L}{\tanh\gamma(\cos\Theta_T - \cos\Theta_L)}\right] \qquad 3.39$$

The lift on any blade is developed from the elementary relation

$$L = \rho V_m \Gamma = c_{l_x} q_x A \qquad 3.40$$

ρ is the density of the fluid and A is the projected area of the section along the chord. The subscript x appearing in the above listed equations indicates that the coefficient of lift and the dynamic head q may be based upon the cascade entrance velocity V_1, the cascade leaving velocity V_2, or the cascade mean velocity V_m. Each of the three coefficients of lift has its reasons for being used in the analysis of cascade performance.

c_l , based upon V_m , permits an aerodynamic tie-in with single airfoil theory, c_{l_1} , based upon V_1 is useful in cascade design because conditions upstream of the cascade are generally known. c_{l_2} based upon V_2 , makes allowance for the deceleration of the flow as it passes through a compressor cascade. Ref. 11 states that acutal cascade tests have shown that the drag-lift ratio reaches a minimum at an approximately constant value of

$c_{l_2} = 0.8$.

In terms of the quantities determined by the previous equations, the coefficient of lift is

$$c_{l_x} = \frac{2}{\sigma} \frac{\cos^2 \alpha_x}{\cos \alpha_m} \left(\tan \alpha_1 - \tan \alpha_2 \right) \qquad 3.41$$

4. EQUIPMENT

The equipment consisted of the specially designed apparatus used to hold the two dimensional, conducting paper, with appurtenances to impose the potential and complete the circuit. Associated with this piece of equipment were various electrical instruments necessary for potential supply and measurements. A list of the instruments with specifications, where applicable, is given in Table 1.

A complete test setup is shown in Fig. 8. The figure shows the conducting paper, the working surface and the associated electrical instruments. The remaining item is the profile template used as a guide in cutting the conducting paper.

4.1 THE WORKING SURFACE

Fig. 9 shows the original working surface which existed at the start of the investigation. It was constructed of 3/4 inch plywood overlaid with 3/16 inch Masonite (rough surface toward the plywood) and was fitted with Birmingham Gage Number 25 copper bus bars, one inch wide and five feet long. These bus bars were positioned on the table parallel and 29.5 inches apart at their inside edges. They served as the electrodes for imposing a potential difference across the paper cascade.

The paper was placed over the bus bars with its conducting (graphite) surface toward the Masonite. It was clamped as shown in Fig. 10. This method of clamping provided a tight, line contact between the bus bars and the paper.

This setup left the ends of the paper as unknown boundaries which were streamlines of the flow. It was necessary to use an iteration process to determine these boundaries. A first approximation was made by eye and the paper cut accordingly. The succeeding approximations were then obtained by flux plotting a streamline from experimentally determined constant potential lines. These plots were made near the middle of the cascade to minimize effects of the previous boundaries. The cascade ends were then cut to this newly determined streamline. This process of refinement was continued until the correction required became as small as the errors of measurement.

In order to by-pass the time and labor consumed in obtaining these boundaries a second table was constructed. This table shown in Fig. 11, was similar to the original in its method of connecting electrodes to the conducting paper. The contact between the electrodes and the paper was obtained by the same manner of clamping. The copper bus bars were widened to 32 inches however, and maintained parallel to $\pm$ 0.003 inches in a three foot length.

The table was lengthened to six feet overall with a foot and a half of each end hinged to the main, three foot section. With this provision, the paper was clamped to the table as in Figs. 10 and 12 and the ends were folded down under the main section thereby bringing the ends of the paper cascade together in a physical and therefore electrical contact. The cascade then had no beginning or end and was, in effect, infinite.

Since cascades of varying solidity required various lengths of paper in order to come to contact at the joint, it was neces-

sary only to lengthen or shorten the bight of the paper at the hinges when securing the paper to the table prior to folding.

The method of obtaining the electrical connection between the ends of the paper cascade is shown in Fig. 13. This method has the disadvantage that the operator cannot see the actual connection and must rely upon the trueness of the hinges, machined parts, etc. To provide sufficient contact pressure along the joint, C-clamps were used outside the aluminum bars.

4.2 THE CONDUCTING MEDIUM

Type "L" Teledeltos paper was used as the conducting medium throughout the investigation. The specific resistance of this paper is given by the manufacturer as 4000 ohms, with an accuracy of $\pm$ 3 to $\pm$ 8 percent with the lower value of resistance along the length of the roll and the higher value across the width of the roll. The quantity specific resistance, is defined and explained in Appendix D. The corresponding specific resistance of the copper bus bars is clearly negligible in comparison with that of the paper. At the hinged ends of the table, and near the electrical joint on the under surface, where the bus bars are necessarily interrupted, the required conductivity was secured by painting the paper on its conducting side with a special silver paint supplied by the manufacturer. The specific resistance of such painted areas is given by the manufacturer as about one to four ohms. While this value is considerably higher than that for the copper bus bars, it is still negligible in comparison with that of the paper. Thus the conductivity of either the bus bars or of the painted areas is es-

sentially infinite in comparison with that of the paper. Each test setup required a new piece of paper making it a consumable item in the investigation.

4.3 THE BLADE TEMPLATES

The following profiles were selected for investigation:

a. The Mutterperl profile, ordinates presented in Ref. 7 and listed in Table II

b. A typical compressor profile, the NACA 65-(15)10 section, ordinates presented in Ref. 9 and listed in Table III

Coordinates of these profiles, scaled to the chord sizes used in this investigation, are presented in Tables IV and V.

In order to transpose the coordinates to the paper in the proper geometry and to maintain accuracy, templates were used as cutting guides. They were made of 1/16 inch, oil hardening flat stock which was left in the spheroidized condition instead of being hardened, thus avoiding distortions.

Tolerance from the tabulated coordinates was held to $\pm$.005 inches. Each template was checked dimensionally at fifteen diameters magnification on the Bausch and Lomb Contour Measuring Projector, Model 33-12-01, at the Supersonic Wind Tunnel of the U. S. Naval Postgraduate School.

To position the templates for cutting on the cascade layout lines, three or more locator holes were drilled in each. These holes were spaced along a line parallel to the chord and offset from it. One of the holes was located at midchord. These profiles are shown in Fig. 14.

4.4 ELECTRICAL CIRCUITRY AND INSTRUMENTS

The electrical circuit of the continuous cascade table and of the associated instruments for measuring percentage potential is shown in Fig. 15. The power supply used was a Heathkit Battery Eliminator, Model BE-4. The voltage output was maintained at about 11 volts in order to give a quicker and more definite response on the null meter. The null meter used was a General Electric DC Micro Ammeter, Type DO-71, Model A292AA1 of 10 microamperes full scale deflection. At a 100 percent potential equal to about 11 volts, 0.01 percent potential was the minimum discernable change on this meter. The voltage divider, manufactured by Electro-Measurements Inc., was a hexadecade type; Model RV622. Its linearity as cited by the manufacturer was $\pm$ 0.0025 percent with an input resistance of 10,000 ohms. As mentioned above, 0.01 percent potential was the minimum detectable change and therefore only the four higher decades of the voltage divider were used. The test probe or stylus was supplied with the General Electric Analog Field Plotter Kit. It was fitted with a shallow tapered needle from a drafting instrument.

The approximate derivative of the mapping function could be determined by graphical means or by direct measurement. The latter method was used. To accomplish this determination, the potential difference over a small distance was measured by a double electrical probe. This probe was adapted from a small bow compass by placing a second, insulated needle in the lead

receptacle and soldering both needles to hookup wires. The compass was adjusted to the smallest needle gap possible and locked in position. This gap measured 0.04048 inches on the measuring projector previously mentioned. The entire compass was finally covered with electrical insulating tape.

Fig. 16 shows the circuit schematic for determining the approximate derivative of the mapping function. The hookup wires from the probe were lead to a Leeds and Northrup Portable Precision Potentiometer No. 8662, where they were connected to the E.M.F. binding posts. This instrument has a range of from 0 to 85 millivolts. The power supply was two six volt batteries connected in series to give approximately 12 volts. Practically all stations on the profile gave voltage increments across the double probe which were within the range of the potentiometer at a battery supply of about 12 volts. The voltage across the cascade (100 percent potential) was measured to the nearest 0.01 volts on a Weston DC Voltmeter, Model 45, having 0-15, 0-150 volts full scale deflection.

5. TEST PROGRAM AND PROCEDURE

The test program was designed to show the effects of various geometric parameters upon the performance of a cascade. The parameters which define the geometry of two dimensional, rectilinear, infinite, cascades are the blade profile, the stagger angle β, and the solidity c/s. The quantities β, c and s are illustrated in Fig. 17.

5.1 DEFINITION OF TERMS

The direction of the incoming flow may be specified in terms of the approach angle α_1, which is measured from a line perpendicular to the cascade.

An alternative parameter which is sometimes useful is the absolute angle of attack α_a, which is defined as the angle between the mean flow direction and the direction of zero lift, Axis I. The mean flow angle α_m, depends both upon the inflow and outflow angles α_1 and α_2. The angle of zero lift α_{L_0}, of the cascade is not initially known, since it depends on the entire cascade geometry in some complex manner, but it may be found from the results of the test measurements in any given case. Once α_{L_0} has been determined, a convenient parameter for further analysis of the cascade is the relative angle of zero lift β_{L_0}, which is defined as the angle between the chord and Axis I, the direction of zero lift of the profile in cascade.

These various relations are shown in Fig. 17.

The performance of a cascade may be expressed in terms of

any convenient parameter which relates the inflow and outflow directions. Among these are the turning angle Θ and the lift coefficients c_l, c_{l_1} or c_{l_2}. The turning angle Θ, represents the net change in direction of flow from inlet to exit. The lift coefficients c_l, c_{l_1} and c_{l_2} represent the ratio of the mean effective pressure difference across the blade to some reference dynamic pressure. They differ only in the reference condition used: c_l uses the mean velocity head, while c_{l_1} and c_{l_2} employ the inlet and outlet velocity heads respectively. All three of these coefficients are closely related to the turning angle, and the choice of parameters is largely a matter of convenience, although for a real fluid the quantity c_{l_2} appears to be an approximate criterion of blade stall.

It can be shown theoretically that for an isolated airfoil

$$c_l = 2\pi \sin\alpha_a \qquad 5.1$$

Similarily, for a cascade of airfoils, it can be shown that

$$c_l = 2\pi K \sin\alpha_a \qquad 5.2$$

where $\alpha_a = \alpha_m - \alpha_{L_0}$ and K is the cascade coefficient which is a constant determined by cascade geometry.

There are two basic parameters, then, which completely determine the performance of a given cascade in ideal fluid flow. These are K and β_{L_0}. They have been calculated for the cascades tested and are reported.

5.2 THE TEST PROGRAM

The method used in this investigation requires that a separate set of measurements be made for each cascade configuration tested, whereupon the effect of variations in inflow direction can be determined analytically. This greatly reduces the amount of testing that is required; nevertheless, the testing procedure was necessarily painstaking, and due to the developmental nature of this investigation only a limited number of tests could be undertaken and analyzed in the time available for this study.

The various combinations of blade profile, solidity and stagger angle which were investigated are summarized in Table VI and discussed below.

The airfoil shape presented by Mutterperl in Ref. 7 was selected for the first series of tests. Published data on this profile had been determined analytically. Tests on the profile in this investigation included solidities of 1.0 and 1.5, both at a stagger angle of 45°. The latter case was not covered by Mutterperl in his report.

The second series of tests was designed around a typical compressor profile at combinations of stagger angle and solidity characteristic of practical compressor geometry (based on the authors' experience with the Gas Turbine Division of General Electric during the 1957 Summer Field Trip from the U. S. Naval Postgraduate School).

Two groups of tests were conducted using an NACA 65-(15)10 profile at stagger angles of 20°, 25°, 30°, and 35°. One group used the six inch chord at a solidity $\sigma = 1.0$ while the other

used the twelve inch chord at σ = 1.5. At least one check point for each test was available from the experimental data presented in Ref. 9.

One of the objectives of this investigation was to demonstrate an extension of the method namely, the determination of the velocity distribution around a blade in cascade. Data for this demonstration was gathered during the test of NACA 65-(15) 10 (12" chord) at σ = 1.5 and β = 35°. Selection of this test provided the opportunity to compare results with those published in Ref. 9.

5.3 PROCEDURE

The procedure is perhaps best illustrated by following a typical cascade setup through to data collection.

The first step of the procedure was preparation of the conducting paper for the table. The paper was supplied in rolls, 34 inches wide and about 20 feet long. The working surface had been designed with the electrodes positioned to accommodate this width so it was necessary only to trim the paper to length. The length required varied with solidity for a given blade chord. For σ = 1.0 and a six inch chord, 88 inches of paper were used. For the tests with σ = 1.5 and the twelve inch chord, 92 inches were required.

The paper was laid out flat on a smooth table and fastened without stretching by masking tape at intervals along the edges. The black (non-conducting) surface was exposed as the drawing surface for layout lines.

Fig. 18 shows a sketch of the layout lines on a typical piece of paper. Fig. 19 shows the template outline on one set of these lines. Included in this latter sketch are the reference lines near the leading and trailing edges which were used to locate data points.

The cascade center line was drawn first. The best results in keeping this line straight occured when using a chalkline of sewing thread and blackboard chalk. The line so obtained was then penciled in using a six foot straight edge. Exact centering of this line on the paper was not necessary as the copper electrodes, being 32 inches apart, allowed some deviation.

The cascade center line was used as the reference for layout of the selected spacing and stagger angles. Care was taken to locate the profiles so that the electrical joint would occur midway between adjacent blades along this reference line. Instances of large stagger angle, where the seam passed through corresponding sections of the cutouts on each end of the paper, could be handled by the joining device.

A drafting machine was utilized to construct the angular stagger and midchord lines shown in Figs. 18 and 19.

In order to maintain accuracy in locating data points, reference lines were drawn on the three center profiles of the paper cascade. These lines were constructed perpendicular to the chord and extended to intersect the contour of the profile cutouts as shown in Fig. 19. The interval along the chord of these lines was 1/40 inch for the six inch chord and 1/20 inch for the twelve inch chord. A jewelers' eyepiece, and 6H pencil, and the scale of the drafting machine arm were used to construct these

lines. Only part of the profile was lined in this manner. Fifteen lines were drawn at the trailing edge in all tests. The number and position of the lines near the leading edge varied with the location of the front stagnation point.

The paper was then removed to a Masonite surface for cutting out the profiles. In this operation the template was located by means of the holes provided. Cutting proceeded from the tail and from the nose toward the midchord where the cuts met. The knife used for cutting was an "Xacto" using the blade having the straight cutting edge. The blade was honed to a shape illustrated in Fig. 20 and stropped on a Masonite surface to remove all burs. In cutting, it was imperative to hold the knife so the cutting edge was at an angle of about 45^{o} to the paper and to guide it in toward the template. All other methods of holding and cutting either did not adhere to the profile shape or produced jagged edges.

The ends of the paper were then folded to fit over the corner of the aluminum bars at the joint of the table. The fold line was marked on the non-conducting (black) surface so the paper was first folded to keep this line exposed as a guide. After this fold had been sharply creased, it was reversed to expose the conducting surface.

Painting the bus bar extensions was the next step in the preparation of the paper cascade. To provide guidelines for this painting, the paper was marked while in its proper position on the working surface. A center line had been scribed on the table during its construction. Bringing the cascade center line into coincidence with the scribed line properly positioned the paper

in one direction. Positioning in the other direction was accomplished by fitting the folds at each end of the paper to the right angle corner on their respective parts of the joining device. This is shown in cross section in Fig. 13, with the paper joined. The end sections of the paper were held by suitable weights on each end section of the table while the middle of the paper was moved along the scribe line of the main table section until the bights of the paper over the hinges were equalized. Fig. 12 shows the paper clamped in this position. The guides for the bus bar extensions were then marked on the paper's conducting surface by pressing it down over the sharp inner edge of the ends of the copper bus bars.

The paper was then removed to the drawing surface and layed out flat with its conducting surface up. At each end of the paper the painting guides were pencil lines which had been extended along the bus bar impressions to the ends of the paper. Painting guides for the bights of the paper were obtained by pencil lines connecting the bus bar impressions at the ends of each bight. Scotch Brand Electric Tape was used as a masking tape. It was placed along the above lines on the side away from the paper edge and extended beyond the bus bar marks. The edges of the paper were then painted with the silver conducting paint along each of the masked areas. When the paint had set but not dried, the masking tape was removed. Unless this tape had been dusted lightly with blackboard chalk or some other dust, the graphite conducting medium was liable to pull away from the paper during tape removal.

At this point various reinforcing sections of tape were ap-

plied to the paper. This was especially needed when using the twelve inch profile cutouts.

After the paint had dried, the paper was aligned on the extended table, non-conducting surface up as when marking, and held. The electrical tape was used in small pieces to hold the paper in position by placing it along the paper edges behind the contact line of the electrodes and over blade cutouts not used for data. The clamps were then applied as shown in Figs. 10 and 12.

The ends of the paper sticking through the slots of the aluminum bars were cut off to leave about 3/8 inch of paper extending beyond the fold. A 3/8 inch wide strip of electrical tape applied to the cut edge of these ends was used to hold the fold over the corner of its respective bar. The relief in the movable bar gave room for the tape and at the joint itself only the two layers of paper, conducting sides together, remained.

The table was turned over and the ends folded toward each other. The folds of the paper were joined simultaneously and a support under the two ends prevented their moving through their closest point of approach. The ends of the table were secured against the middle by bolts. Insulating paper was then slipped between the conducting paper and aluminum bar and pushed to the joint to prevent the curled cutout edges from contacting the aluminum bars. C-clamps were applied to press the bars together and make a tight contact between the folds on the ends of the paper.

The table was turned over and the circuit connected as in Fig. 15.

The data points were numbered from leading edge to trailing edge. Stations every 1/8 inch along the chord on the six inch profile were numbered consecutively. Data points between these lines were lettered a, b, c, and d. The data consisted of the value of $\mathcal{E}$ at the leading edge, the points near $\mathcal{E}_1$, and at the fifteen upper and lower points near the trailing edge. To obtain $\frac{\partial \mathcal{E}}{\partial x}$, a line perpendicular to the electrodes and the cascade center line was drawn from the electrode ahead of the cascade. It was marked at intervals of one inch for five or six inches from the bus bar. The value of $\mathcal{E}$ was recorded for each of these points. All values of $\mathcal{E}$ were read and recorded to 0.01 percent potential.

When obtaining the derivative approximation $\frac{\Delta \mathcal{E}}{\Delta z}$ it was necessary to use the circuit of Fig. 16. Percent potential could be obtained simultaneously by connecting the voltage divider with null meter and probe across the battery supply.

The data in this test consisted of $\mathcal{E}$ at various points around the profile edge, corresponding values of ΔE in millivolts obtained from the precision potentiometer and total potential E* in volts. The double probe was positioned so that its interval between probes was centered about the point where $\mathcal{E}$ was obtained and with its needles just making contact at the edge of the profile. The value of ΔE was read and recorded to the nearest .01 millivolt.

6. DEVELOPMENT OF RESULTS

A sample of the data taken during these tests for the determination of turning angles is presented in Table VII. A sample of the data taken for the determination of velocity is presented in Table VIII. Table IX contains the input quantities used for the determination of turning angles herein reported.

Results of tests on the cascade analyzed in Ref. 7 are presented in Fig. 21 as a curve of coefficient of lift versus mean velocity direction.

Results of tests made on the NACA 65-(15)10 airfoil are presented in Figs. 22 through 31. In Figs. 22 and 25 the values of turning angle for various blade stagger angles are plotted versus cascade entrance angle with lines of constant coefficient of lift c_{l_1} crossplotted. Fig. 22 is for a solidity of 1.0 and Fig. 25 is for a solidity of 1.5. Figs. 23 and 26 contain, for a solidity of 1.0 and 1.5 respectively, curves of coefficient of lift c_{l_1} for various blade stagger angles, as a function of cascade entrance angle. Figs. 24 and 27 show, for a solidity of 1.0 and 1.5 respectively, curves of coefficient of lift c_{l_2} for various blade stagger angles, as a function of cascade entrance angle. Fig. 28 is a plot of cascade coefficient K versus blade stagger angle β Fig. 29 is a plot of relative zero lift angle β_{L_0} versus blade stagger angle β.

Figs. 30 and 31 contain the results of the test of this method to predict velocity distribution about the NACA 65-(15)10 airfoil in cascade at stagger angles of 35° and solidity of 1.5. The results are plotted as $\left(\frac{V_2}{V_1}\right)^2$ versus percentage distance along the

chord.

The recorded data necessary to determine turning angles and coefficients of lift for a given cascade (blade, stagger, and solidity) consisted in part of readings of the percentage voltage at several stations of known location in the vicinity of $\mathcal{E}_1$, $\mathcal{E}_2$, and $\mathcal{E}_T$. See Table VII. Data were recorded for at least three blades in each cascade test, but final values of this report are based on the median blade for each case. These percentage readings near $\mathcal{E}_1$ and $\mathcal{E}_2$ could be plotted versus distance along the chord to permit utilization of several voltage readings to insure greater accuracy in the determination of the values of $\mathcal{E}_1$ and $\mathcal{E}_2$. See Fig. 32.

Finding $\mathcal{E}_T$ was a more difficult problem. Fig. 3 indicates that the curve of $\mathcal{E}$ versus percentage of the chord becomes tangent to the line representing 100% chord at the trailing edge. Determination of $\mathcal{E}_T$, the point of tangency, by experimental measurement meant reliance upon a single potential reading because of the physical nature of the very sharp trailing edge.

The method used in this investigation to determine $\mathcal{E}_T$ more accurately involved obtaining an analytical curve of $\mathcal{E}$ near the trailing edge of the airfoil. The form of the curve was that of potential flow around a straight sided wedge. The curve was obtained by fitting this form to several experimental points in a finite but small distance near the trailing edge. Curve fitting was accomplished by means of the method of least squares. The point of tangency $\mathcal{E}_T$ was then determined analytically. Appendix E contains the details of this curve fitting procedure.

The value of $\frac{\partial \mathcal{E}}{\partial x}$ was obtained by plotting. Near the bus

bars readings of $\mathcal{E}$ were plotted versus perpendicular distance from the bus bars. The slope of this straight line was $\frac{\partial \mathcal{E}}{\partial x}$. See Fig. 32.

The determination of the velocity at a point on the blade required the measurement of ΔE at that point. A sample of recorded readings of ΔE is contained in Table VIII. These readings were converted to $\frac{\Delta \mathcal{E}}{\Delta z}$ by means of the relation

$$\frac{\Delta \mathcal{E}}{\Delta z} = \frac{\Delta E}{E^*} \frac{1}{d} \qquad \text{where} \qquad 6.1$$

d is the separation of the double probe. Values of $\frac{\Delta \mathcal{E}}{\Delta z}$ are also shown in Table VIII. Values of $\frac{V_2}{V_1}$ were then obtained by means of the formula

$$\frac{V_2}{V_1} = \frac{\Delta \mathcal{E}}{\Delta z} \frac{\cos \alpha_1}{V_a} \left[1 - \frac{\tanh \gamma}{\tan \theta} \tan \alpha_m + \frac{\Delta T}{m} \frac{\sinh \gamma}{\sin \theta} \right] \qquad 6.2$$

The NCR 102A electronic, digital computer of the U. S. Naval Postgraduate School was used to compute $\mathcal{E}_T$, α_1, α_2, α_i, and $\frac{V_2}{V_1}$. Machine assistance proved indispensible for the extensive calculations required by the many cascade combinations tested during this investigation.

One program on the computer was used to determine $\mathcal{E}_T$. Input data consisted of twenty potential readings, ten from the upper surface on the airfoil near the trailing edge and ten from the lower surface near the trailing edge, together with their respective distances from the trailing edge and the value of p. See Appendix E. The computer solved for $\mathcal{E}_T$.

A second computer program was used to determine α_1, α_2, and α_i. Input data consisted of $\mathcal{E}_1$, $\mathcal{E}_2$, $\mathcal{E}_L$, $\mathcal{E}_T$, s, and $\left(-\frac{\partial \mathcal{E}}{\partial x}\right)_\infty$. In addition, inputs of $\mathcal{E}$ and $\frac{\Delta \mathcal{E}}{\Delta z}$ were required for

each of the points at which velocity ratios $\frac{V_2}{V_1}$ were desired.

7. DISCUSSION

7.1 GENERAL

The discussion of this method for predicting the flow of an ideal fluid across any arbitrary cascade first examines the results of the tests made on various cascades. The analysis of the results then provides the basis for a critique of the method and for suggested improvements in equipment and in technique. Possible applications of this method to other aspects of engineering are also suggested.

7.2 RESULTS

The geometric parameters which determine a cascade are the blade profile, the stagger angle, and the solidity. For a given cascade the quantities K and β_{L_0} are the fundamental parameters which were determined by this investigation for indicating the performance of a cascade over a wide range of mean velocity directions. Turning angles were also calculated for each cascade. From this information other parameters were calculated to permit cascade analysis from different viewpoints and to permit comparison with published reports.

It first seemed appropriate to compare the results of the method herein discussed with a published analytical solution. Ref. 7 contains an analytical solution of potential flow across a given cascade of $\sigma = 1$ and $\beta = 45^\circ$. This report was used for comparative purposes because it contained coordinates for the profile used and because results were reported over a range of

directions of the mean velocity. The blade profile used is similar in camber and thickness to those presently found in compressors. The blade, however, has a trailing edge of zero thickness. The pointed trailing edge is difficult to duplicate exactly in the paper cutouts and would not be used in actual compressors. Reference to Fig. 21 indicates that the method of this paper apparently predicts coefficients of lift which are about 14% greater than those contained in Ref. 7. The difference represents about 5° in turning angle. This difference was greater than had been expected, but it is subsequently shown that this disparity can be reduced. Subsequent tests indicated that an increased error in turning angle resulted from tests on cascades with large stagger angles. The larger stagger angle cascades are more susceptible to errors caused by the variation of specific resistance of the paper between width and length directions. Possible solutions to this problem are discussed later.

Fig. 21 does indicate that the slopes of the curves of c_l vs. α are almost the same. Calculations reveal that the cascade of Ref. 7 has a coefficient K of .74 while the cascade coefficient determined by this method is .72. Thus if determination of the angle of zero lift were made separately, the turning angle predicted by this method would be within a fraction of a degree of the turning angles reported in Ref. 7.

Fig. 21 indicates that increase of the solidity of this cascade to 1.5 changes the cascade coefficient to .49. The 1.5 solidity cascade is not analyzed in Ref. 7.

Ref. 9 is a report of systematic two dimensional cascade tests of NACA 65 series compressor blades. Cascades considered

to be most typical of present compressor design were selected from the report for investigation by this method.

The NACA test data was taken by varying cascade stagger angle. This was required because of the difficulty of varying the direction of the approaching velocity in the two dimensional wind tunnel. The method of this report permits variation of the direction of approaching velocity for constant cascade geometry. Comparison, then, was possible only at certain points, indicated in Figs. 22, 23, 25 and 26.

It must be borne in mind that Ref. 9 is a report of tests performed using an actual fluid. The magnitude of the effect of viscosity is uncertain, but one could not expect results based on viscous fluid flow to be identical to those for ideal fluid flow. Comparison serves to indicate, nevertheless, that predictions based upon ideal fluid flow are sufficiently close to measured values for air to be of value in actual cascade design.

Figs. 22 and 25 give the results for the cascade of the NACA 65-(15)10 airfoils with $\sigma = 1$ and 1.5 respectively. The figures show that the relationship between turning angle and cascade entrance angle is almost a linear one, indicating that the exit angle remains nearly constant. For a given cascade entrance angle, turning angle is of course increased by decreasing the stagger angle. The effect of increasing solidity on turning angle (and therefore on the quantity σC_l) is small. Hence the cross plots indicate an appreciable reduction in C_l, with increase in solidity. These are all general results which one would expect.

The cascade designer wonders what represents optimum condi-

tions and the extent of variation permissible for satisfactory performance. The cross plotted values of c_{l_1} give an indication of the coefficient of lift associated with a certain turning angle. This information together with the plot of ideal angle of attack helps to denote an area of satisfactory operation based upon upstream conditions. However, for the decelerating flow experienced in a compressor, information showing the extent of the range of operation for an optimum drag-lift ratio is desired. For this reason Figs. 24 and 27 have been presented. Ref. 11 says tests show that the drag-lift ratios of cascades varying from turbine to compressor types show a minimum at an approximately constant value of c_{l_2} of about .8. For blades of the types generally used in cascades the drag coefficient is low and almost constant over a range which extends perhaps five degrees above and fifteen degrees below the minimum drag-lift ratio. These general criteria for determining range of operation are indicated on Figs. 22 and 25.

The effect of changing cascade stagger is apparent from Figs. 22 and 25. One would expect the spacing between lines of constant β to be more uniform than this test indicated. This variation is considered to be a manifestation of the experimental error of the method. For the whole series of tests the error is believed to be $\pm 1^{\circ}$. A test program which included a wider range of stagger angles or which provided for smaller test increments in this same range would serve to assist in reducing this random error by permitting the application of statistical data smoothing techniques.

There is again an indication, particularly for the cascade

test at $\sigma = 1.5$ and $\beta = 35^\circ$ that the high stagger angle cascade is subject to an additional error. The turning angles predicted for this case seem to be greater than one would expect, considering the other three cascades. As in the 45° stagger angle cascade first discussed, some of this difference is probably attributable to the paper.

This particular cascade was also analyzed to see what value of ε_σ would give results in agreement with the NACA report. The point on the blade cutout which had the value of ε so determined was located on the upper side of the blade profile very near the trailing edge. This suggests that the real fluid in the NACA tests, under the influence of viscosity and adverse pressure gradient, separated from the airfoil at a point closely approximating this same location on the blade cutout.

For the $\sigma = 1$ cascade the predicted turning angles compare remarkably well with the NACA test points for a cascade entrance angle $\alpha_1 = 45^\circ$. The comparison is not as close for the two NACA points plotted at a cascade approach angle $\alpha_1 = 30^\circ$. For $\beta = 20^\circ$ a line drawn between the two NACA test points at $\alpha_1 = 30^\circ$ and $\alpha_1 = 45^\circ$ would not have the same slope as the corresponding line produced by this method. The same thing is true to a lesser extent for $\beta = 25^\circ$. These differences in slope are considered to be a consequence of viscosity.

For the $\sigma = 1.5$ cascade there is a somewhat larger difference between predicted turning angles and reported NACA test results, but the comparison is still close. Twelve inch chord blade templates were used for three of the four cascades of $\sigma = 1.5$. Only the $\beta = 25^\circ$ cascade was cut out using a six

inch template. The somewhat increased error due to bus bar location for the larger template is not discernable; so use of the larger blade is probably warranted for high solidity cascades when the reduction in cut out time and in labor are considered. A series of analyses for various values of β and σ such as is contained in Appendix F for $\sigma = 1$ and $\beta = 45^\circ$ would permit approximate determination of the largest sized blade permissable for a given acceptable percentage error.

Fig. 28 presents a concise summary of the effects of solidity and stagger angle upon cascade performance. The variation of cascade coefficient K with changes in stagger angle are shown for each solidity. For purposes of approximate comparison values of K for a flat plate cascade having the same nominal value of solidity and stagger as the actual cascade are also plotted and are seen to be quite similar.

Another concise representation of cascade characteristics is contained in Fig. 29 which shows the effect of changing stagger angle upon the relative angle of zero lift α_{L_0}. This presentation amplifies and clearly shows the variation in the angle of zero lift with changes in stagger angle. It suggests that a similar plot for a much larger number of tests would permit the determination of a smooth curve of β_{L_0} vs. β. If the magnitude of random error were thus partially removed from the determination of α_{L_0}, a more uniform spacing of the constant β lines in Figs. 22 and 25 would result and the error indicated in Fig. 21 would be considerably reduced. Unfortunately time did not permit conducting the additional number of tests which would be required to determine this curve.

The curve of Fig. 31, $\left(\frac{V_2}{V_1}\right)^2$ vs. percent chord compares favorably with the NACA curve for a similar cascade entrance angle. However, Fig. 31 is a smooth curve determined from calculations based upon raw data by means of a method of least squares developed by Professor Gawain. Before extensive tests of velocity could be undertaken, the double probe and perhaps the technique of obtaining ΔE readings would require improvement. Fig. 31 does indicate, however that the velocity distribution can be determined by this method.

7.3 ACCURACY

The accuracy of the results obtained by this method of cascade analysis is a function of the approximations made and of the accuracy of the measured input data. The results are more sensitive to errors in some input quantities than to errors in others, and certain measured quantities can be determined more accurately than others.

Table X gives an indication of the sensitivity of results to variation of input data. It lists the change in calculated turning angle caused by individually increasing each of the input quantities $\mathcal{E}_1$, $\mathcal{E}_2$, $\mathcal{E}_T$, and $\frac{\partial \mathcal{E}}{\partial x}$ by one percent of its measured value. This information was compiled for a cascade of the airfoil contained in Ref. 7 with $\beta = 45^\circ$ and $\sigma = 1$, but it is considered to be representative of the other blades and cascades tested. The table indicates that the results are particularly sensitive to changes of $\mathcal{E}_2$ and $\mathcal{E}_T$. It indicates the desirability of obtaining the input measured values to an accuracy of one part in ten thousand.

Many operations were required for each cascade layout, and every step had some effect on the value of the final measured quantities. The largest of the construction errors was due to the conducting medium. The value of the specific resistance of this material was given by the manufacturer as 4000 ohms. This value was specified accurate from ± 3 to ± 8 percent with the lower value of resistance along the length of the roll and the higher value across the width of the roll. This variation is explained by the manner of manufacturing. These errors were necessarily accepted as the particular conducting medium used was basic to this investigation.

Wood was used for structural members of the working surface. The position of the bus bars was held to the tolerance mentioned in the equipment section, but the trueness of the joint depended upon the ability of the wood to maintain its dimensions under continued use. It was found that after three or four tests, the table required cleaning because the graphite deposit on the table caused a change in the conductivity of subsequent papers when not removed.

In the layout of the cascade on the paper several sources of probable error were encountered, such as dimensioning, constructing layout and reference lines and setting stagger angles. These were subject to the same limits of error encountered in engineering drawings A reading glass and a jewelers' eyepiece were used to provide magnification for greater accuracy in layout. Dimensions could be held to a tolerance of .01 inch. Lines were maintained to widths of from four to six thousandths of an inch and angles were maintained correct to 10 minutes of arc.

The templates introduced a systematic error due to the tolerance of manufacture and a random error in the process of positioning. The manufacturing tolerance was ± 0.005 inches. The profile cutouts were maintained to their respective coordinates with a tolerance of about .010 inches.

Reading and determination errors of the instruments were encountered only with the null meter and with the probe. Since a zero reading or null was required on the meter prior to reading the voltage divider, detecting a null was reduced to detecting motion of the meter needle. The sensitivity of the instruments permitted reading potential on the voltage divider to one part in ten thousand. Readout was directly in percent potential; so constancy of imposed voltage was not required. Errors in probe location depended upon all previous dimensioning and construction of reference lines. With optical aids it was possible to place the probe within the actual width of the pencil lines. Distance from the cutout edges of the profile could not be determined to comparable accuracy. However, the constant potential lines are normal to the cutout near the profile edge; so this distance is not as critical.

The velocity distribution around the profile was determined to demonstrate in preliminary fashion one of the capabilities of the method. This involved measuring small changes in potential and distance as a means of determining potential gradient. Tests were not conducted to determine the accuracy of these measurements nor the validity of the final results. Ref. 12 states that for a liquid electrolyte it is possible to obtain an accuracy of two to five parts in a thousand with respect to

the theoretical value when using a double probe of five millimeters separation. The method of determining the error of such an instrument was to rotate it around a point in the field in which case a sinusoidal variation should result.

It might seem, when first considered, that a comparison of the potential readings at corresponding points on adjacent profiles would give an indication of the overall accuracy actually obtained. However, this is not a definite criterion. In fact it was not uncommon for the measured potentials at corresponding points on adjacent profiles to differ by 2% without producing a noticeable change in results. The reason for this is that the quantities τ and f which determine conditions in the picture plane contain ratios of differences between measured quantities. The measured values of the various $\mathcal{E}$'s could therefore differ from profile to profile without necessarily affecting the values of τ and f .

A better indication of the overall accuracy actually obtained in construction and measurement was the repeatability of results. Fig. 33 gives an indication of the degree of repeatability of the method and procedure as finally evolved. The three layouts shown were distinct in every respect even to the use of Teledeltos paper from three separate rolls.

The indication of repeatability does not, however, purport to show the accuracy of the method in its degree of approximation to the true conditions for an infinite cascade. The bus bars were located a finite distance from the cascade and can only approximate the conditions an infinite distance away. Although the error accepted with this assumption cannot be deter-

mined exactly with the present equipment, a close approximation of this error based on a cascade of flat plates is derived analytically in Appendix F. From the figure and the data in this appendix it is evident that for the geometry selected, the error introduced by the location of the bus bars is negligible. Only one cascade of flat plates was investigated, but the analytic means is at hand for determining cases of different solidity and stagger angle.

The effect of the foregoing limitations on the accuracy of K and β_{1_o} cannot presently be determined directly. Further testing is needed to provide statistical data for determination of the error as well as means for its reduction.

The closely related parameter of cascade performance θ, when compared to published data, agreed within the limits of $\pm 1^{o}$.

7.4 CRITIQUE OF THE METHOD AND SUGGESTED IMPROVEMENTS

The given conducting paper was taken as fundamental to this investigation. The scope of this work could not include a search for nor an evaluation of various conducting mediums. However, removal of the directional properties of the conducting medium and reduction of the variation in its specific resistance should greatly improve the accuracy of the method. Perhaps the present type of conducting paper could be improved. Other conducting mediums may be available. Considerable work has been done in France and at Rensselaer Polytechnic Institute in this country with electrolytic tanks. See Refs. 12 and 13. A solid conducting medium is believed to be preferable for the method herein described. The solid medium obviates such problems

as leveling and polarization. The test set-up is much simpler as only a single template is required for all of the cascades using that airfoil.

If after investigation the teledeltos paper still proved to be the best solid medium available, allowance for the directional properties could be made by use of a scale factor. For the work reported here a scale factor correction of profile coordinates was not considered practical because of the range of variation of specific resistance in a given direction. Summarizing, even if directionality cannot be removed, variation of specific resistance in a given direction should be decreased.

A minor suggestion for increased ease in cascade layout is to change the black color of the backing side of the sheet to more clearly show-up the penciled layout lines.

The layout table undoubtedly would be further modified if this method were to be used commercially. It is considered desirable to bring the meridional ends of the paper together to establish an electrically continuous sheet although the original flat table produced satisfactory results when the approximate streamlines were used as boundaries. The cascade test at $\sigma = 1.0$ and $\beta = 30^{\circ}$ was done on the original table. If a paper were used which was sufficiently long in the direction of the cascade axis the effect of straight-cut ends would probably be small at the center blade cutouts. This would be particularly true for the cascades of small stagger angle.

If a table be constructed of design similar to the one herein described, particular care should be taken to insure that the table hinges be dimensionally true. Their trueness

also will require periodic checking because of the dependence of the electrical connection upon them.

Perhaps a clip-board type of springed clamp could be designed for establishing electrical contact between bus bars and paper. Such an arrangement could save time over the bolted clamping system used for these tests.

Another suggestion for improvement is to design the layout table such that the bus bars as well as the paper would be electrically continuous. Although the conductivity of both the copper bus bars and the silver painted areas on the paper is large relative to the paper, their conductance would improve the approximation of uniform conditions at large distances from the cascade.

The method is dependent upon the technique of the operator. With an increasing number of cascades tested, the operator can be expected to improve in accuracy and increase in speed. The angle of holding the probe, the depth of probe penetration, the eyesight of the operator, and his ability to position the probe accurately are all personal factors which will affect the results to a certain small degree.

The statistical curve fitting technique for determining the value of $\mathcal{E}_T$ probably could be improved. There is a requirement for reduction of the random error. The method used in this report seemed attractive because of the similarity of its equations to those for perfect fluid flow. It proved to be practical for solution. This same form perhaps could be modified to allow for the curvature of the blade profile near the trailing edge.

This method of cascade analysis has the great advantage of being much less expensive than actual cascade tests. The teledeltos paper is the principal consumable item. The templates can be manufactured without difficulty or excessive expense.

The time saving of this method over other methods of cascade analysis is considered to be one of its principal advantages. With improvement in technique it was found that a typical cascade layout could be completed and measurements taken for determination of turning angle in slightly more than one working day. This of course depended to some extent upon cascade geometry. Calculations of turning angles from the raw data were accomplished in three to four hours and would be much faster on newer digital computers. The use of the computer is not required for this method. It was used here principally to save time and thus permit the testing of a greater number of cascades. The measurements required for the determination of velocities at 60 stations on the profile required an additional two hours. Calculating time to find these velocity ratios required approximately 20 minutes for each angle of mean velocity.

Analyzing the method from another viewpoint, it experimentally accomplishes conformal transformation of an arbitrary cascade onto a circle. When one considers the well known transformation which maps a circle into a cascade of flat plates, he might in one sense consider that this method determines an equivalent flat plate cascade for any arbitrary cascade. The performance of a cascade of flat plates is defined theoretically by two parameters K and θ_{4_0} . These quantities are determined in this method simply by making the measurements required to find τ and f_T.

This method has greater capability, however, than simply the determination of these two parameters. A point to point correspondence between blade profile and circle is obtained which permits determination of the local velocity ratio at any point on the blade profile.

In review, a method of cascade analysis has been developed. It was shown to be capable of predicting, with reasonable accuracy, the turning angles of perfect fluid flow across an arbitrary cascade. Because of the nature of the present conducting medium the accuracy seems somewhat poorer at large stagger angles but no limits of solidity or camber are known to exist. The time required to accomplish the procedure is short enough to make the method suitable for engineering application. The method is not expensive.

Extension of the method to the analysis of radial and conical (mixed flow) cascades is analytical once the basic transformation of a rectilinear cascade has been achieved.

The method could be analytically supplemented to permit consideration of viscous conditions. Some estimate of compressibility effects could be made using the Prandtl-Glauert method.

The method of experimental conformal transformation used herein should be a valuable tool when applied to the many other engineering problems which are characterized by LaPlace's equation. Examples are problems in the theory of elasticity, in heat transfer, and in electric field theory.

8. CONCLUSIONS AND RECOMMENDATIONS

The principal conclusions of this investigation are:

The method herein described determines the ideal fluid flow, including turning angles and pressure distribution along the blades, for any two dimensional cascade. A practical technique, partly experimental and partly analytical, of conformally transforming an arbitrary cascade to a corresponding circle is provided as the basis of the method.

At its present state of development the method appears to determine turning angles to an overall accuracy of $\pm 1^{\circ}$, but further refinement can undoubtedly reduce this error.

The cascade analysis is accomplished in approximately one working day and at nominal expense.

No limitations in the method due to cascade geometry are known to exist.

For further refinement of the method it is recommend that:

A more nearly homogeneous and isotropic conducting medium be used.

Cascade layout and measurement procedures be mechanized.

9. REFERENCES AND BIBLIOGRAPHY

Ref. 1: Durand, William F.: Aerodynamic Theory, Vol. II, Div. E, Reprinted ed., 1943.

Ref. 2: Weinig, Fritz S.: Die Strömung um die Schaufeln von Turbomaschinen, Johann Ambrosius Barth (Leipzig) 1935 - English translation printed by Code 338, Research and Standards Branch, Bureau of Ships, Navy Department, May 1946.

Ref. 3: Collar, A. R.: The Flow of a Perfect Fluid through Cascades of Aerofoils. The Journal of the Royal Aeronautical Society, 1941, Vol. XLV, No. 365, pp 183-213.

Ref. 4: Tyler, R. A.: The Available Theoretical Analyses of Two-Dimensional Cascade Flow. National Research Council of Canada. Aero Note AN-4, 1949.

Ref. 5: Vazsonyi, Andrew: On the Aerodynamic Design of Axial Flow Compressors and Turbines. Journal of Applied Mechanics, 1948, Vol. 15, No. 1, pp 53-64.

Ref. 6: Weinig, Fritz S.: New Approach to the Theory of Thin, Slightly Cambered Profiles. Journal of Applied Mechanics, 1957, Vol. 24, No. 2, p 177.

Ref. 7: Mutterperl, William: A Solution to the Direct and Inverse Potential Problems for Arbitrary Cascades of Airfoils. NACA ARR L4K22b, Dec. 1944.

Ref. 8: Garrick, I. E.: On the Plane Potential Flow Past a Lattice of Arbitrary Airfoils. NACA Rep. No. 788, 1944.

Ref. 9: Herrig, L. Joseph; Emery, James C.; and Erwin, John R.: Systematic Two-Dimensional Cascade Tests of NACA 65-Series Compressor Blades at Low Speeds. NACA TN 3916, 1957.

Ref. 10: Bradfield, K. N. E., Hooker, S. G., and Southwell, R. B.: Conformal Transformation with the Aid of an Electrical Tank. Royal Society of London, Proceedings, 1937, Vol. 159 A, pp 315-346.

Ref. 11: Shepard, D. G.: Principles of Turbomachinery, 1956, 1st ed., The MacMillan Co., New York.

Ref. 12: Malavard, L.: The Technique of Electric Analogies. Centre National de Recherche Scientifique. Transl. by Begue, Joseph and Brower, W. B., Jr., Rensselaer Polytechnique Inst., Issued as Rep. No. OSR-TN-54-299. Contract AF 18(600)499.

Ref. 13: Brower, W. B., Jr.: The Application of the Electric Analogy to Two Dimensional Problems in Aeronautics. Rensselaer Polytechnic Inst. Rep. No. TR AE 5406, 1953. Contract AF 18(600)499.

Bibliography of material used as background but not referred to specifically in the text.

Streeter, Victor L.: Fluid Dynamics, 1948, 1st ed., McGraw-Hill Book Company, Inc.

Glauert, H.: Airfoil and Airscrew Theory, 1926, reprinted 1943, 1st ed., The Macmillan Company, New York.

Dwinnel, J. H.: Principles of Aerodynamics, 1949, 1st ed., McGraw-Hill Book Company, Inc.

Vavra, M. H.: Lecture Notes from Course in Gas Turbines, U. S. Naval Postgraduate School, Monterey, California.

Karo, D.: Electrical Measurements and the Calculation of the Errors involved, Part I, 1950, MacDonald and Company, Ltd., London.

DeLella, Amelia, compiler,: Five Place Table of Natural Trigonometric Functions to Hundredths of a Degree, 1934, John Wiley and Sons, Inc., New York.

Lamb, Sir Horace: Hydrodynamics, 1932, 6th ed., reprint, 1945, Dover Publications, New York.

TABLE 1

INSTRUMENTS

1. Potential supply - Heathkit Battery Eliminator, Model BE-4.

2. Null meter - General Electric DC Micro Ammeter, Type DO-71, Model A29AA1, coil resistance of 1700 ohms, detecting sensitivity power on the order of 8 micro-micro watts.

3. Voltage divider - Electro-Measurements Inc. Dekavider, Model RV622, linearity of $\pm$0.0025 percent, input resistance of 10,000 ohms, Serial 13,049.

4. Potentiometer - Leeds and Northrup Portable Precision Potentiometer, Number 8662, Serial 1318768.

5. Voltmeter - Weston DC Voltmeter, Model 45, Serial 49400.

TABLE II

AIRFOIL ORDINATES FROM NACA ARR. NO. L4K22b

(Stations and ordinates in percent of airfoil chord)

Upper surface		Lower surface	
Station	Ordinate	Station	Ordinate
0	0	0	0
.23	.97	.77	-.43
.44	1.24	1.06	-.44
.88	1.66	1.62	-.46
2.03	2.63	2.97	-.37
4.43	4.17	5.57	-.13
6.87	5.44	8.13	.18
9.34	6.56	10.66	.48
14.34	8.46	15.66	1.08
19.38	9.98	20.62	1.64
24.44	11.24	25.56	2.16
29.55	12.20	30.45	2.60
34.64	12.90	35.36	2.96
39.72	13.39	40.28	3.29
44.82	13.64	45.18	3.58
49.96	13.65	50.04	3.91
55.07	13.37	54.93	4.23
60.17	12.78	59.83	4.48
65.26	11.92	64.74	4.68
70.30	10.81	69.70	4.77
75.32	9.53	74.68	4.67
80.29	8.04	79.71	4.39
85.23	6.40	84.77	3.94
90.17	4.56	89.83	3.10
95.10	2.57	94.90	1.89
100	0	100	0

TABLE III

ORDINATES FOR NACA 65-010 BASIC THICKNESS FORMS

(Stations and ordinates in percent of chord)

Station, x	Ordinates, ±y
	65(216)-010 airfoil combined with y = 0.0015x
0	0
.5	.752
.75	.890
1.25	1.124
2.5	1.571
5.0	2.222
7.5	2.709
10	3.111
15	3.746
20	4.218
25	4.570
30	4.824
35	4.982
40	5.057
45	5.029
50	4.870
55	4.570
60	4.151
65	3.627
70	3.038
75	2.451
80	1.847
85	1.251
90	.749
95	.354
100	.150
L.E. radius	.666

TABLE IV

COORDINATES OF 6" and 12" NACA ARR NO. L4K22b AIRFOILS

6" Chord (Stations and ordinates in inches)

Upper surface		Lower surface	
Station, x	Ordinate, y	Station, x	Ordinate, y
0	0	0	0
.0138	.0582	.0462	-.0258
.0264	.0744	.0636	-.0264
.0528	.0996	.0972	-.0276
.1218	.1578	.1782	-.0222
.2658	.2502	.3342	-.0078
.4122	.3264	.4878	+.0108
.5604	.3936	.6396	.0288
.8604	.5076	.9396	.0648
1.1628	.5988	1.2372	.0984
1.4664	.6744	1.5336	.1296
1.7730	.7320	1.8270	.1560
2.0784	.7740	2.1216	.1776
2.3832	.8034	2.4168	.1974
2.6892	.8184	2.7108	.2148
2.9976	.8190	3.0024	.2346
3.3042	.8022	3.2958	.2538
3.6102	.7668	3.5898	.2688
3.9156	.7152	3.8844	.2808
4.2180	.6486	4.1820	.2862
4.5192	.5718	4.4808	.2802
4.8174	.4824	4.7826	.2634
5.1138	.3840	5.0862	.2364
5.4102	.2736	5.3898	.1860
5.7060	.1542	5.6940	.1134
6.0000	0	6.0000	0

TABLE IV (Cont.)

12" Chord (Stations and ordinates in inches)

Upper surface		Lower surface	
Station, x	Ordinate, y	Station, x	Ordinate, y
0	0	0	0
.0276	.1164	.0924	-.0516
.0528	.1488	.1272	-.0528
.1056	.1992	.1944	-.0552
.2436	.3156	.3564	-.0444
.5316	.5004	.6684	-.0156
.8244	.6528	.9756	+.0216
1.1208	.7872	1.2792	.0576
1.7208	1.0152	1.8792	.1296
2.3256	1.1976	2.4744	.1968
2.9328	1.3488	3.0672	.2592
3.5460	1.4640	3.6540	.3120
4.1568	1.5480	4.2432	.3552
4.7664	1.6068	4.8336	.3948
5.3784	1.6368	5.4216	.4296
5.9952	1.6380	6.0048	.4692
6.6084	1.6044	6.5916	.5076
7.2204	1.5336	7.1796	.5376
7.8312	1.4304	7.7688	.5616
8.4360	1.2972	8.3640	.5724
9.0384	1.1436	8.9616	.5604
9.6348	.9648	9.5652	.5268
10.2276	.7680	10.1724	.4728
10.8204	.5472	10.7796	.3720
11.4120	.3084	11.3880	.2268
12.0000	0	12.0000	0

TABLE V

COORDINATES OF 6" and 12" NACA 65-(15)10 AIRFOILS

6" Chord (Stations and ordinates in inches)

Upper surface		Lower surface	
Station, x	Ordinate, y	Station, x	Ordinate, y
0	0	0	0
.0059	.0606	.0541	-.0156
.0181	.0776	.0719	-.0146
.0438	.1079	.1062	-.0116
.1122	.1701	.1878	-.0027
.2558	.2680	.3442	+.0164
.4033	.3465	.4967	.0351
.5526	.4132	.6474	.0521
.8544	.5229	.9456	.0828
1.1587	.6079	1.2413	.1085
1.4643	.6746	1.5356	.1309
1.7709	.7254	1.8291	.1494
2.0780	.7603	2.1220	.1667
2.3853	.7850	2.4147	.1789
2.6934	.7944	2.7672	.1911
3.0000	.7886	3.0000	.2042
3.3066	.7669	3.2934	.2186
3.6120	.7307	3.5880	.2332
3.9160	.6796	3.8840	.2474
4.2184	.6188	4.1816	.2560
4.5191	.5486	4.4809	.2569
4.8181	.4675	4.7819	.2489
5.1152	.3763	5.0848	.2294
5.4114	.2761	5.3886	.1892
5.7070	.1622	5.6930	.1222
6.0000	.0090	6.0000	-.0090

LEADING EDGE RADIUS = .03996 inches

TABLE V (Cont.)

12" Chord (Stations and ordinates in inches)

Upper surface		Lower surface	
Station, x	Ordinate, y	Station, x	Ordinate, y
0	0	0	0
.0118	.1213	.1082	-.0313
.0362	.1553	.1438	-.0293
.0876	.2159	.2124	-.0233
.2245	.3401	.3755	-.0053
.5116	.5359	.6884	+.0328
.8066	.6930	.9934	.0702
1.1053	.8264	1.2947	.1042
1.7088	1.0459	1.8911	.1655
2.3174	1.2158	2.4826	.2172
2.9287	1.3492	3.0713	.2618
3.5417	1.4507	3.6583	.2989
4.1559	1.5206	4.2440	.3334
4.7707	1.5700	4.8293	.3578
5.3868	1.5888	5.5344	.3822
6.0000	1.5771	6.0000	.4083
6.6131	1.5337	6.5868	.4373
7.2241	1.4614	7.1759	.4664
7.8321	1.3592	7.7679	.4949
8.4367	1.2375	8.3633	.5121
9.0382	1.0971	8.9618	.5139
9.6362	.9351	9.5638	.4977
10.2304	.7527	10.1696	.4587
10.8228	.5522	10.7772	.3784
11.4141	.3245	11.3859	.2443
12.0000	.0180	12.0000	-.0180

LEADING EDGE RADIUS = .07992 inches

TABLE VI

TEST PROGRAM

A. Turning Angles:

1. First series:

Profile - Mutterperl (NACA ARR No. L4K22b)
Tests (a) $\beta = 45^{\circ}$; $\sigma = 1.0$
(b) $\beta = 45^{\circ}$; $\sigma = 1.5$

2. Second series:

Profile - NACA 65-(15)10
Tests - Group one (six inch chord)
(a) $\beta = 20^{\circ}$; $\sigma = 1.0$
(b) $\beta = 25^{\circ}$; $\sigma = 1.0$
(c) $\beta = 30^{\circ}$; $\sigma = 1.0$
(d) $\beta = 35^{\circ}$; $\sigma = 1.0$

Group two
(a) $\beta = 20^{\circ}$; $\sigma = 1.5$ (twleve inch chord)
(b) $\beta = 25^{\circ}$; $\sigma = 1.5$ (six inch chord)
(c) $\beta = 30^{\circ}$; $\sigma = 1.5$ (twelve inch chord)
(d) $\beta = 35^{\circ}$; $\sigma = 1.5$ (twelve inch chord)

B. Velocity Distribution:

Profile - NACA 65-(15)10 (twelve inch chord)
Test - $\beta = 35^{\circ}$; $\sigma = 1.5$

TABLE VII

SAMPLE DATA FOR TURNING ANGLE DETERMINATION

Station	Upper Surface $\mathcal{E}$ (Percent)
3b	71.88
c	71.88
d	71.89
4	71.90
4a	71.89
b	71.88
46	34.91
a	34.70
b	34.47
c	34.26
d	34.00
47	33.77
a	33.52
b	33.28
c	33.01
d	32.76
48	32.50
a	32.20
b	31.93
c	31.59
d	31.24
49	30.68
Center Tail	30.52

Station	Lower Surface $\mathcal{E}$ (Percent)
46	30.69
a	30.61
b	30.55
c	30.49
d	30.42
47	30.37
a	30.29
b	30.24
c	30.18
d	30.12
48	30.08
a	30.03
b	30.01
c	29.99
d	30.00
49	30.18

$\left(\frac{\partial \mathcal{E}}{\partial x}\right)_{\infty}$:

Station	$\mathcal{E}$ (Percent)
0	98.53
1	95.74
2	92.97
3	90.24
4	87.58
5	84.84

TABLE VIII

SAMPLE DATA AND INPUT VALUES FOR DETERMINATION OF VELOCITY RATIOS

Percent Chord From L.E.	Upper Surface $\mathcal{E}$ (Percent)	Upper Surface ΔE (Volts)	Upper Surface $\frac{\Delta E}{\Delta \mathcal{E}}$ (Percent)	Lower Surface $\mathcal{E}$ (Percent)	Lower Surface ΔE (Volts)	Lower Surface $\frac{\Delta E}{\Delta \mathcal{E}}$ (Percent)
0	68.38	67.84	14.17			
2.08	71.31	10.22	2.353	65.30	34.86	7.983
4.17	71.75	3.58	0.824	63.67	29.33	6.752
6.25	71.85	-	-	62.22	27.45	6.319
8.33	71.75	2.57	0.592	61.00	22.97	5.288
10.42	71.53	4.77	1.098	59.85	21.70	4.995
12.50	71.23	6.06	1.395	58.74	19.71	4.537
16.67	70.40	8.91	2.051	56.71	19.29	4.441
20.83	69.29	10.69	2.461	54.65	18.75	4.316
25.00	67.99	13.14	3.025	52.81	18.70	4.305
29.17	66.51	13.93	3.207	51.00	16.30	3.752
33.33	64.88	15.76	3.628	49.26	16.23	3.736
37.50	63.06	18.23	4.197	47.56	15.75	3.626
41.67	61.21	18.43	4.243	45.95	16.25	3.741
45.83	59.18	18.73	4.312	44.34	15.77	3.630
50.00	57.15	20.31	4.675	42.74	15.77	3.630
54.17	55.06	20.12	4.632	41.22	14.70	3.384
58.33	52.98	19.64	4.521	39.81	13.15	3.027
62.50	50.87	19.53	4.496	38.44	13.08	3.011
66.67	48.81	18.30	4.213	37.14	12.17	2.802
70.83	46.68	18.98	4.369	35.94	11.25	2.590
75.00	44.57	19.40	4.466	34.79	11.54	2.657
79.17	42.52	18.45	4.247	33.72	10.00	2.302
83.33	40.39	18.34	4.222	32.77	9.22	2.122
87.50	38.23	19.31	4.445	31.89	8.21	1.890
91.67	36.10	20.55	4.731	31.05	6.80	1.565
93.75	34.91	20.02	4.609	30.69	5.94	1.367
95.83	33.97	19.85	4.570	30.37	5.35	1.232
97.92	32.50	20.70	4.765	30.08	3.71	0.854

$\Delta \mathcal{E}$ = .0405 inches

TABLE IX

INPUT VALUES FOR DETERMINATION OF TURNING ANGLES

σ	β Degrees	ε_1 Percent	ε_2 Percent	ε_T Percent	$-\frac{\partial \varepsilon}{\partial x}$ Percent	s Inches
			MUTTERPERL AIRFOIL			
1.0	45	61.86	39.42	40.29	2.870	6.00
1.5	45	62.61	38.02	38.54	2.825	4.00
			NACA 65-(15)10			
1.0	20	61.65	40.54	40.63	3.060	6.00
1.0	25	61.14	40.32	40.50	3.072	6.00
1.0	30	62.14	39.01	39.30	3.259	6.00
1.0	35	62.34	40.82	41.26	2.882	6.00
1.5	20	71.38	30.26	30.36	2.943	8.00
1.5	25	61.63	39.70	39.83	3.019	4.00
1.5	30	72.26	30.03	30.44	2.761	8.00
1.5	35	71.90	29.99	30.49	2.761	8.00

TABLE X

SENSITIVITY OF RESULTS TO VARIATION OF INPUT VALUES

Quantity	Value	ΔQuantity	$\frac{\Delta \text{Quantity}}{\text{Quantity}}$	$\Delta\Theta$ at $\alpha_m = 35^\circ$	$\Delta\Theta$ at $\alpha_m = 60^\circ$
$\mathcal{E}_1$	62.91	+6	.001	$+ .012^\circ$	$+.026^\circ$
$\mathcal{E}_2$	38.58	+4	.001	$+1.105^\circ$	$+.641^\circ$
$\mathcal{E}_T$	39.68	+4	.001	-1.104°	$-.647^\circ$
$-\frac{\partial \mathcal{E}}{\partial x}$	30.80	+3	.001	$+ .029^\circ$	$+.016^\circ$

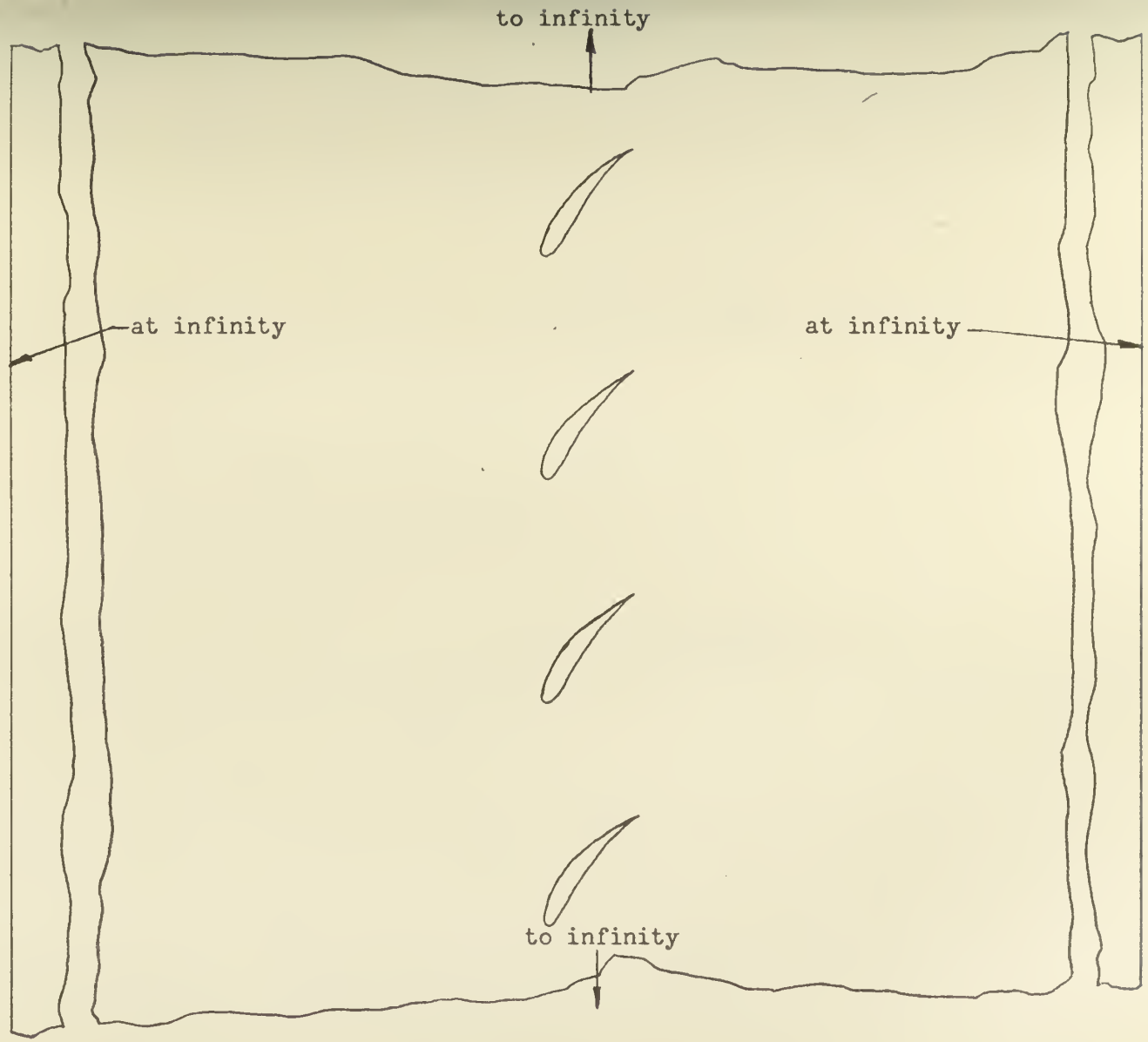

Figure 1 - Conducting Sheet of Infinite Extent in Two Dimensions

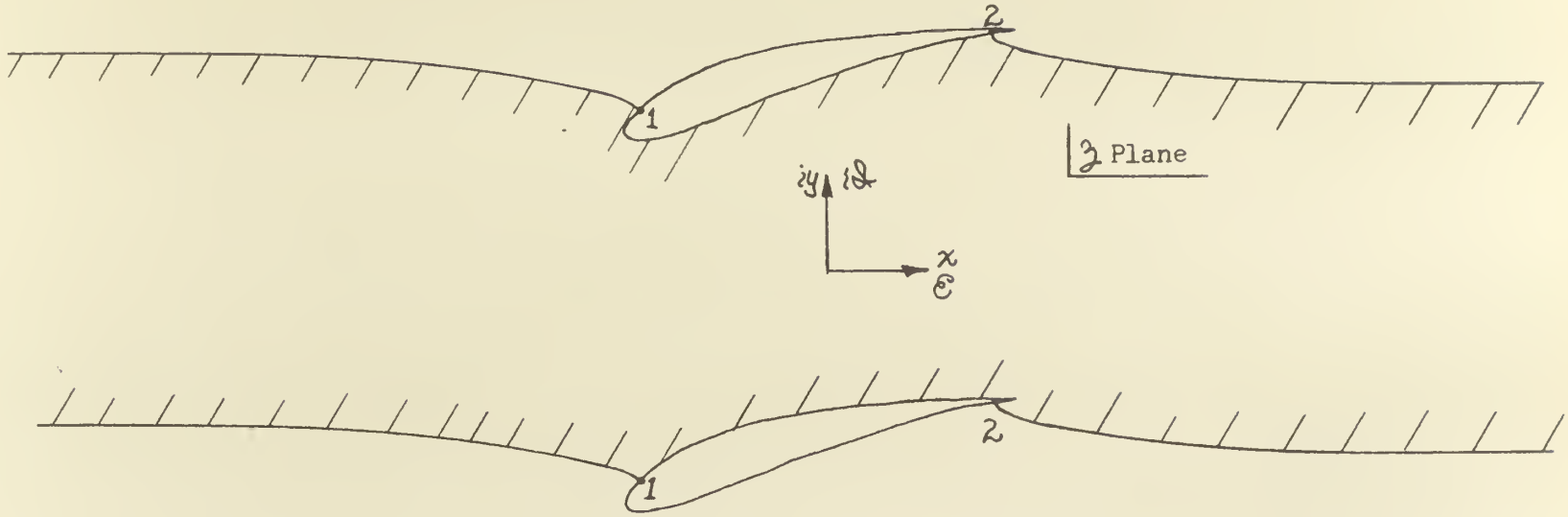

Figure 2 - Single Strip from Infinite Cascade

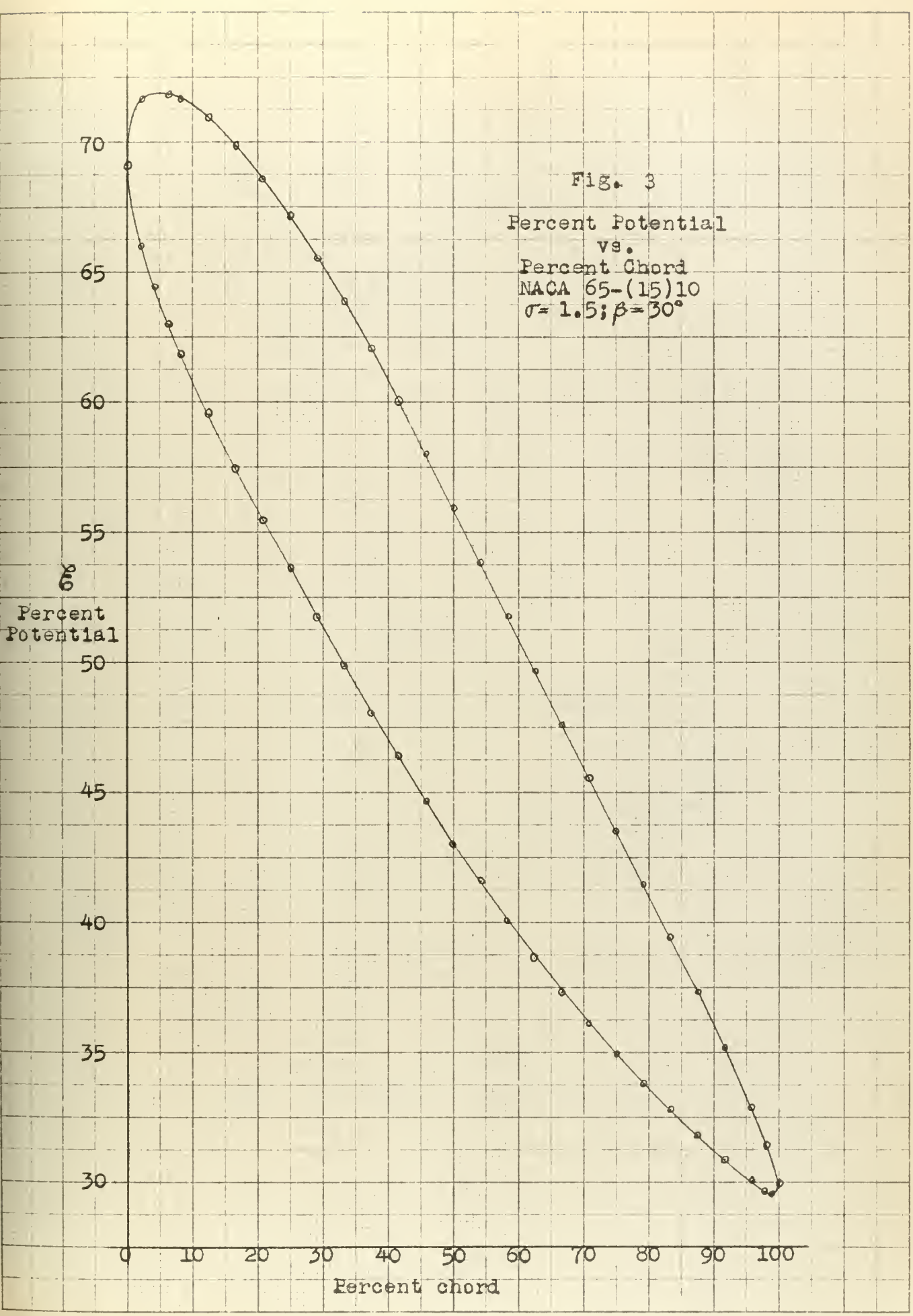
Fig. 3
Percent Potential
vs.
Percent Chord
NACA 65-(15)10
σ= 1.5; β=30°
70
65
60
55
50
45
40
35
30
Percent Potential
0
10
20
30
40
50
60
70
80
90
100
Percent chord

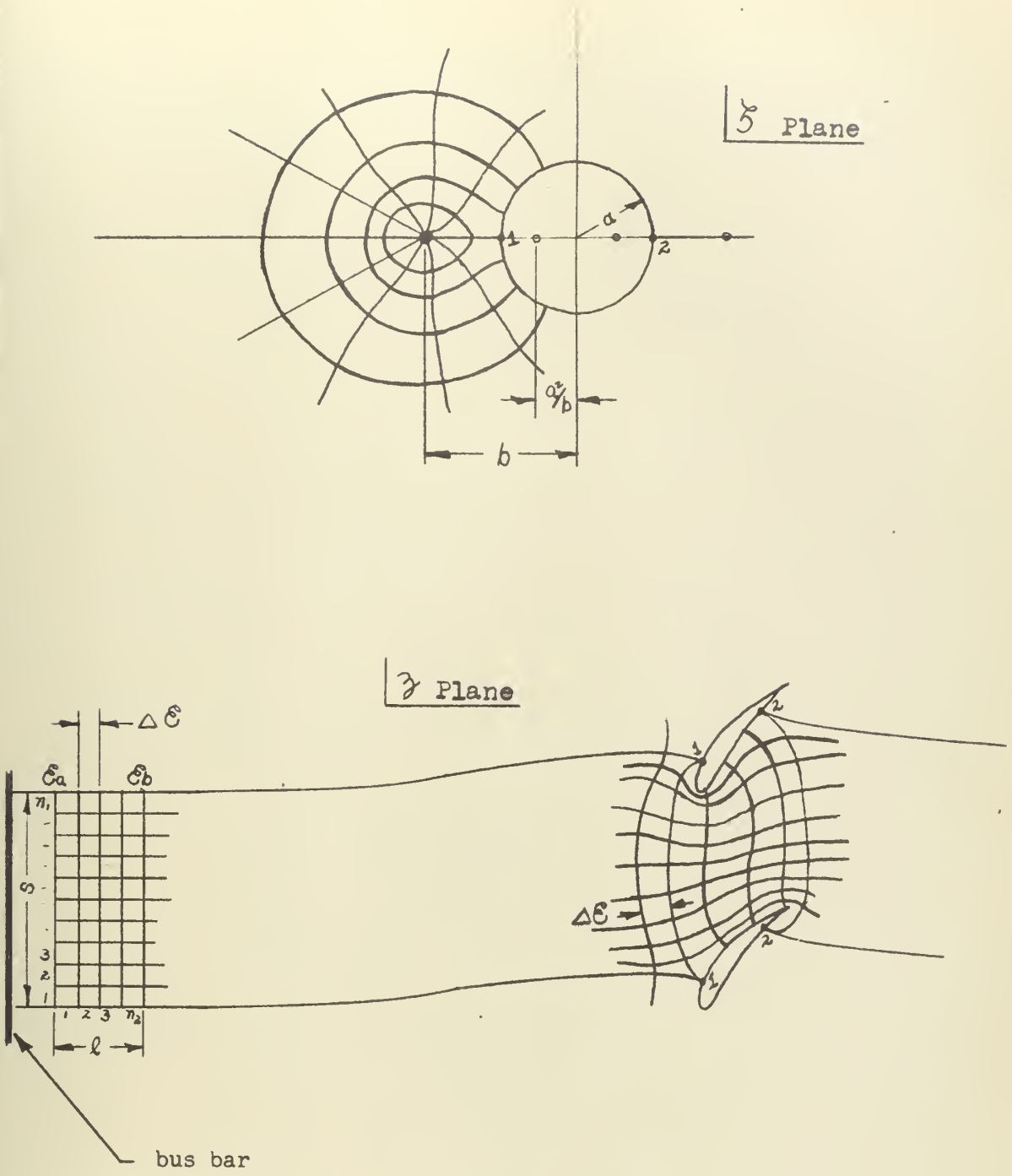

Figure 4 - Transformations Between The Real and Picture Planes

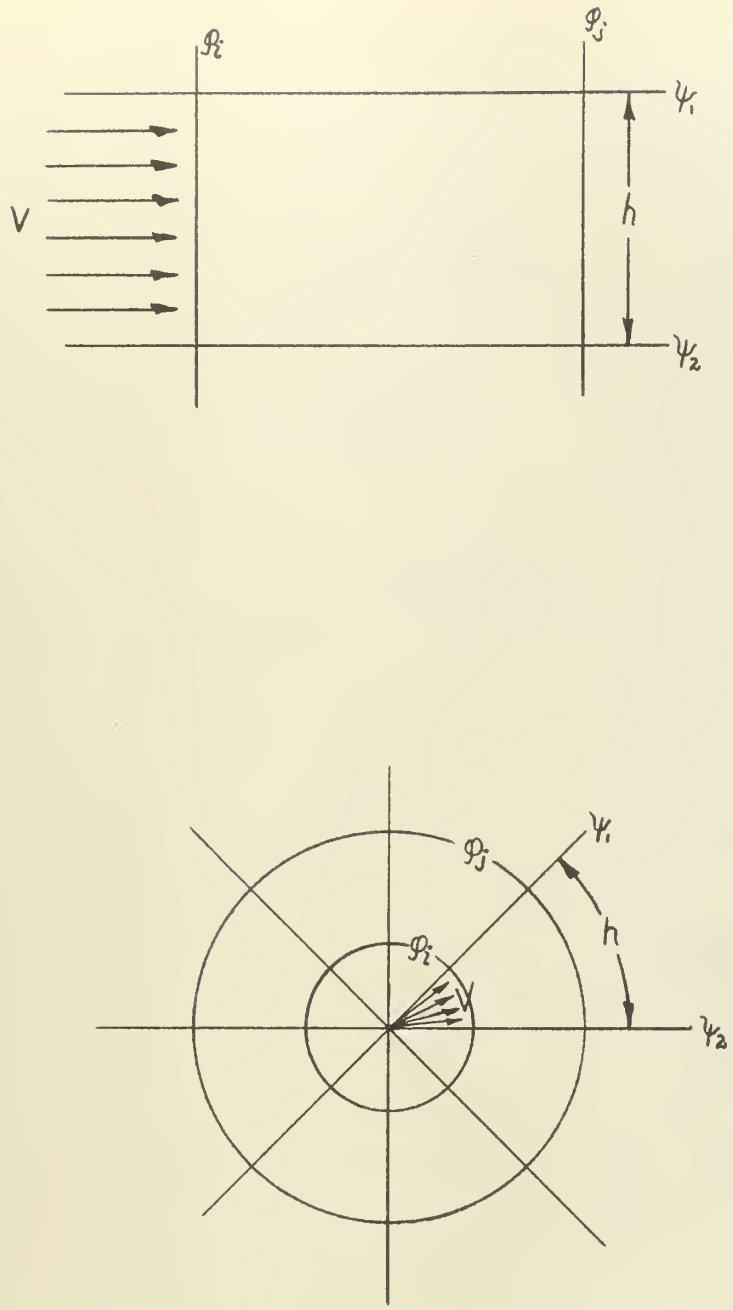

Figure 5 -Simple Two Dimensional Flows

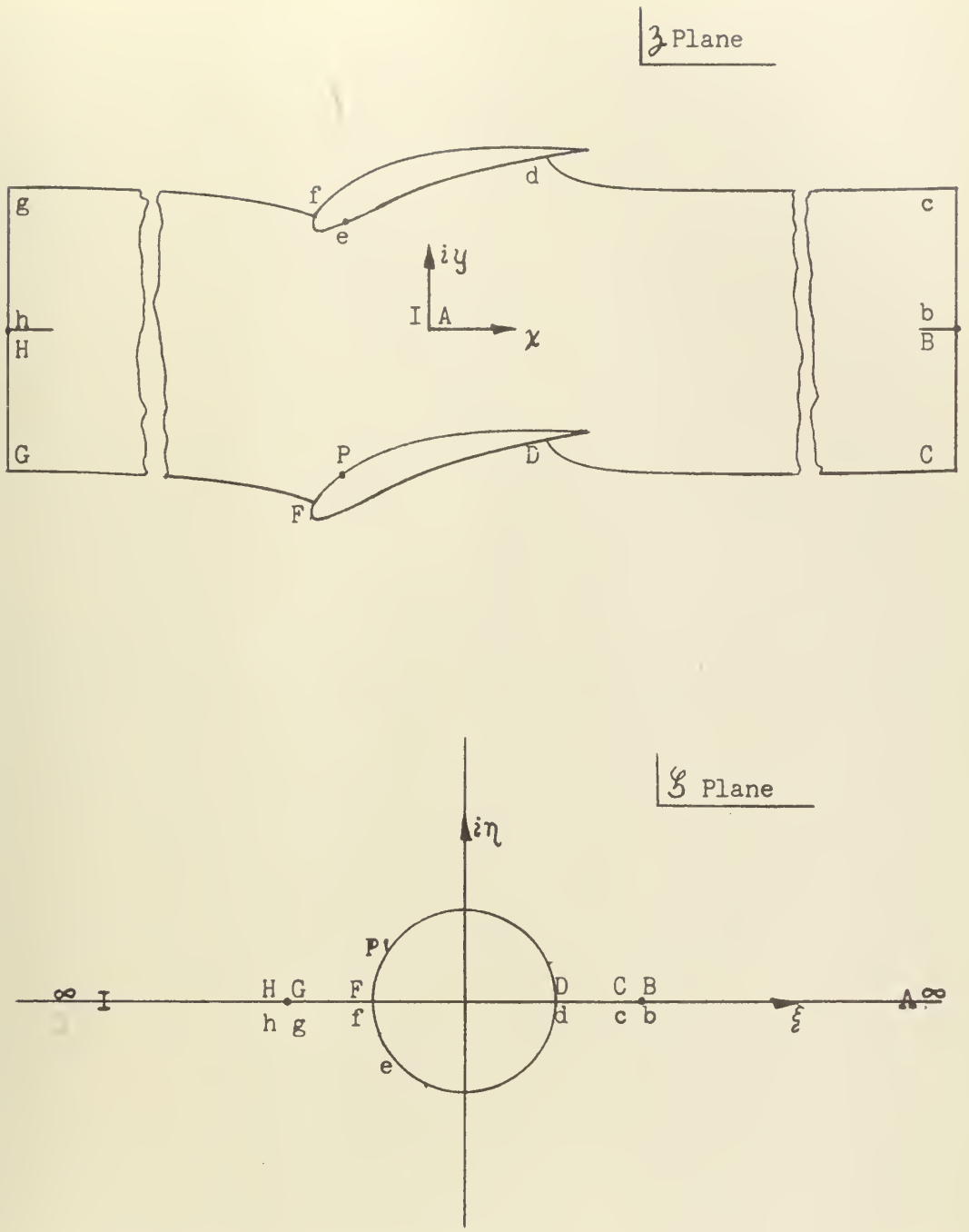

Figure 6 -Correspondence Between The Real and Picture Planes

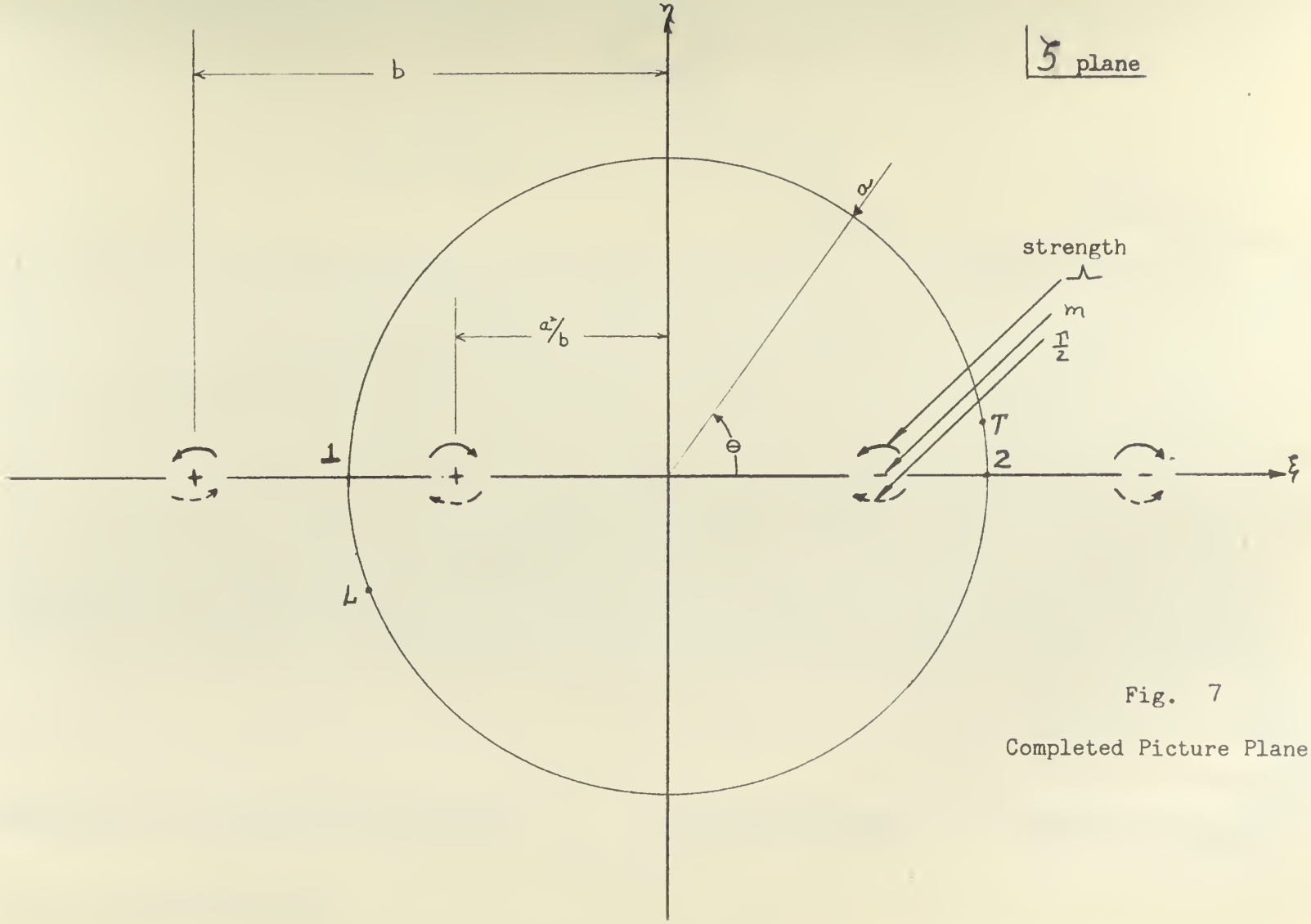

Fig. 7

Completed Picture Plane

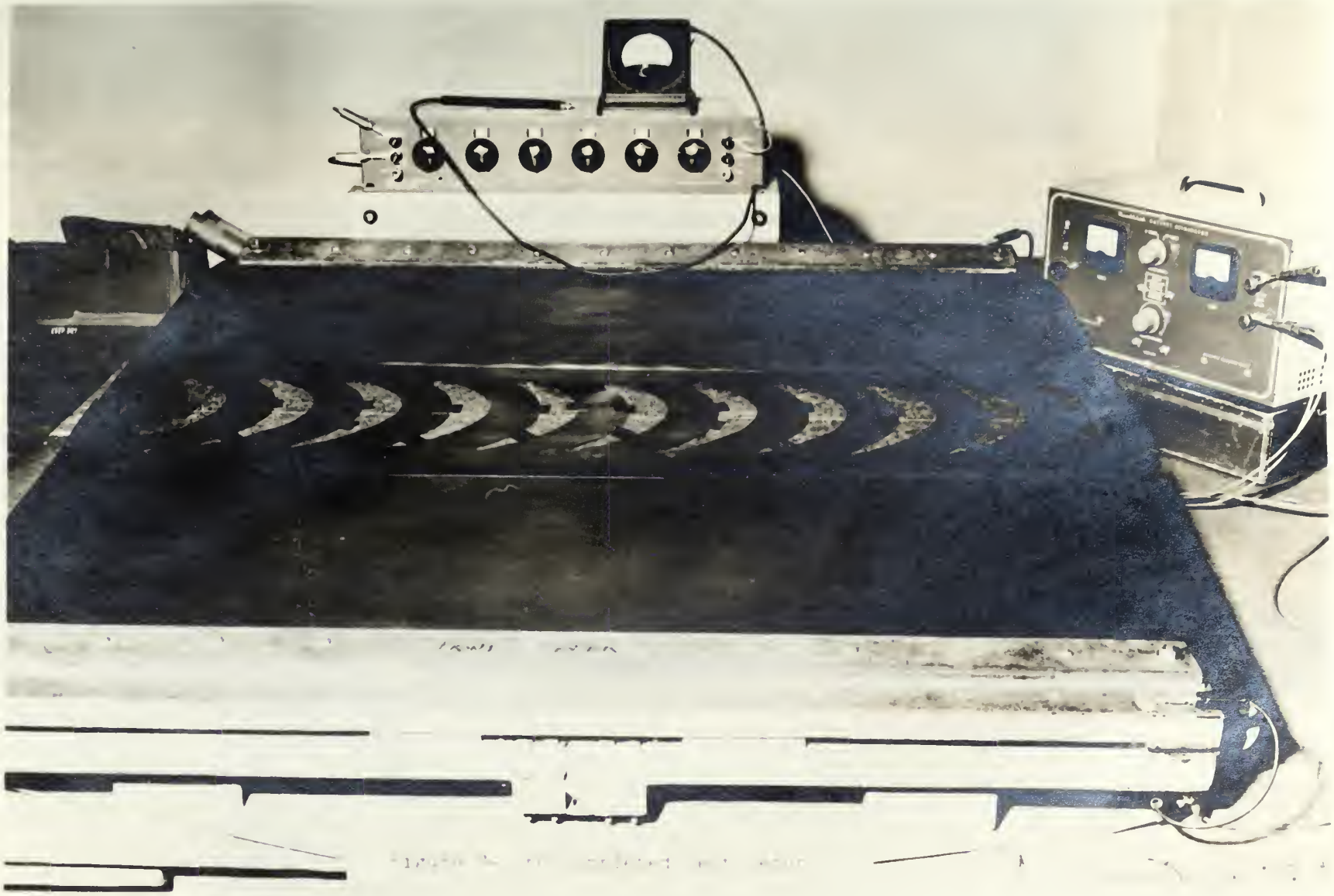

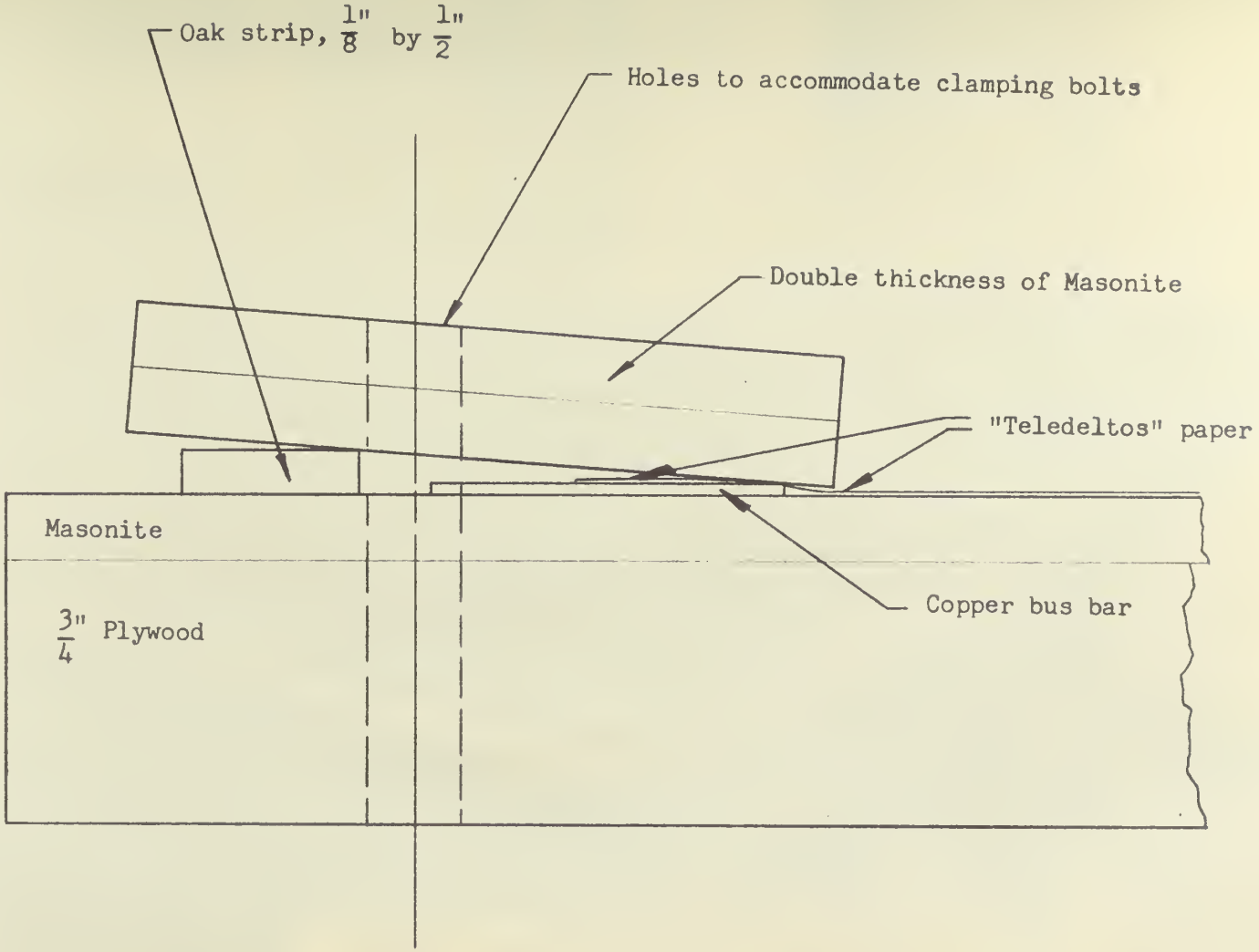

Figure 10.- Cross section through the paper clamping device.

Figure 11- The Folding Table Without Paper

Figure 12- The Folding Table With Paper

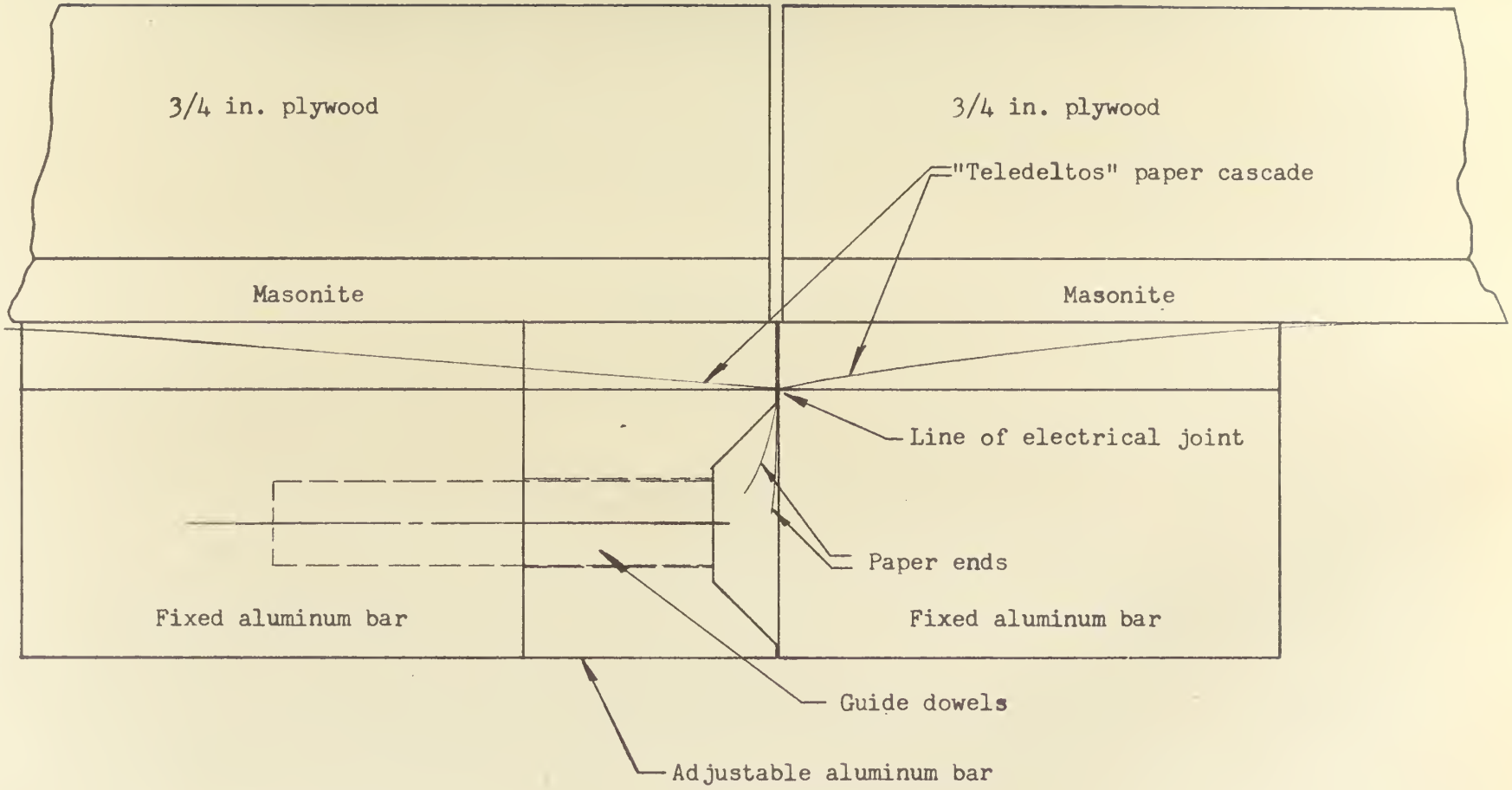

Figure 13.—Cross section through electrical joining device.

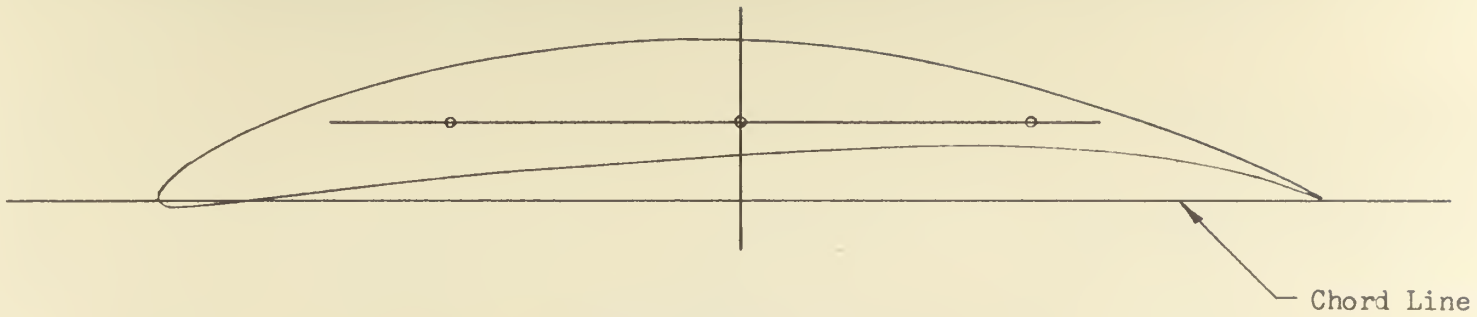

Mutterperl Profile

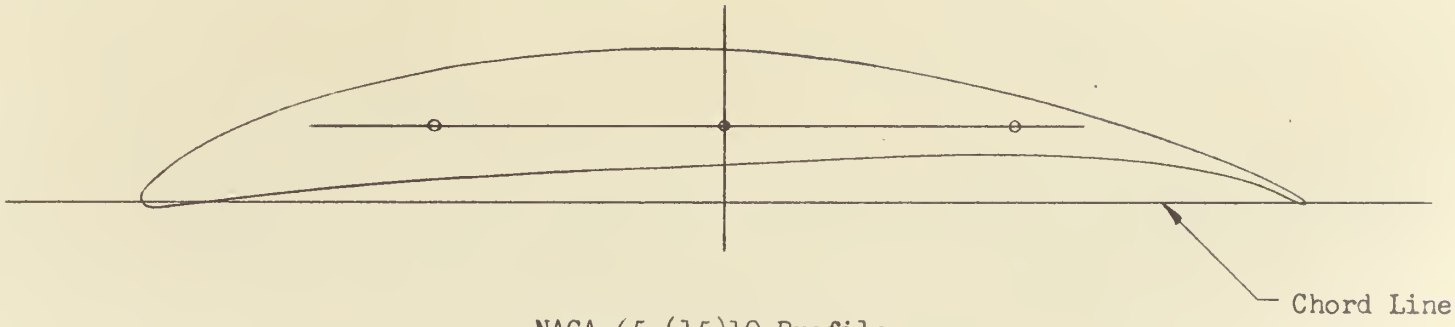

NACA 65-(15)10 Profile

Figure14.- Compressor blade sections.

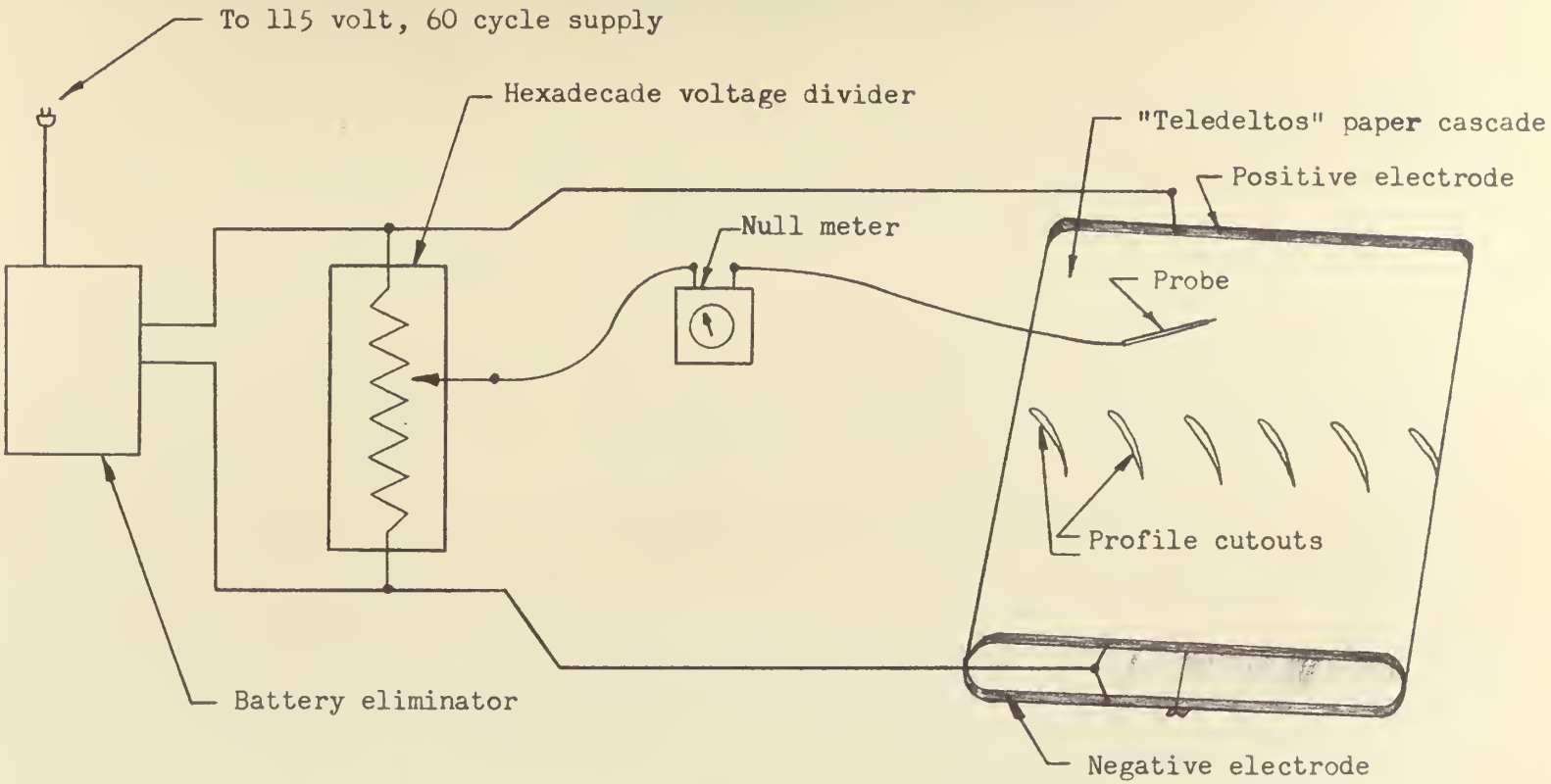

Figure 15 .-Circuit schematic for potential data.

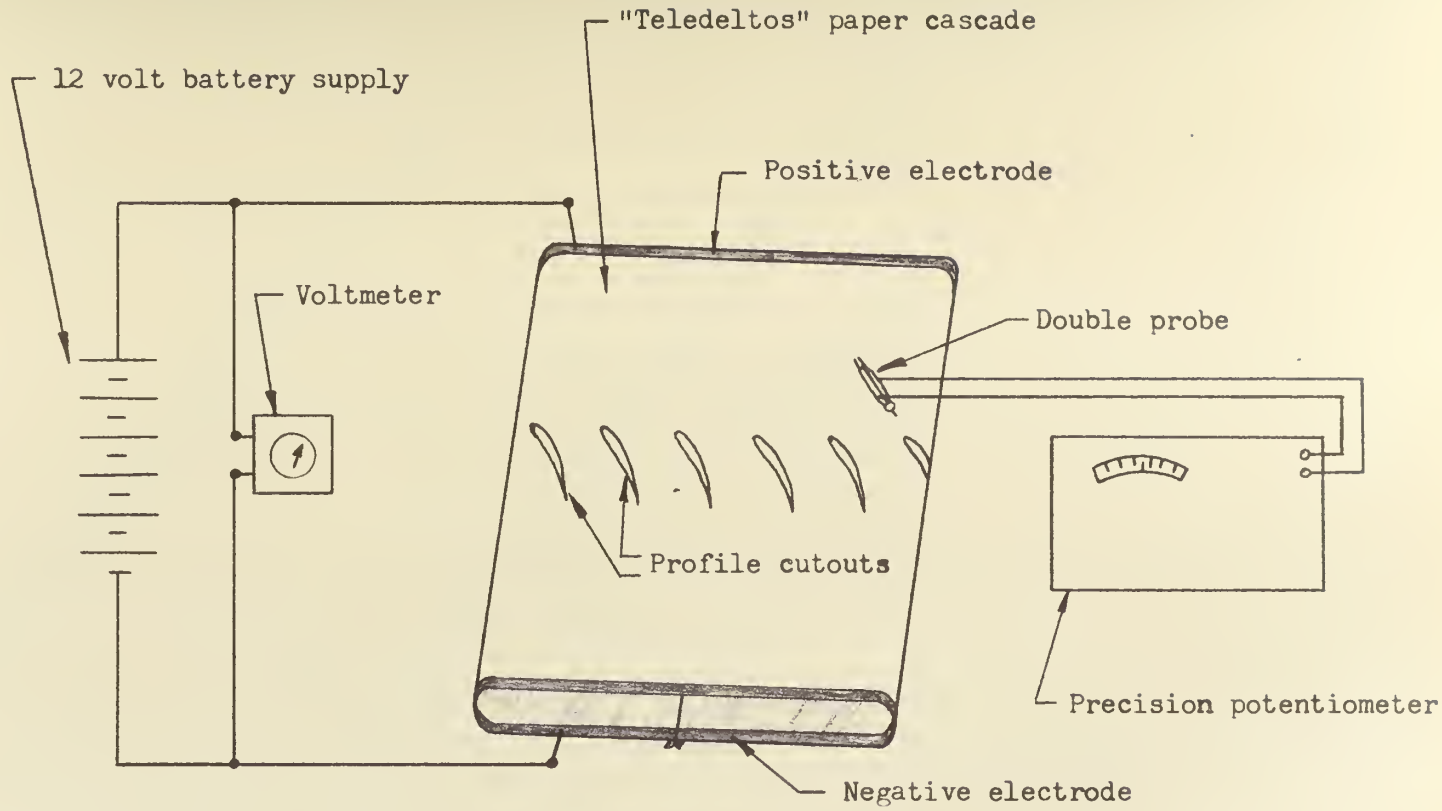

Figure 16.-Circuit schematic for derivative data.

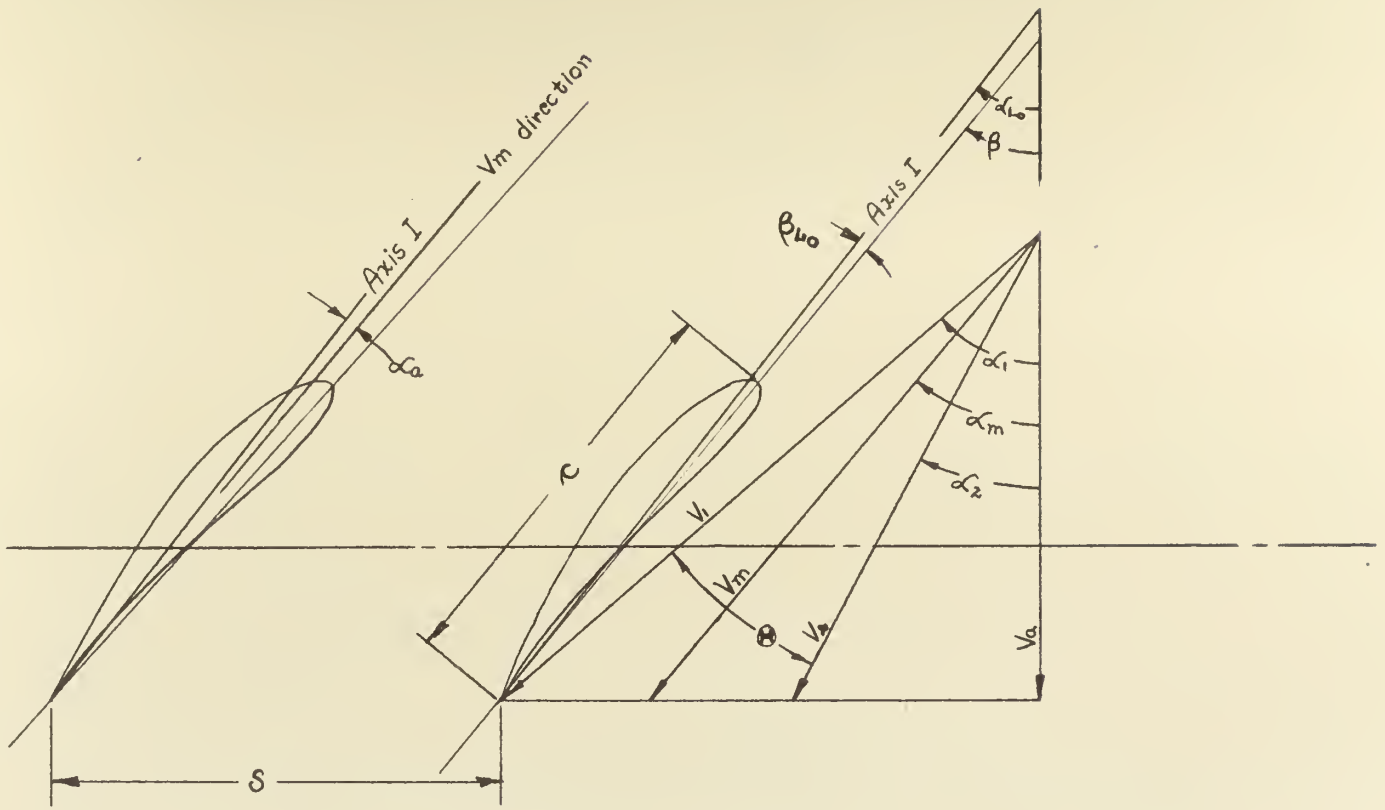

Figure 17 - Typical Velocity Vector Diagram

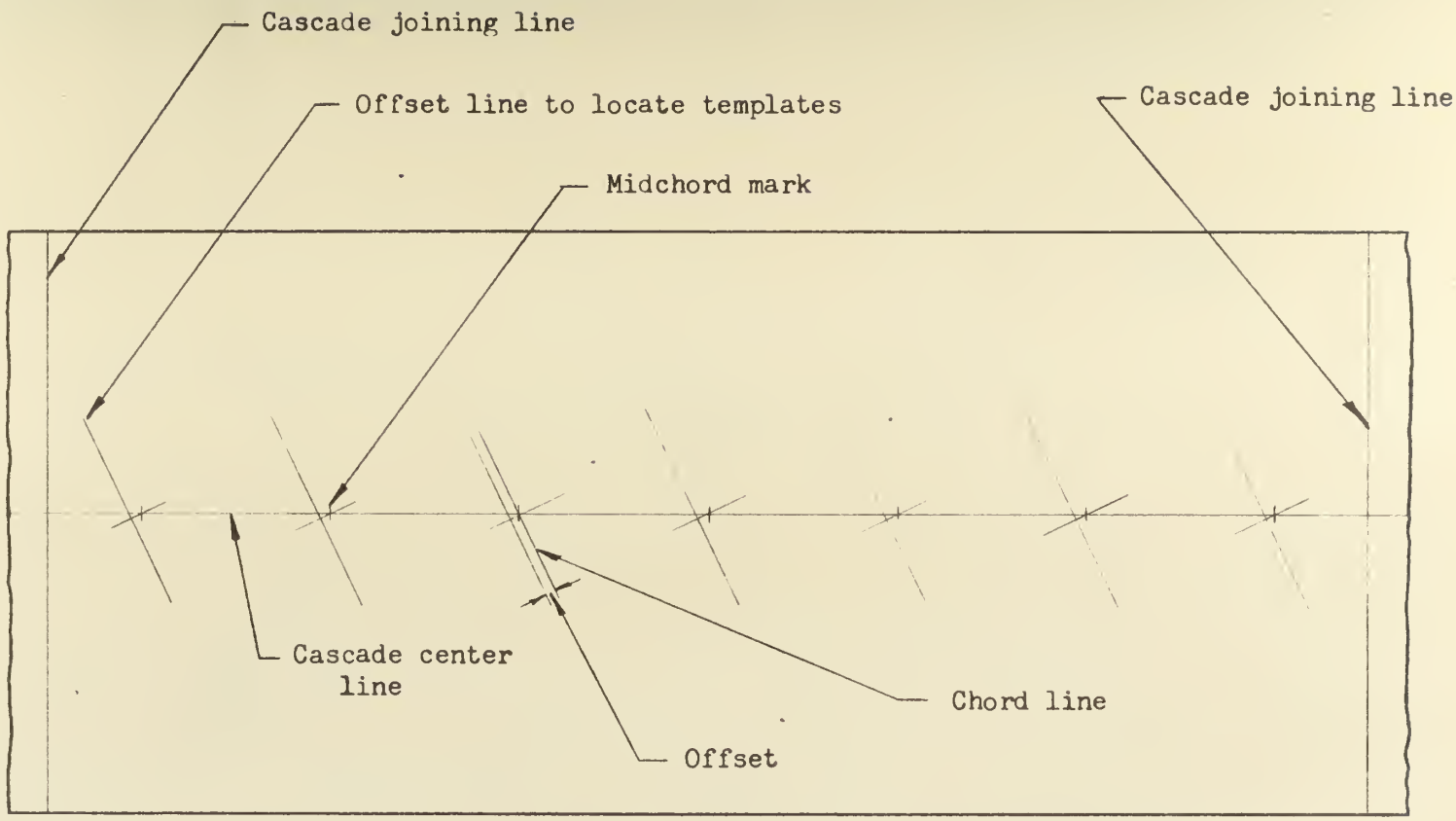

Figure 18.- Cascade layout lines.

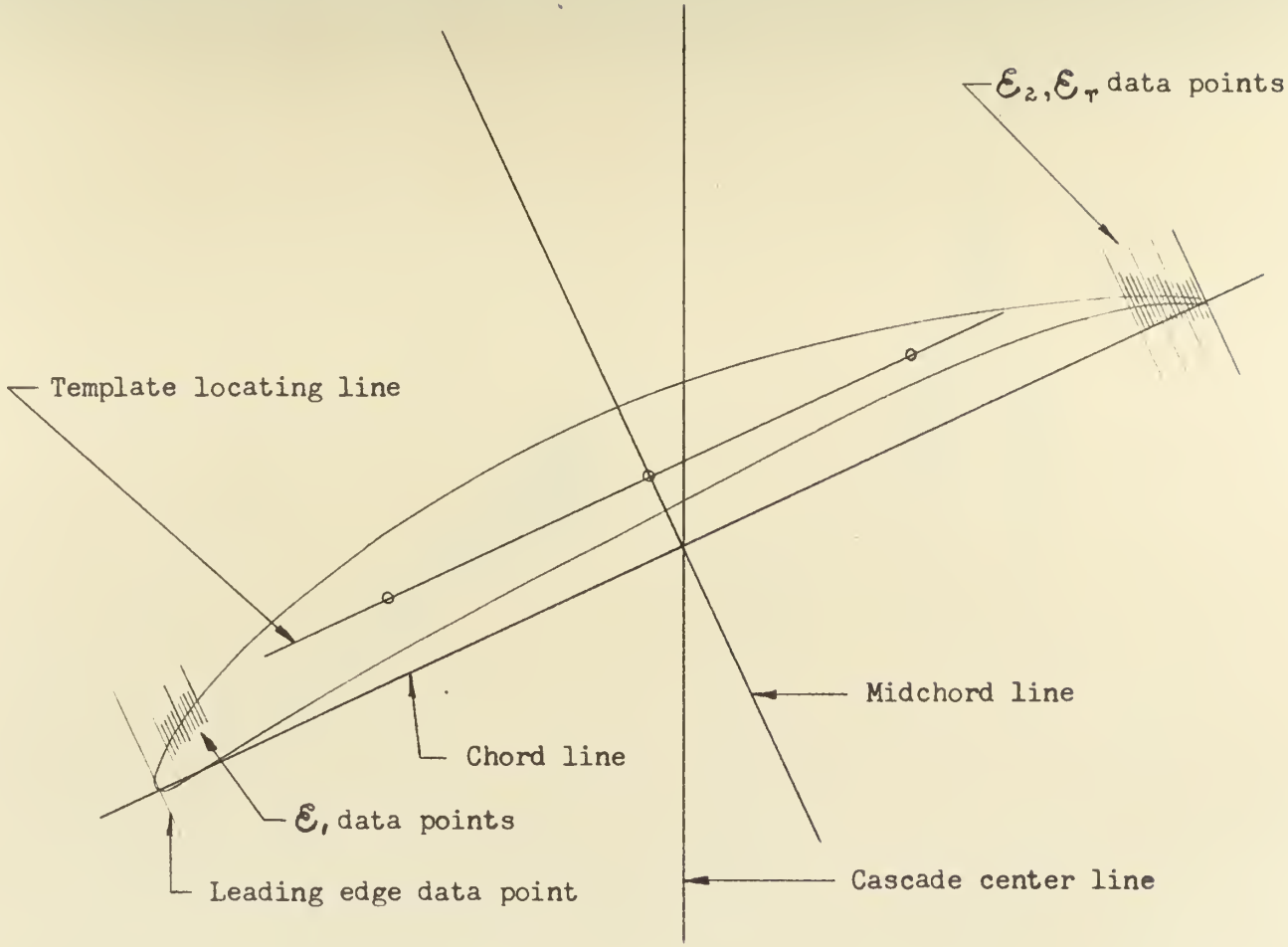

Figure 19.- Layout lines for the NACA 65-(15)10 template.

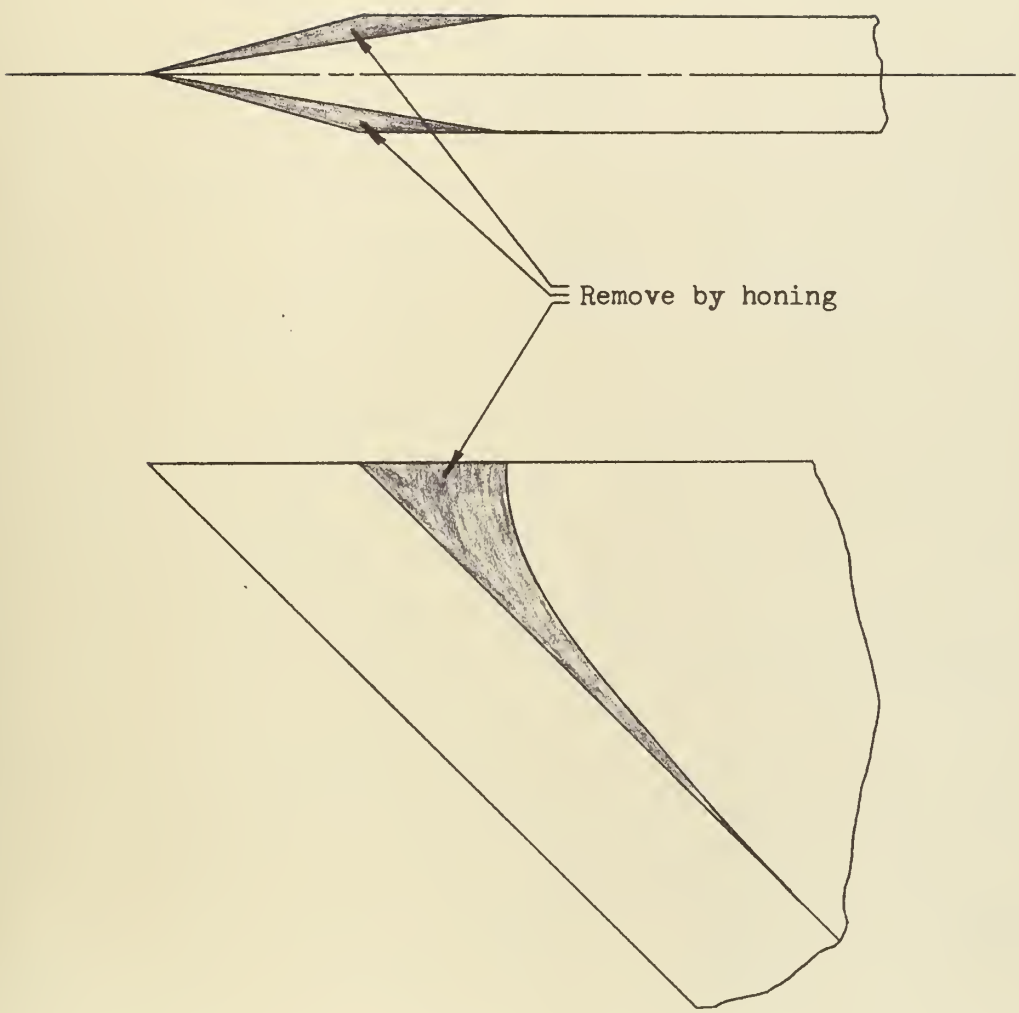

Figure 20.- Cutting knife modifications.

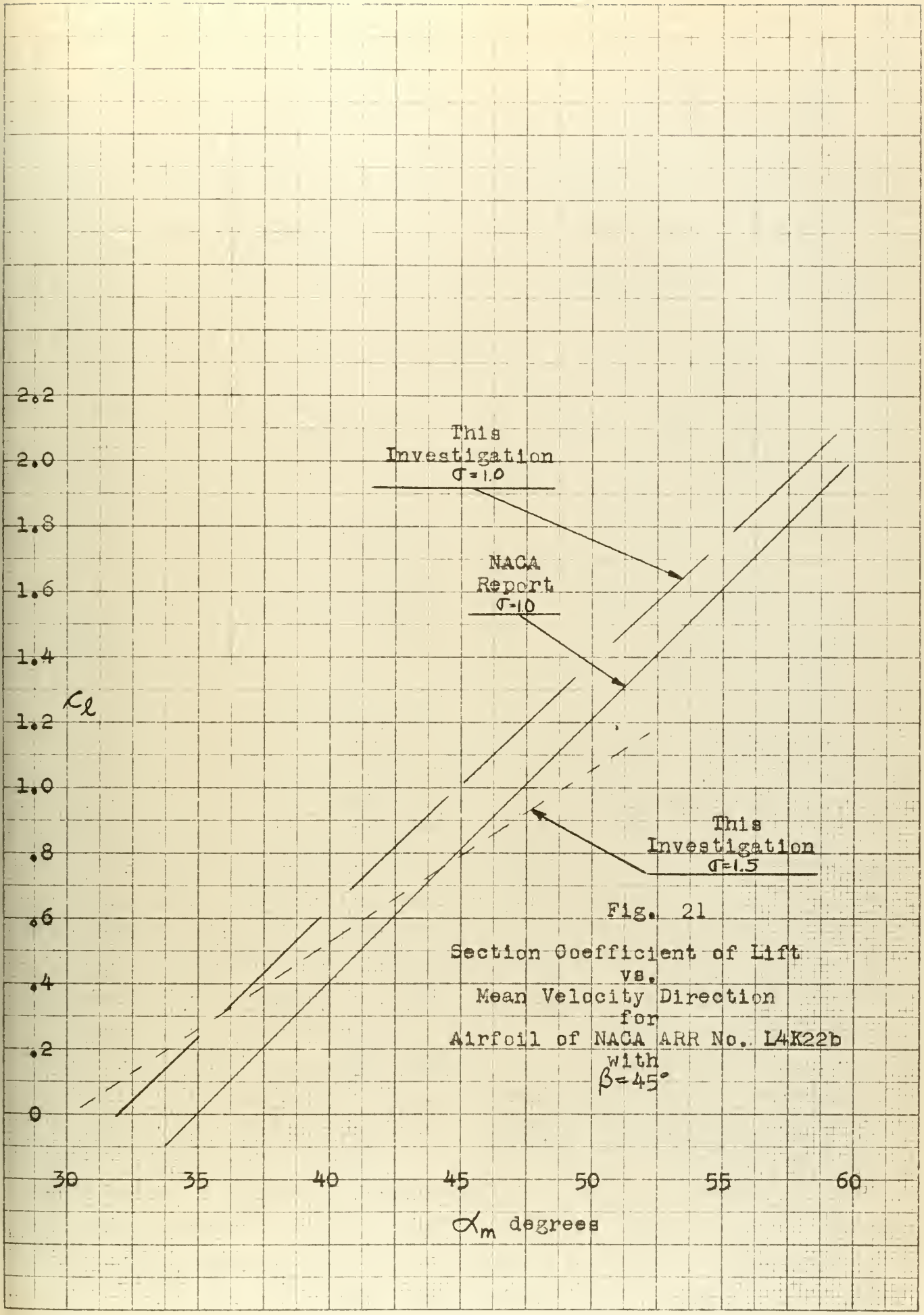

Fig. 21

Section Coefficient of Lift vs. Mean Velocity Direction for Airfoil of NACA ARR No. L4K22b with $\beta = 45°$

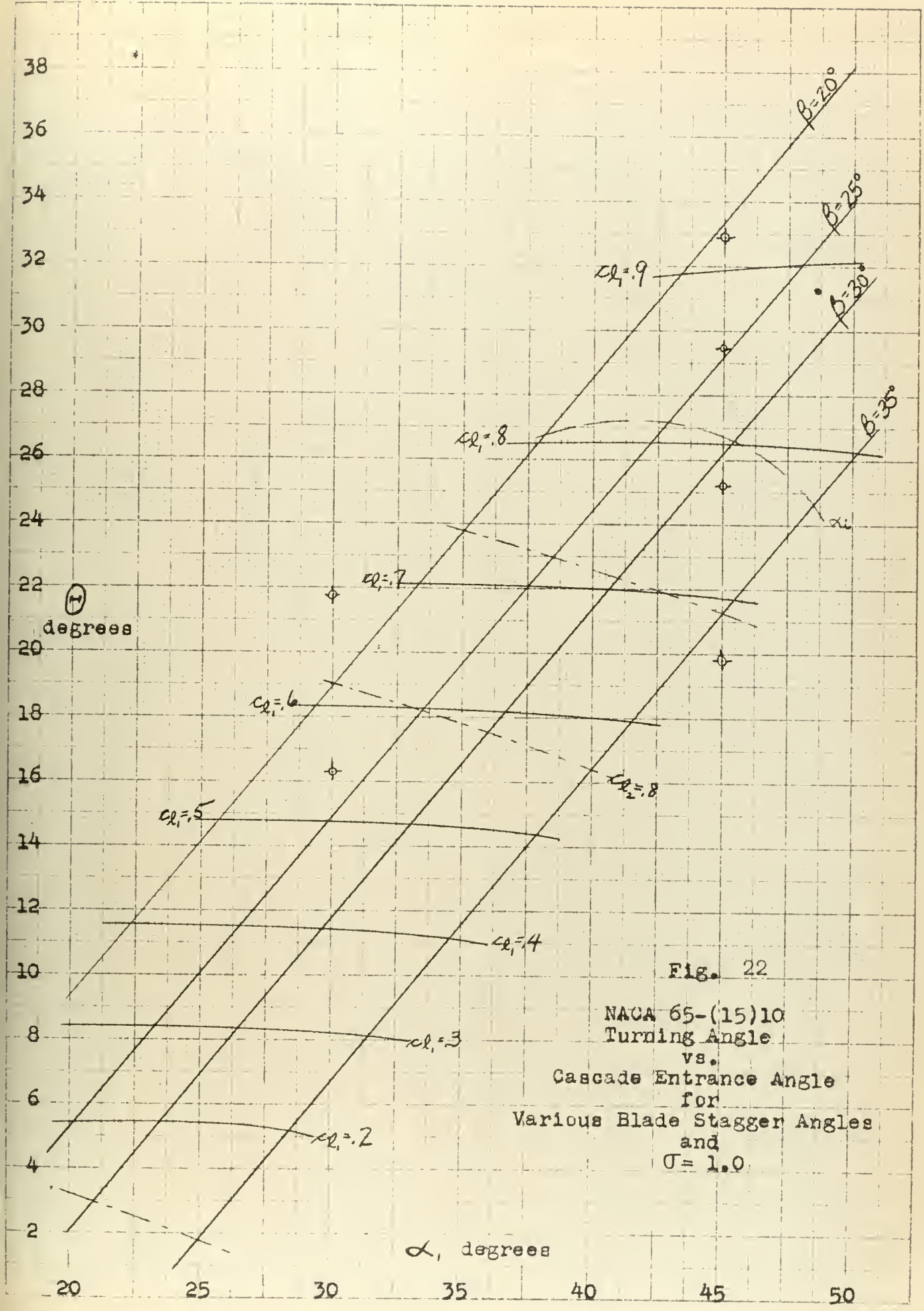

Fig. 22

NACA 65-(15)10
Turning Angle
vs.
Cascade Entrance Angle
for
Various Blade Stagger Angles
and
σ= 1.0

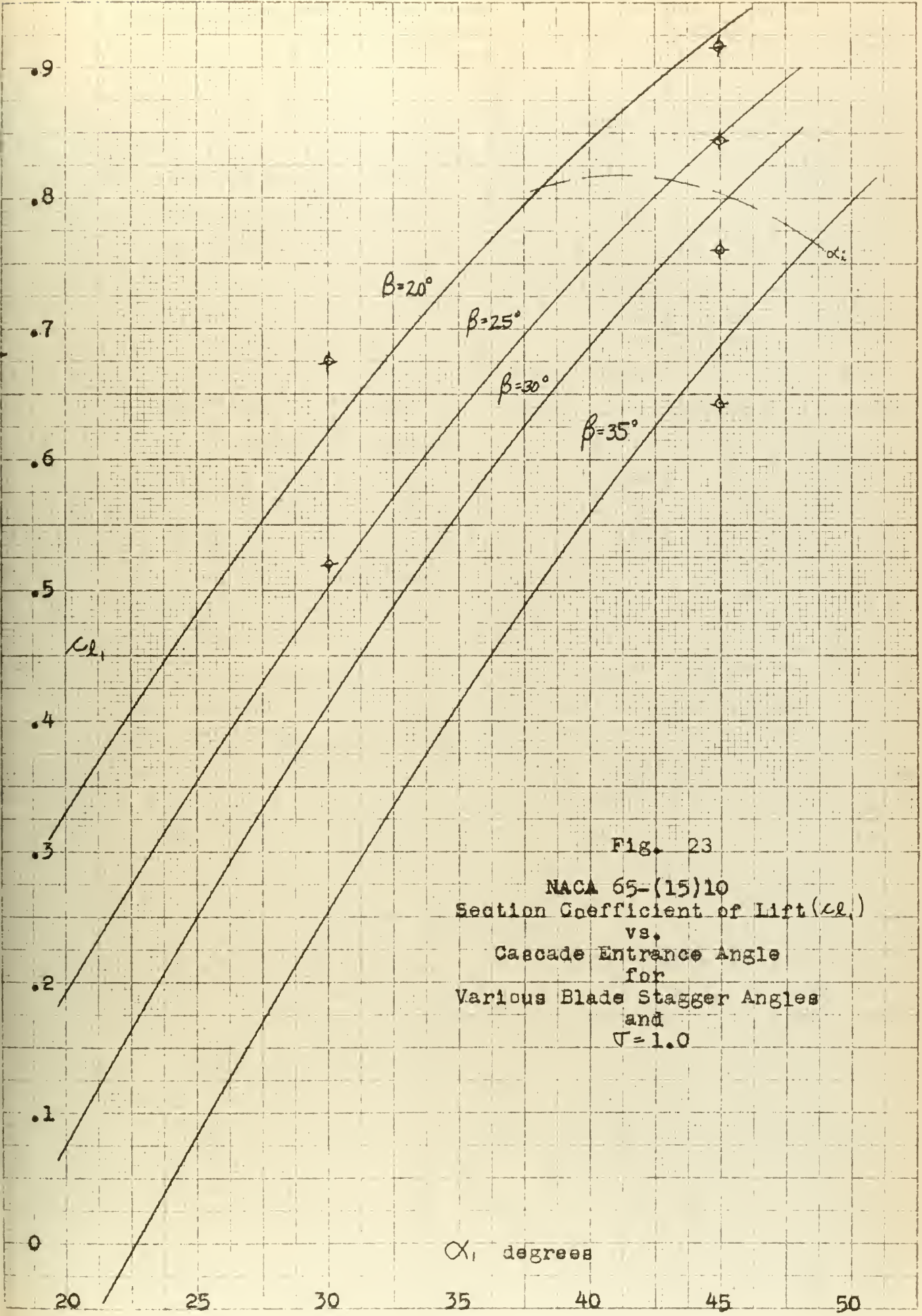

Fig. 23

NACA 65-(15)10
Section Coefficient of Lift (c_{l_i})
vs.
Cascade Entrance Angle
for
Various Blade Stagger Angles
and
$\sigma = 1.0$

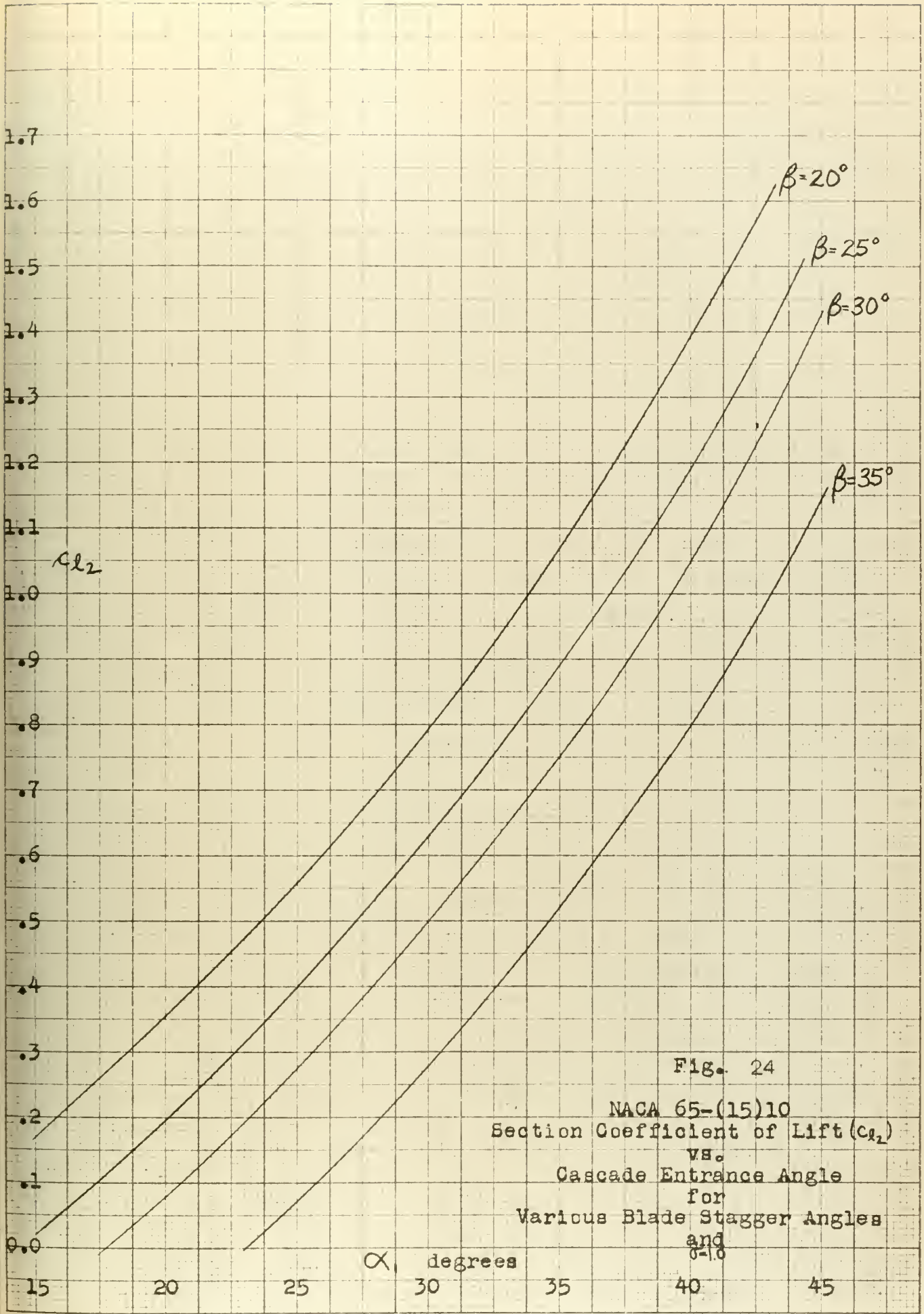

Fig. 24

NACA 65-(15)10
Section Coefficient of Lift (c_{l_2})
vs.
Cascade Entrance Angle
for
Various Blade Stagger Angles
and
σ=1.0

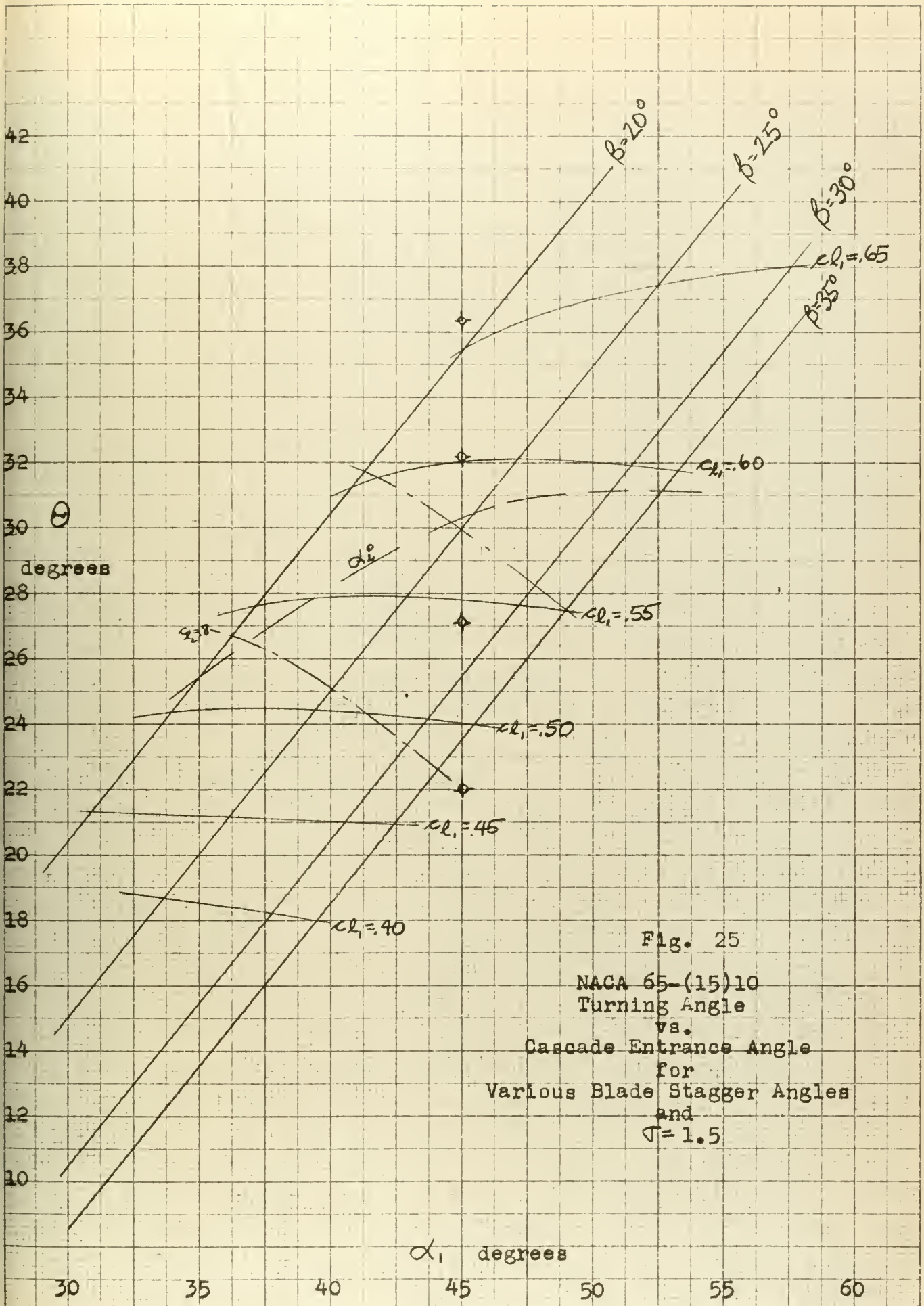

Fig. 25

NACA 65-(15)10
Turning Angle
vs.
Cascade Entrance Angle
for
Various Blade Stagger Angles
and
σ = 1.5

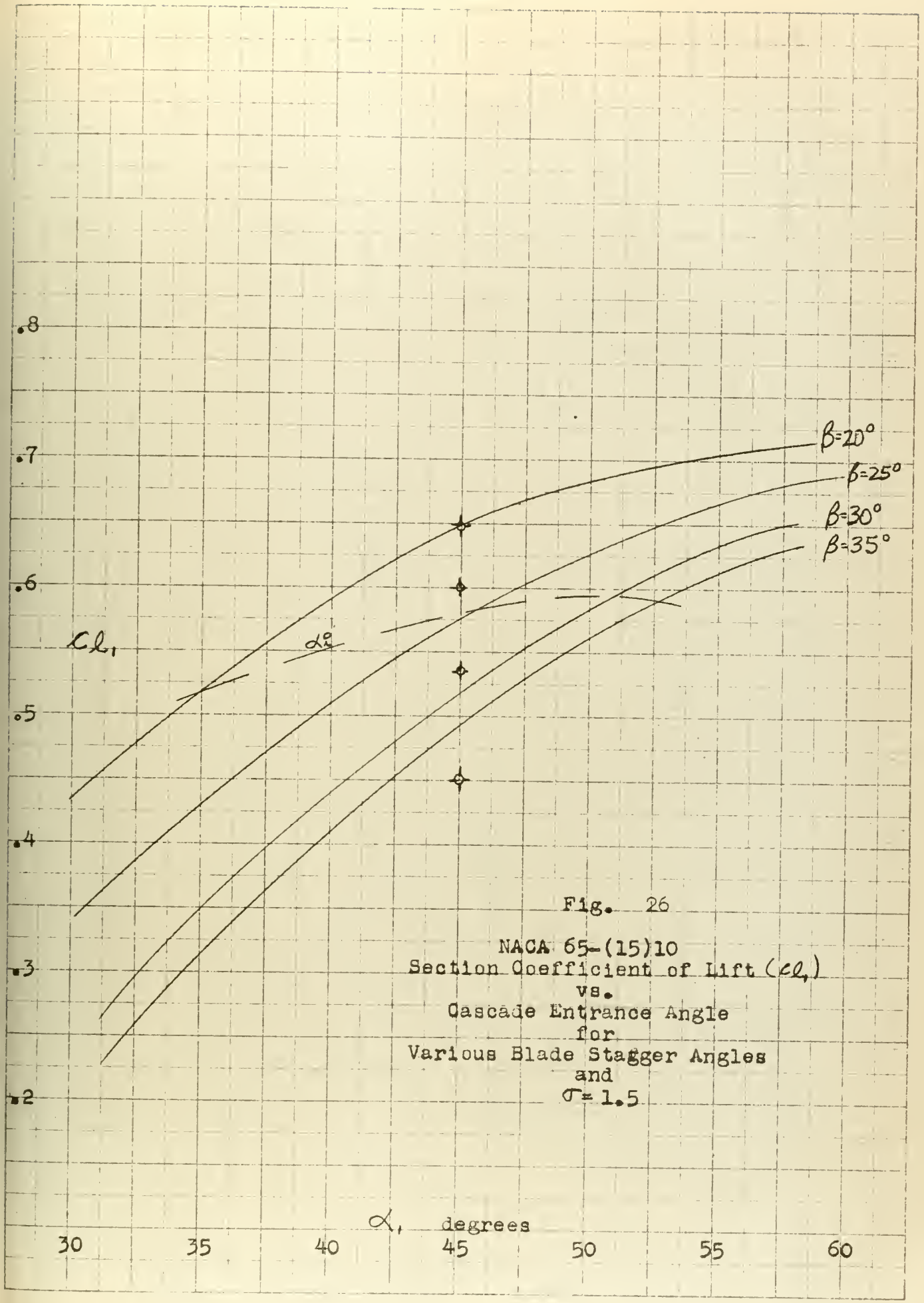

Fig. 26

NACA 65-(15)10
Section Coefficient of Lift (c_{l_1})
vs.
Cascade Entrance Angle
for
Various Blade Stagger Angles
and
σ= 1.5

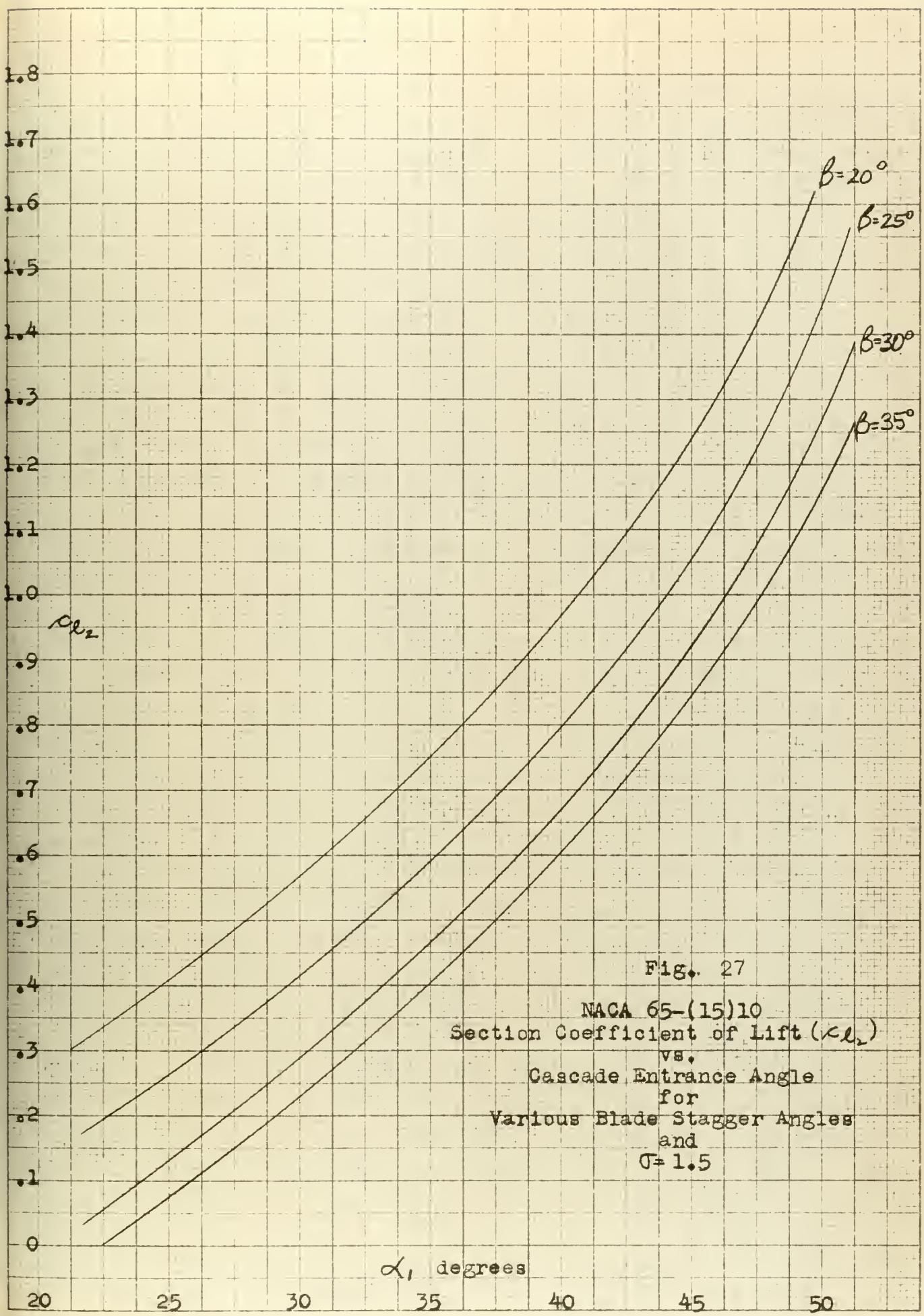

Fig. 27

NACA 65-(15)10
Section Coefficient of Lift (c_{l_2})
vs.
Cascade Entrance Angle
for
Various Blade Stagger Angles
and
$\sigma = 1.5$

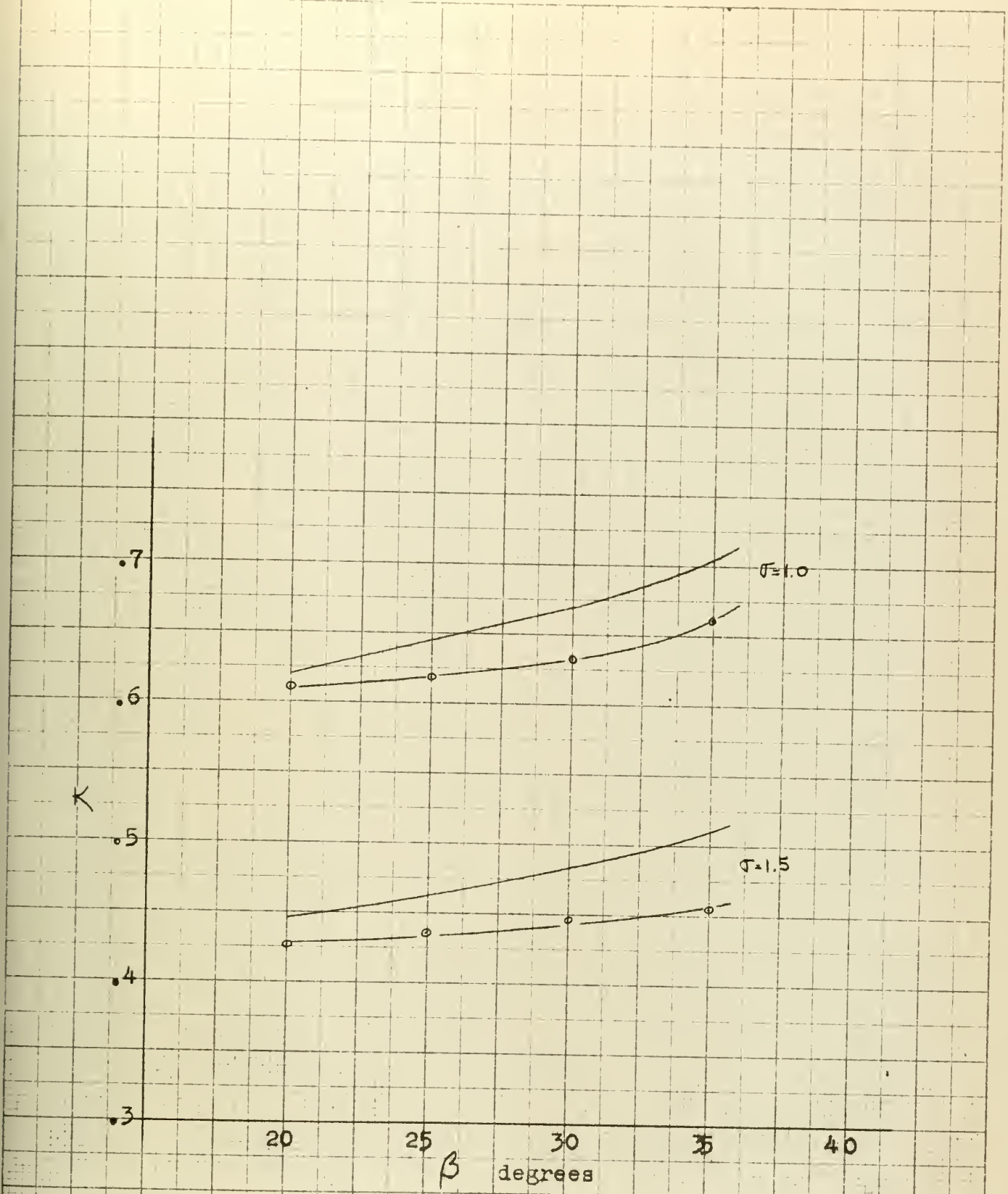

Fig. 28

Cascade Coefficient

vs.

Blade Stagger Angle

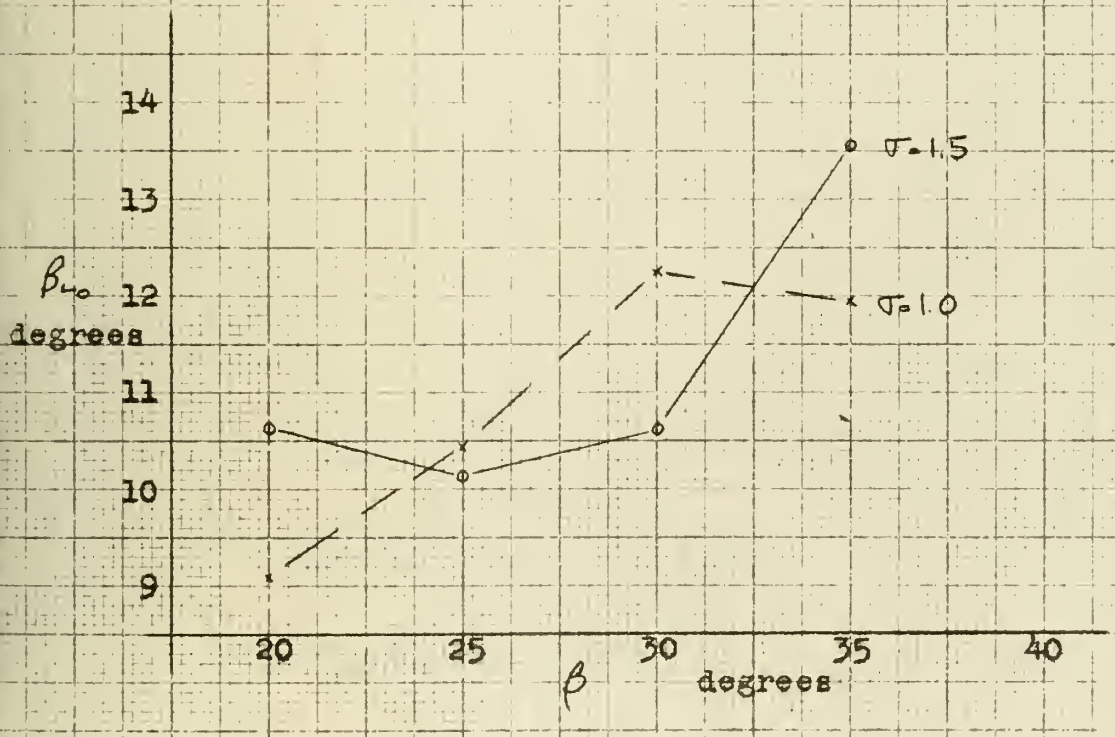

Fig. 29

Relative Zero Lift Angle
vs.
Blade Stagger Angle

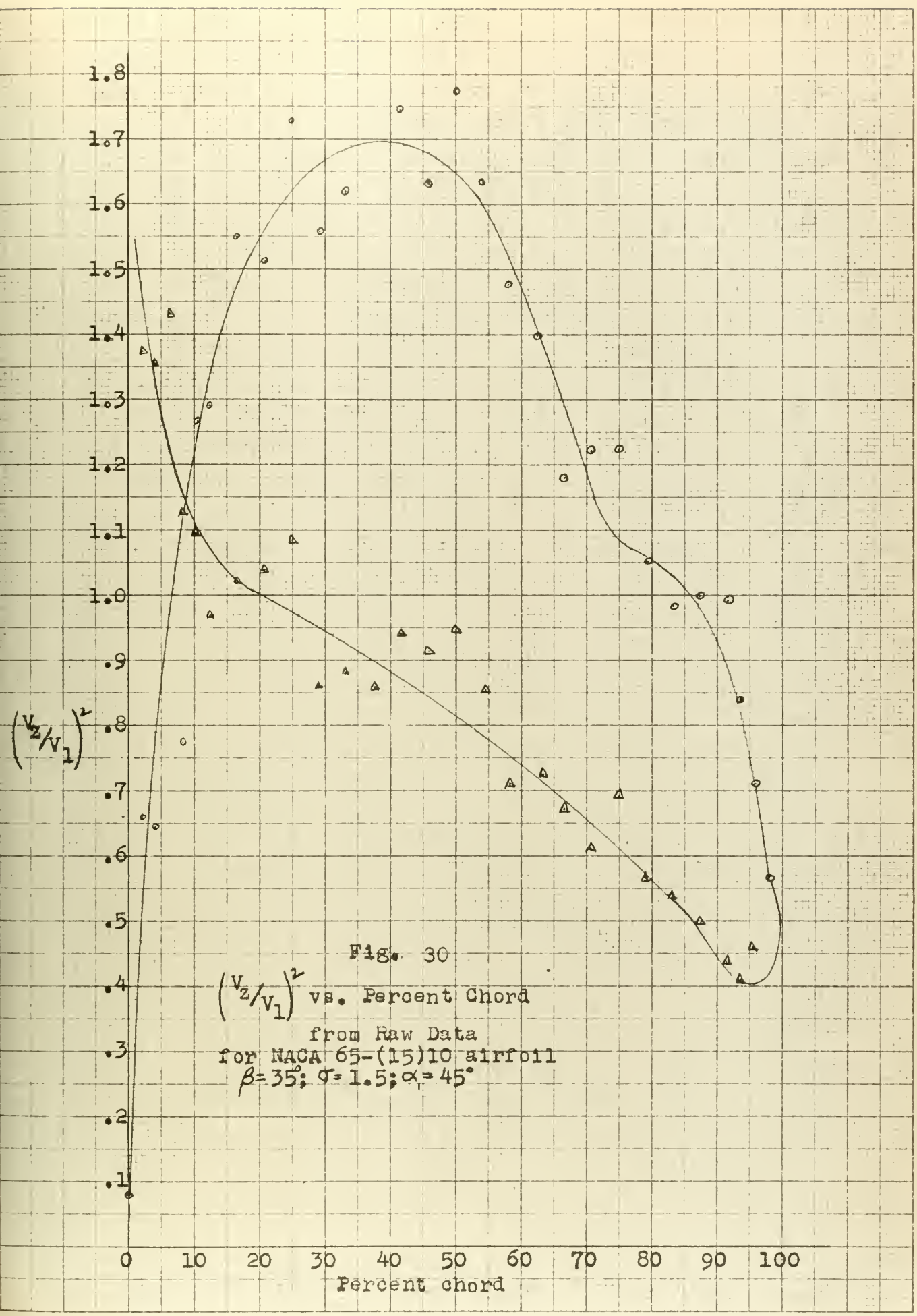

Fig. 30

$\left(V_2/V_1\right)^2$ vs. Percent Chord

from Raw Data

for NACA 65-(15)10 airfoil

$\beta = 35°$; $\sigma = 1.5$; $\alpha_1 = 45°$

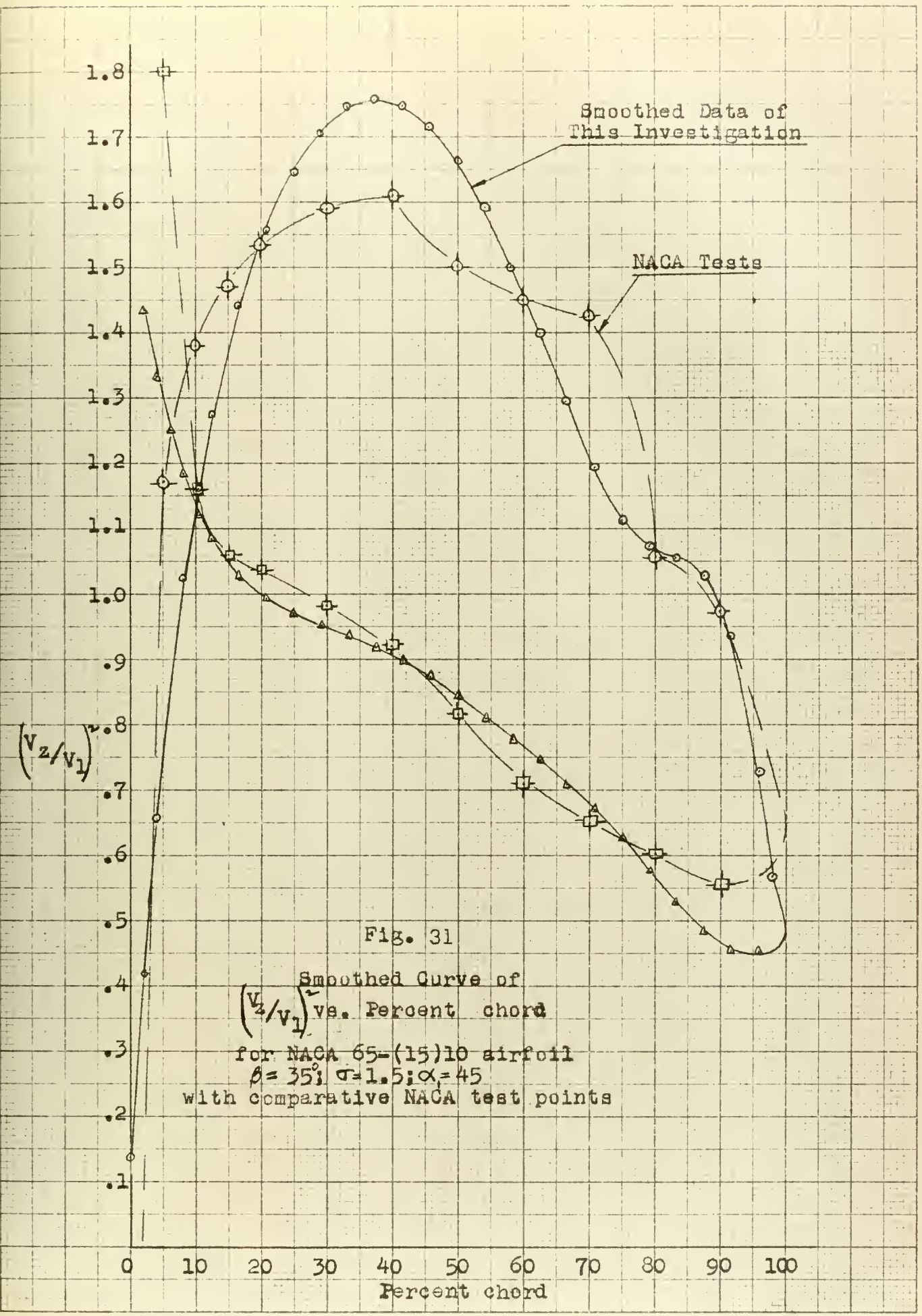

Fig. 31

Smoothed Curve of $\left(V_2/V_1\right)^2$ vs. Percent chord
for NACA 65-(15)10 airfoil
$\beta = 35°$; $\sigma = 1.5$; $\alpha_1 = 45$
with comparative NACA test points

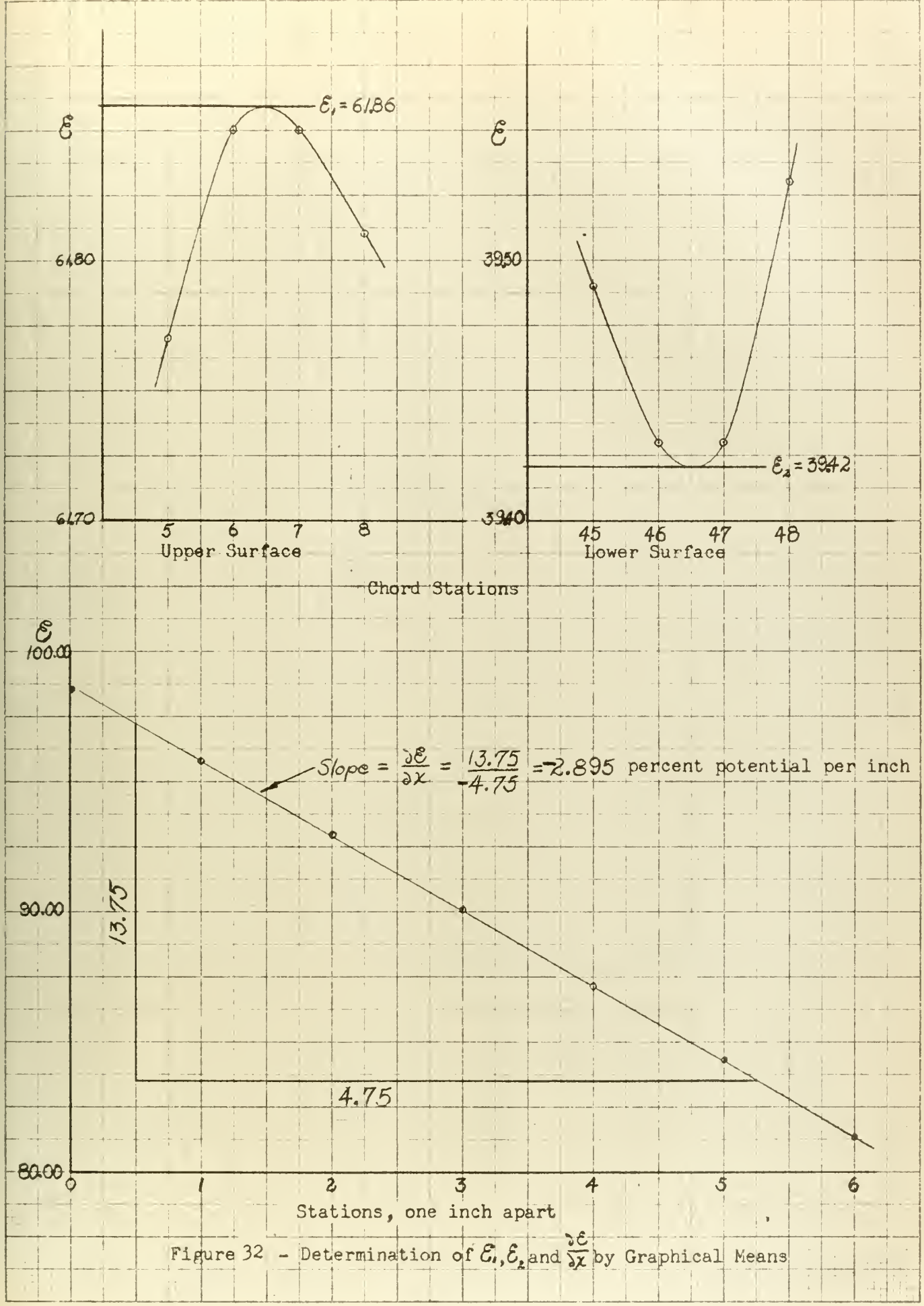

Figure 32 - Determination of $\mathcal{E}_1, \mathcal{E}_2$ and $\frac{\partial \mathcal{E}}{\partial x}$ by Graphical Means

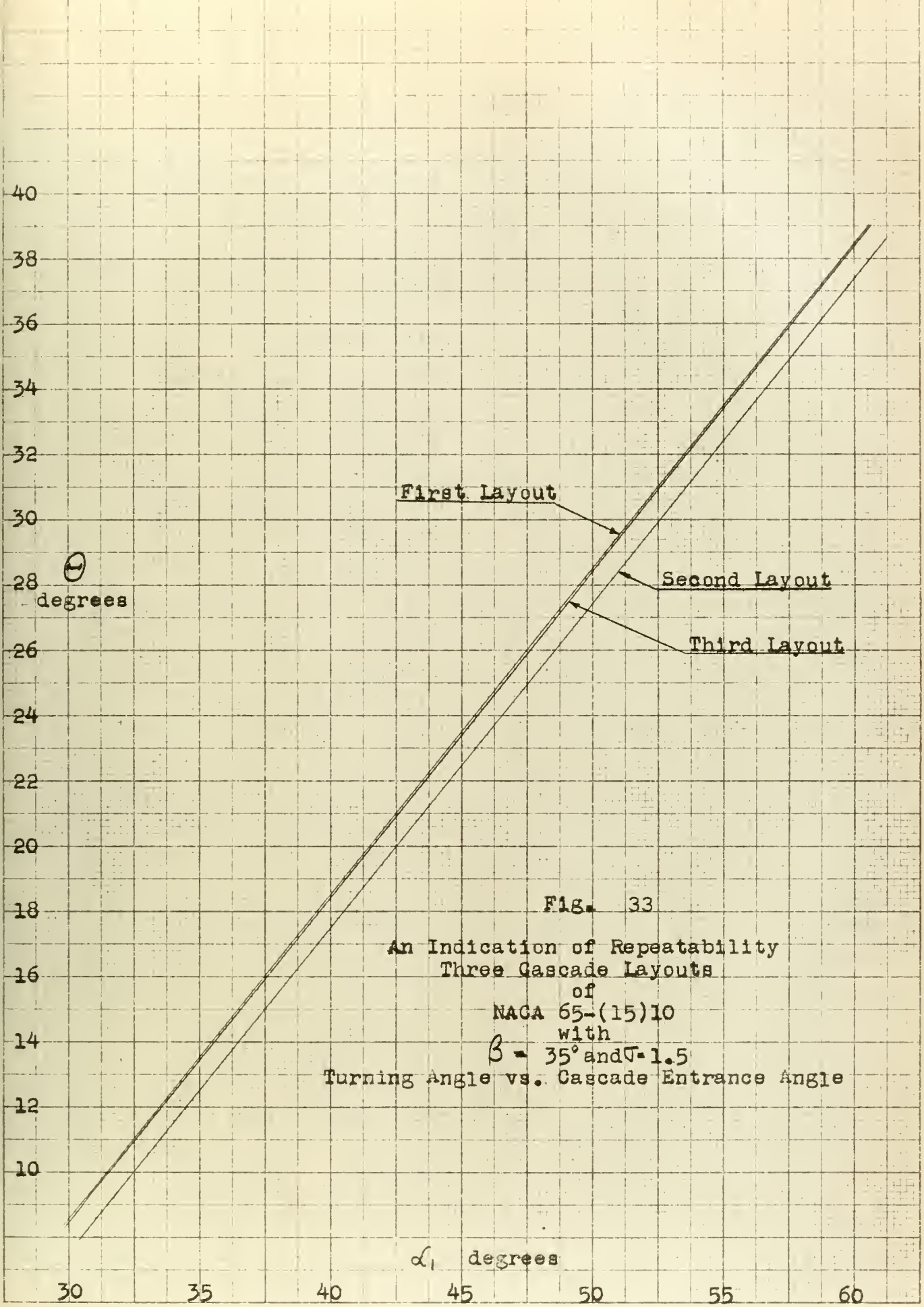

Fig. 33

An Indication of Repeatability
Three Cascade Layouts
of
NACA 65-(15)10
with
β = 35° and σ = 1.5
Turning Angle vs. Cascade Entrance Angle

APPENDIX A

THE ANALOGY

In potential, two dimensional, ideal fluid flow there is a complex velocity potential $w = \phi + i\psi$ such that the Cauchy-Riemann differential equations are satisfied

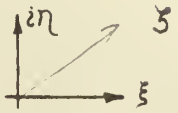

$$\frac{\partial \phi}{\partial \xi} = \frac{\partial \psi}{\partial \eta} \quad \text{and} \quad \frac{\partial \phi}{\partial \eta} = -\frac{\partial \psi}{\partial \xi} \qquad \text{A1}$$

Then the complex velocity may be written

$$\frac{dw}{d\zeta} = \frac{\partial \phi}{\partial \xi} - i\frac{\partial \phi}{\partial \eta} = \frac{\partial \psi}{\partial \eta} + i\frac{\partial \psi}{\partial \xi} = u + iv \,. \qquad \text{A2}$$

Considering the flow of a steady current in a flat sheet of uniform resistance per unit square ν .

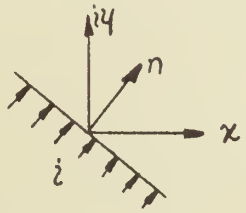

$$\nu i_n = -\frac{\partial E}{\partial n} \qquad \text{A3}$$

where i_n is the current line intensity. Let I be a total current function analagous on the sheet to the stream function in the ideal fluid flow such that

$$i_x = -\frac{\partial I}{\partial y} \quad \text{and} \quad i_y = \frac{\partial I}{\partial x} \,. \qquad \text{A4}$$

It follows:

$$\nu \frac{\partial I}{\partial y} = -\frac{\partial E}{\partial x} \quad \text{and} \quad \nu \frac{\partial I}{\partial x} = \frac{\partial E}{\partial y} \qquad \text{A5}$$

which indicates that E and I also satisfy the Cauchy-Riemann differential equations. Equations A5 may be used to obtain

$$E + i\nu I = f(x + iy) = f(z) \,, \qquad \text{A6}$$

or if we divide by the maximum potential

$$E^* = R^* i^* \,, \tag{A7}$$

$$\frac{E}{E^*} + i\,\frac{\nu I}{i^* R^*} = \mathcal{E} + i\,\mathcal{I} = f_1(z) \,. \tag{A8}$$

Hence we may list the following analogies:

z Plane	ζ Plane	
$i_x = -\frac{1}{\nu}\frac{\partial E}{\partial x} = -\frac{\partial I}{\partial y} = \frac{E^*}{\nu}\left(-\frac{\partial \mathcal{E}}{\partial x}\right)$	$u = \frac{\partial \varphi}{\partial \xi} = \frac{\partial \psi}{\partial \eta}$	A9
$i_y = -\frac{1}{\nu}\frac{\partial E}{\partial y} = \frac{\partial I}{\partial x} = \frac{E^*}{\nu}\left(-\frac{\partial \mathcal{E}}{\partial y}\right)$	$v = \frac{\partial \varphi}{\partial \eta} = -\frac{\partial \psi}{\partial \xi}$.	

APPENDIX B

DERIVATION OF EQUATIONS FOR CONFORMAL TRANSFORMATION

This appendix develops the equations needed to achieve conformal transformation of the cascade of blades in the z plane to the circle in the ζ plane. It also defines the quantity $\frac{d\zeta}{dz}$ which is important in later work for relating velocities in the picture plane to those in the real plane.

Conformal transformation is possible between the real, z plane and the picture, ζ plane if there exists a function in the picture plane of the real plane complex variable z such that for every assigned value of the variable the function has a definite value or system of values and also a definite derivative. The advantage of this definition is that it does not require the existence of an analytical expression of the function.

It was shown in the main text that any point on the real plane may be designated by its coordinates x, y or by the values of $\mathcal{E}$ and α which characterize it. See also Appendix A. Furthur, the parameter $\tau = \frac{\mathcal{E}_1 - \mathcal{E}_2}{s\left(-\frac{\partial \mathcal{E}}{\partial x}\right)_\infty}$ was shown to be the unique and invariant quantity which must be maintained to achieve conformal transformation.

The basic potential relations for a point of strength m are

$$\varphi = \frac{m}{2\pi} \ln R \quad \text{and} \quad \psi = \frac{m}{2\pi} \theta \qquad \text{B1}$$

where m is real. The point is called a source if m is positive and a sink if m is negative. R is the radial distance from the point and θ is the angular coordinate with respect to the point as origin.

In the picture plane of Fig. 4, let sources of strength m be located on the real axis at $\xi = -b, -a^2/b$ and let sinks of equal strength be located on the real axis at $\xi = b, a^2/b$.

Then the complex potential in the picture plane is

$$w = \frac{m}{2\pi} \ln \frac{b+\zeta}{b-\zeta} + \frac{m}{2\pi} \ln \frac{\zeta + a^2/b}{\zeta - a^2/b} = \varphi + i\psi \quad . \qquad \text{B2}$$

Now any point in the picture plane can be designated by its coordinates ξ , η or by the values of φ and ψ which characterize it. Combining the factors of eq. B2 ,

$$w = \frac{m}{2\pi} \ln \frac{b+\zeta}{b-\zeta} \cdot \frac{\zeta + a^2/b}{\zeta - a^2/b} \quad . \qquad \text{B3}$$

On the circle $|\zeta| = a$,

$$w = \frac{m}{2\pi} \ln \frac{ae^{i\theta}\left[ae^{i\theta} + ae^{-i\theta} + b/a + a/b\right]}{-ae^{i\theta}\left[ae^{i\theta} + ae^{-i\theta} - b/a + a/b\right]} \qquad \text{B4}$$

and with $b/a = e^{\gamma}$

$$w = \frac{m}{2\pi} \ln \frac{\cosh\gamma + a\cos\theta}{\cosh\gamma - a\cos\theta} \quad . \qquad \text{B5}$$

We may let a = 1, giving

$$w = \frac{m}{2\pi} \ln \frac{\cosh\gamma + \cos\theta}{\cosh\gamma - \cos\theta} = \varphi + i\psi \qquad \text{B6}$$

which shows that the circle is a line of constant ψ .

If 1 and 2 are the points indicated in Fig. 4

$$\varphi_2 - \varphi_1 = \frac{m}{2\pi} \ln \frac{\cosh\gamma + 1}{\cosh\gamma - 1} \quad . \qquad \text{B7}$$

By Appendix A, φ corresponds to $\mathcal{E}$; so we may impose the relation

$$\varphi = k_1 - k_2 \mathcal{E} \quad , \qquad \text{B8}$$

where k_1 and k_2 are arbitrary constants. It follows that

$$\varphi_2 - \varphi_1 = k_2(\mathcal{E}_1 - \mathcal{E}_2) \qquad \text{B9}$$

and if

$$m = s k_2 \left(-\frac{\partial \mathcal{E}}{\partial x}\right)_\infty \ , \qquad \text{B10}$$

then

$$\frac{\varphi_2 - \varphi_1}{m} = \tau = \frac{k_2(\mathcal{E}_1 - \mathcal{E}_2)}{k_2 s\left(-\frac{\partial \mathcal{E}}{\partial x}\right)_\infty} \ . \qquad \text{B11}$$

This establishes the existance of a function relating the z and ζ planes conformally.

Eq. B7 may be solved to give

$$\gamma = \cosh^{-1}\left[\frac{e^{\pi\frac{\varphi_2-\varphi_1}{m}} + 1}{e^{\pi\frac{\varphi_2-\varphi_1}{m}} - 1}\right] = \cosh^{-1}\left[\frac{e^{\pi\tau} + 1}{e^{\pi\tau} - 1}\right] \ . \qquad \text{B12}$$

Knowing γ , the locations of the sources and sinks in the picture plane are determined. For any point P on the circle and a corresponding point P' on a blade profile, let there be a quantity f such that

$$\frac{\varphi_P - \varphi_1}{\varphi_2 - \varphi_1} = f = \frac{\mathcal{E}_1 - \mathcal{E}_{P'}}{\mathcal{E}_1 - \mathcal{E}_2} \ . \qquad \text{B13}$$

By substitution of eqs. B6 and B7 into eq. B13 we obtain

$$f = \frac{1}{2}\frac{\ln\frac{\cosh\gamma + \cos\theta}{\cosh\gamma - \cos\theta} + \ln\frac{\cosh\gamma + 1}{\cosh\gamma - 1}}{\ln\frac{\cosh\gamma + 1}{\cosh\gamma - 1}} \qquad \text{B14}$$

and solving for $\cos\theta$:

$$\cos\theta = \cosh\gamma\left[\frac{\left(\frac{\cosh\gamma+1}{\cosh\gamma-1}\right)^{2f-1} - 1}{\left(\frac{\cosh\gamma+1}{\cosh\gamma-1}\right)^{2f-1} + 1}\right] = \cosh\gamma\left[\frac{e^{\pi\tau(2f-1)} - 1}{e^{\pi\tau(2f-1)} + 1}\right] \ . \qquad \text{B15}$$

The derivative $\left|\frac{d\zeta}{dz}\right|$ is the operator which relates infinitesimal vectors in the picture plane to corresponding vectors in the real plane, and vice versa. In particular,

$$V_z = \frac{dw}{dz} = \frac{dw}{d\zeta}\left|\frac{d\zeta}{dz}\right| = V_\zeta \left|\frac{d\zeta}{dz}\right| \quad , \tag{B16}$$

but recalling our parameter f this may be written,

$$V_z = V_\zeta \left|\frac{\frac{df}{dz}}{\frac{df}{d\zeta}}\right| \quad . \tag{B17}$$

Now V_ζ is known in the picture plane and is given by eq. C5 of Appendix C.

The numerator of eq. B17 can be written as

$$\left|\frac{df}{dz}\right| \cong \left|\frac{\Delta E}{\Delta z}\right| \frac{1}{E_1 - E_2} \quad . \tag{B18}$$

The denominator of eq. B17 can be written as

$$\left|\frac{df}{d\zeta}\right| = \left|\frac{\sin\theta \cosh\gamma}{(\cosh^2\gamma - \cos^2\theta)\ln\frac{\cosh\gamma + 1}{\cosh\gamma - 1}}\right| \quad . \tag{B19}$$

APPENDIX C

DERIVATION OF FLOW EQUATIONS

This appendix derives the equations required to develop an arbitrary flow about the circle $|\zeta| = a$.

The sources and sinks used to accomplish transformation can be considered to create an axial flow velocity V_a such that $m = V_a s$. On the circle $|\zeta| = a$ this flow produces a velocity. From eq. B3

$$\frac{1}{R}\frac{\partial \varphi}{\partial \theta} = V_\theta = -\frac{2V_a s}{\pi}\frac{\cosh\gamma \sin\theta}{\cosh 2\gamma - \cos 2\theta} \quad . \qquad \text{C1}$$

The basic velocity and stream potential relations for a point vortex of strength Λ are

$$\varphi = \frac{\Lambda}{2\pi}\theta \qquad \text{and} \qquad \psi = -\frac{\Lambda}{2\pi}\ln R \ , \qquad \text{C2}$$

where Λ is positive if counterclockwise.

If vortices of strength Λ and with direction indicated in Fig. 7 be placed in the picture plane in addition to the sources and sinks the resulting complex potential is

$$w = \frac{V_a s}{2\pi}\left(\ln\frac{b+\zeta}{b-\zeta} + \ln\frac{\zeta + a^2/b}{\zeta - a^2/b}\right) - i\frac{\Lambda}{2\pi}\left(\ln\frac{b+\zeta}{b-\zeta} + \ln\frac{\zeta - a^2/b}{\zeta + a^2/b}\right) \qquad \text{C3}$$

and the corresponding velocity on the circle is

$$V_\theta = -\frac{2V_a s}{\pi}\frac{\cosh\gamma\sin\theta}{\cosh 2\gamma - \cos 2\theta} + \frac{2\Lambda}{\pi}\frac{\sinh\gamma\cos\theta}{\cosh 2\gamma - \cos 2\theta} \quad . \qquad \text{C4}$$

If $V_a = \frac{m}{s}$ and $V_t = \frac{\Lambda}{s}$,

$$\frac{V_t}{V_a} = \tan\alpha_m = \frac{\Lambda}{m} \quad . \qquad \text{C5}$$

Since the value of m is determined in the process of transforma-

tion, from $m = sk_2\left(-\frac{\partial \mathcal{E}}{\partial x}\right)_\infty$, the arbitrary choice of a mean velocity direction α_m determines the strength Λ. Then if additional vortices of strength $\frac{\Gamma}{2}$ and with direction indicated in Fig. 7 be placed in the picture plane, the resulting velocity on the circle $|\zeta| = a$ is:

$$V_\zeta = V_\theta = -\frac{2V_a s}{\pi}\left(\frac{\cosh\gamma\sin\theta - \tan\alpha_m \sinh\gamma\cos\theta}{\cosh 2\gamma - \cos 2\theta}\right) - \frac{\Gamma}{2\pi}\left(\frac{\sinh 2\gamma}{\cosh 2\gamma - \cos 2\theta}\right). \quad C6$$

At the point on the circle where $\theta = \theta_T$, $V_\theta = 0$. Solving for $\frac{\Gamma}{2m}$,

$$\frac{\Gamma}{2V_a s} = \tan\alpha_m \frac{\cos\theta_T}{\cosh\gamma} - \frac{\sin\theta_T}{\sinh\gamma} \quad . \quad C7$$

The circulation given by this equation insures satisfaction of the Kutta condition.

The velocity triangle is now complete.

$$\tan\alpha_1 = \tan\alpha_m + \frac{\Gamma}{2V_a s} \quad C8$$

$$\tan\alpha_2 = \tan\alpha_m - \frac{\Gamma}{2V_a s} \quad C9$$

$$\tan(\alpha_1 - \alpha_2) = \frac{\frac{\Gamma}{V_a s}}{1 + \tan^2\alpha_m - \left(\frac{\Gamma}{2V_a s}\right)^2} \quad C10$$
$$= \tan\Theta .$$

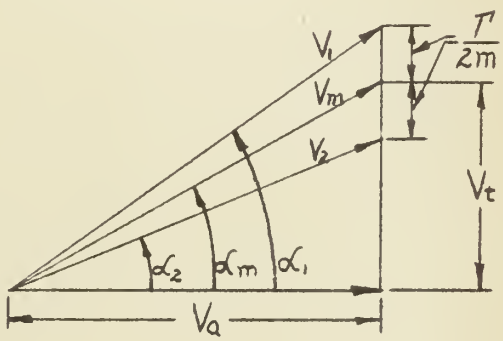

Of aerodynamic interest is the ideal angle of attack. At this angle the front stagnation point is at the leading edge of the airfoil. If $V_\theta = 0$ for $\theta = \theta_L$ equation C6 may be solved to give,

$$\tan\alpha_i = \frac{\sin\theta_T - \sin\theta_L}{\tanh\gamma(\cos\theta_T - \cos\theta_L)} \quad . \quad C11$$

For the determination of lift coefficients,

$$L = c_{l_x}\frac{\rho}{2}V_x^2 c = \rho V_m \Gamma \quad . \quad C12$$

From eqs. C8 and C9, $\Gamma = V_a s(\tan\alpha_1 - \tan\alpha_2)$. C13

Substituting and solving,

$$c_{l_x} = \frac{2V_m V_a s}{V_x^2 c}(\tan\alpha_1 - \tan\alpha_2) \qquad \text{C14}$$

but $V_m = \frac{V_a}{\cos\alpha_m}$ and $m = V_a s$; so, $c_{l_x} = \frac{2V_a^2}{\cos\alpha_m}\frac{s}{c}\frac{\cos^2\alpha_x}{V_x^2}(\tan\alpha_1 - \tan\alpha_2)$.

Hence,

$$c_{l_x} = \frac{2}{\sigma}\frac{\cos^2\alpha_x}{\cos\alpha_m}(\tan\alpha_1 - \tan\alpha_2) . \qquad \text{C15}$$

APPENDIX D

DEFINITION AND EXPLANATION OF THE TERM "SPECIFIC RESISTANCE"

Consider an element of the conducting medium of length Δl and width ΔW. Assume constant thickness h and resistivity ρ. Let ΔV be the potential drop along the length Δl of the element, and Δi be the corresponding current.

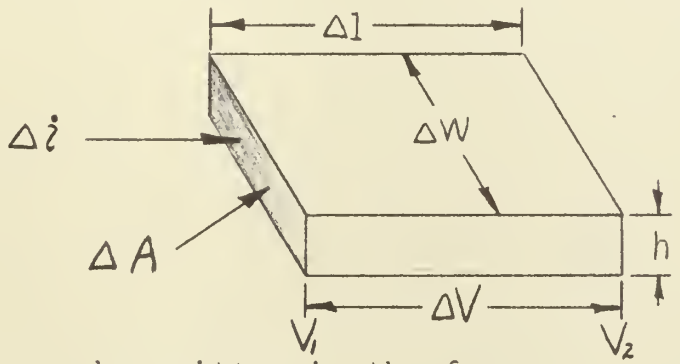

Ohm's Law may be written in the form:

$$\Delta V/\Delta l = \rho\, \Delta i/\Delta A = (\rho/h)(\Delta i/\Delta W) \text{ where } \Delta A = h(\Delta W).$$

The constant of proportionality ρ/h is defined as the specific resistance ν, of the conducting medium. Solving the above equation for this term:

$$\nu = (\rho/h) = \Delta V/\Delta i\ (\Delta W/\Delta l)\ \frac{\text{volts in.}}{\text{amp.} \quad \text{in}} = \text{ohms}.$$

The net resistance of the element may be written:

$$R = \Delta V/\Delta i = \nu(\Delta l/\Delta W).$$

Thus if the element is square ($\Delta l = \Delta W$), its net resistance R, will be numerically equal to the specific resistance ν, of the medium, regardless of the size of the square.

APPENDIX E

DETERMINATION OF $\mathcal{E}_T$

Let $$w_a = A z^{P_a} = \mathcal{E} + i \psi \qquad \text{E1}$$

be the complex potential for conditions symmetrical on the top and bottom of a wedge, Fig. E1, where $$P_a = \frac{1}{1 - \frac{\theta}{2\pi}} \cdot \qquad \text{E2}$$

The sides of the wedge are two separate lines which join at the wedge vertex to form a single line bisecting the obtuse angle formed by the vertex. Along each line $\psi = 0$; so,

$$\mathcal{E}_a = A r^{P_a} \cdot \qquad \text{E3}$$

Similarly let $$w_b = B z^{P_b} \cdot \qquad \text{E4}$$

be the complex potential for conditions where a single line of constant ψ coincides with the top and bottom boundaries of the wedge. Here $$P_b = \frac{\frac{1}{2}}{1 - \frac{\theta}{2\pi}} = \frac{1}{2} P_a = P \qquad \text{E5}$$

and as above, $$\mathcal{E}_b = \pm B r^{P_b} \qquad \text{E6}$$

on the wedge profile. The + sign is for the upper side of the wedge and the - sign is for the lower side of the wedge.

Superposition of these two complex potentials results in

$$\mathcal{E}_c = \mathcal{E}_a \pm \mathcal{E}_b = A r^{2P} \pm B r^{P} \cdot \qquad \text{E7}$$

Let the wedge approximate the trailing edge of the airfoil being investigated. Let r be the straight line distance of a point on the profile from the trailing edge. With the trailing edge at the point r = 0, eq. E7 will result in $\mathcal{E}$ being zero at r = 0; so with the addition of a constant, the resultant equation is, $$\mathcal{E}_d = \mathcal{E}_T + A r^{2P} \pm B r^{P} \cdot \qquad \text{E8}$$

Desired is the determination of the constants $\mathcal{E}_T$, A, B, and p, such that the curve of the above expression will as closely as possible approximate the measured values of $\mathcal{E}$ in the neighborhood of the trailing edge of the airfoil and permit determination of $\mathcal{E}_T$. The constant p is determined by a plotting procedure described later in the appendix. The determination of $\mathcal{E}_T$ is accomplished by the method of least squares which is mathematically expressed by making the sum of the squares of the deviations of the experimental points from the analytical curve a minimum:

$$\Delta = \sum (\mathcal{E}_i - \mathcal{E}_d)^2 = \text{minimum}. \qquad \text{E9}$$

This requires that,

$$\frac{\partial \Delta}{\partial \mathcal{E}_d} = 0 = \frac{\partial \Delta}{\partial A} = \frac{\partial \Delta}{\partial B} \quad . \qquad \text{E10}$$

The resulting set of equations is

$$\begin{aligned} a_{11}\mathcal{E}_T + a_{12}A + a_{13}B &= M_1 \\ a_{21}\mathcal{E}_T + a_{22}A + a_{23}B &= M_2 \\ a_{31}\mathcal{E}_T + a_{32}A + a_{33}B &= M_3 \end{aligned} \qquad \text{E11}$$

where

$$\begin{aligned} a_{11} &= 1, & a_{22} &= \frac{1}{N}\sum_{i=1}^{N} r_i^{4P} & M_1 &= \frac{1}{N}\sum_{i=1}^{N} \mathcal{E}_i \\ a_{12} = a_{21} &= \frac{1}{N}\sum_{i=1}^{N} r_i^{2P}, & a_{23} = a_{32} &= \frac{1}{N}\sum_{i=1}^{N} r_i^{3P} & M_2 &= \frac{1}{N}\sum_{i=1}^{N} r_i^{2m}\mathcal{E}_i \\ a_{13} = a_{31} &= \frac{1}{N}\sum_{i=1}^{N} \pm r_i^{P}, & a_{33} &= \frac{1}{N}\sum_{i=1}^{N} r_i^{2P} & M_3 &= \frac{1}{N}\sum_{i=1}^{N} \pm r_i^{m}\mathcal{E}_i \end{aligned} \qquad \text{E12}$$

and N is the number of experimental points.

The matrix solution for $\mathcal{E}_T$ is obtained, yielding

$$\mathcal{E}_T = \frac{M_1(a_{22}a_{33} - a_{23}^2) + M_2(a_{23}a_{13} - a_{12}a_{33}) + M_3(a_{12}a_{23} - a_{22}a_{13})}{2a_{12}a_{13}a_{23} + a_{22}a_{33} - a_{23}^2 - a_{12}^2 a_{33} - a_{13}^2 a_{22}} \quad . \qquad \text{E13}$$

For this investigation a sketch of the trailing edge of the airfoil was drawn to a scale ten times that of the 6 inch chord templates used. Straight line distances were measured on this sketch from the trailing edge of the airfoil to the locations along the top and bottom surface where potential readings were taken. A curve was plotted of $\mathcal{E}_u$ and $\mathcal{E}_\ell$ versus these distances r: See Fig. E2. From this curve the values of $\mathcal{E}_u$ and $\mathcal{E}_\ell$ were obtained at equal values of r. On log-log coordinates $(\mathcal{E}_u - \mathcal{E}_\ell)$ was plotted as a function of r. The slope of this straight line is the coefficient p. See Fig. E3.

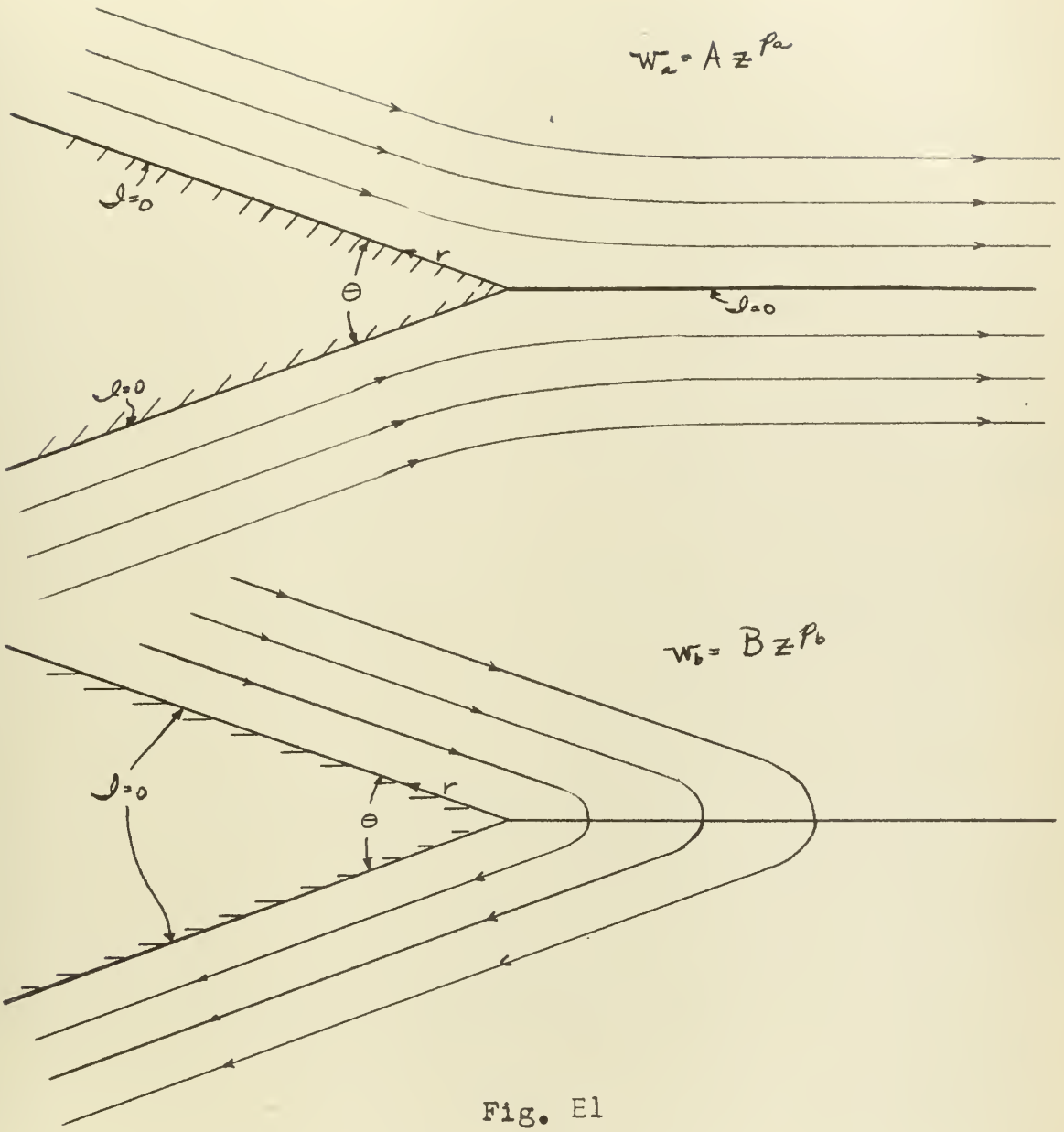

Fig. E1

Complex potentials
for Determining ε_r

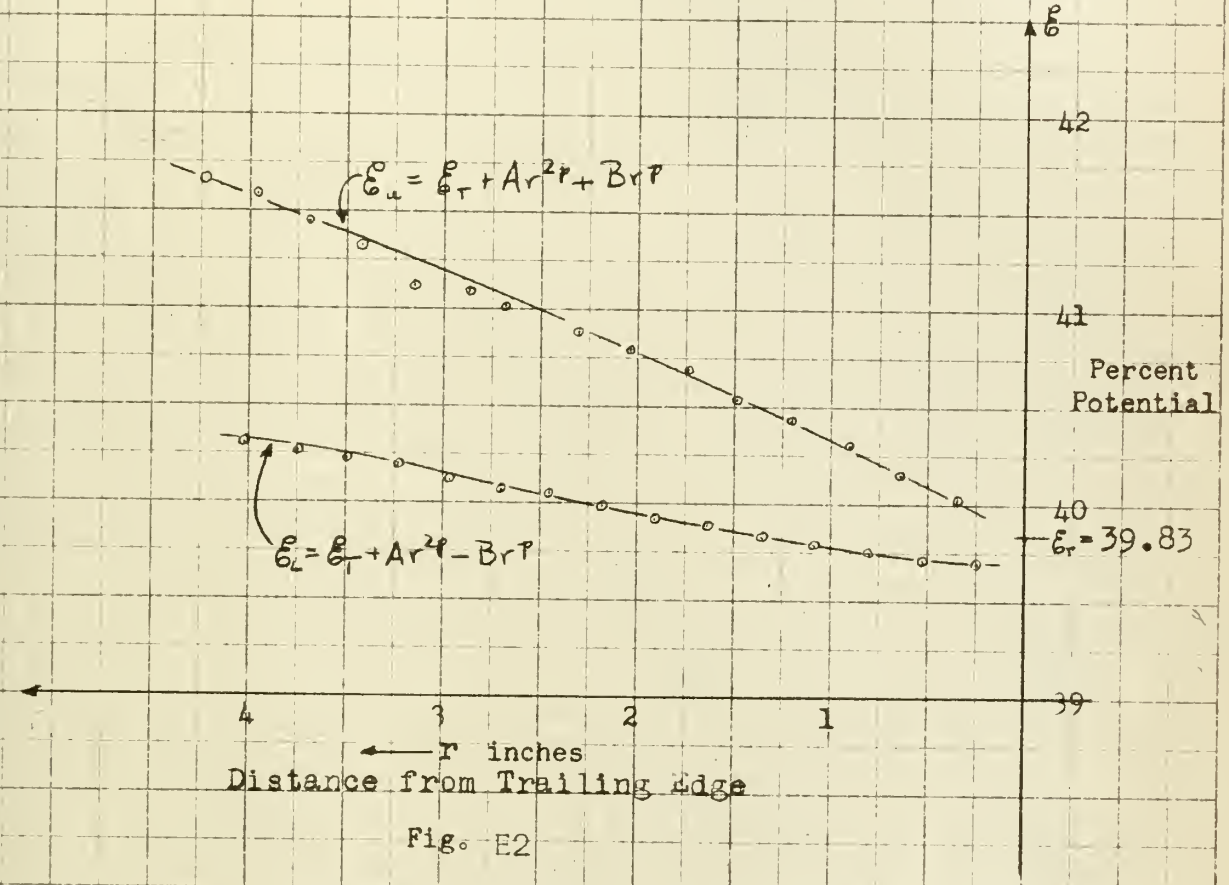

Fig. E2

Percent Potential
vs.
Distance from Trailing Edge
NACA 65-(15)10
$\sigma = 1.5$; $\beta = 25°$

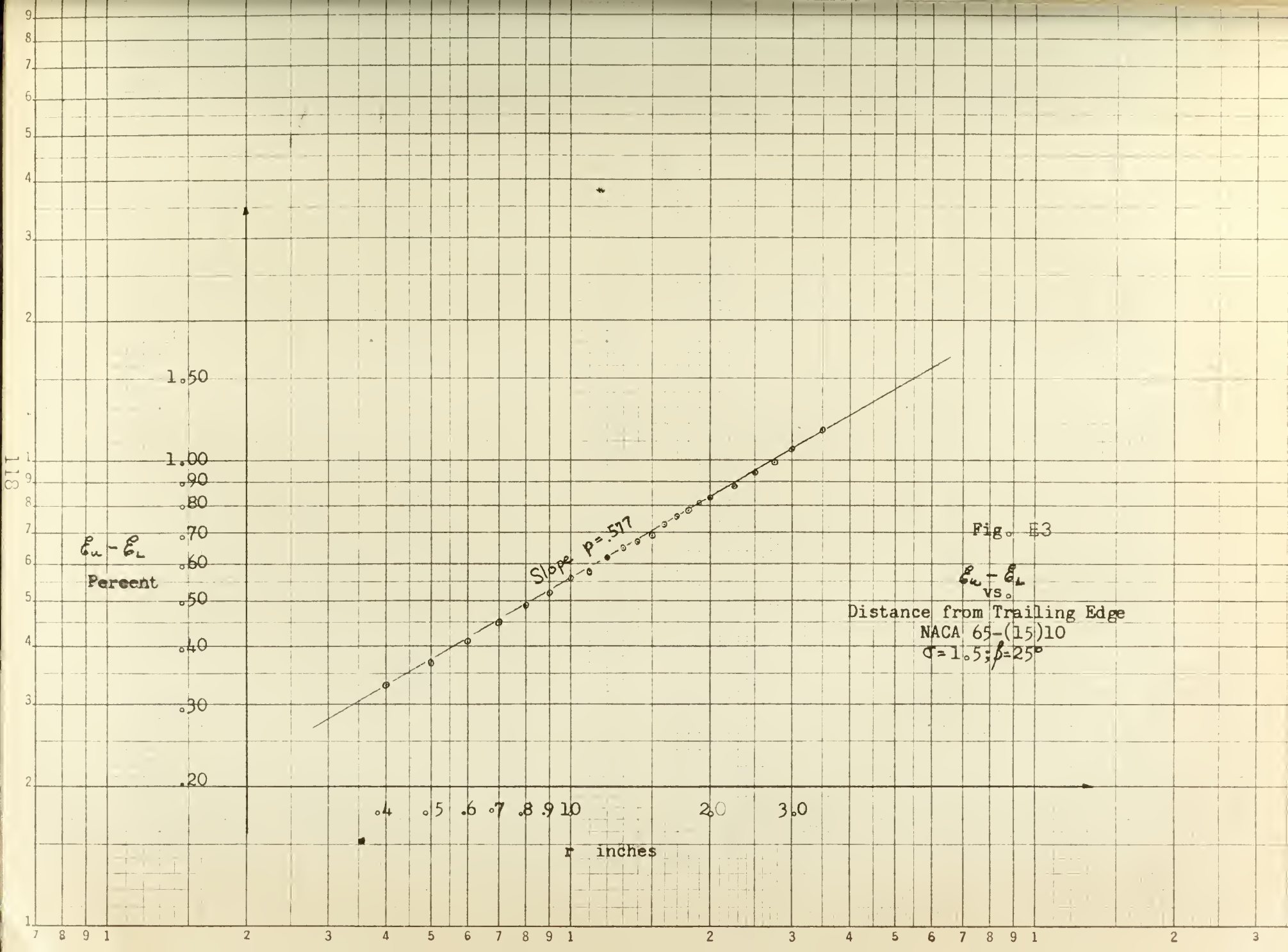

Fig. E3

$\epsilon_u - \epsilon_L$ vs.
Distance from Trailing Edge
NACA 65-(15)10
$\sigma = 1.5; \beta = 25°$

APPENDIX F

APPROXIMATION OF THE ERROR DUE TO THE BUS BAR LOCATION

In adapting equipment to provide the electrical analogy to flow through cascades, it was necessary to locate the bus bars a finite distance from the cascade. Thus the location of the bus bars introduced an error in the measured data. The determination of this error cannot readily be made when the airfoils of the cascade have camber and thickness. However, a good approximation of the error may be found by considering a cascade of flat plates.

Tests of this investigation were conducted under conditions equivalent to straight through flow with no circulation. The same conditions may be achieved over a flat plate cascade by imposing a potential flow composed of sources and sinks onto the conformal map of the cascade.

THE CASCADE OF FLAT PLATES

Considering $\zeta' = f(\zeta)$ as a complex potential function, then

$$\zeta' = S\frac{\cos\beta}{2\pi}\left[\ln\frac{\zeta+b}{\zeta-b} + \ln\frac{\zeta+a^2/b}{\zeta-a^2/b}\right] + \zeta S\frac{\sin\beta}{2\pi}\left[\ln\frac{\zeta+b}{\zeta-b} - \ln\frac{\zeta+a^2/b}{\zeta-a^2/b}\right] \qquad \text{F1}$$

gives the mapping function between a circle with the radius a in the ζ plane and a staggered lattice composed of straight airfoils in the ζ' plane (Fig. F1).

The first term of the above equation can be considered as originating from sources and sinks of equal strength located as shown in the figure, while the second term originates from

vortices of equal magnitude superimposed on the sources and sinks. The sense of the vortices is shown by the direction of the arrows in Fig. F1.

The spacing of the airfoils along the cascade is a constant s and β if the stagger angle of the blades.

The parameter b is connected with the chord spacing ratio. In order to establish the relation between them, it is necessary to calculate the chord. By setting $\frac{d\zeta'}{d\zeta} = 0$ for $\zeta = \zeta_L$ (L, Fig. F1) and $\zeta = \zeta_T$ (T, Fig. F1) which points correspond to the leading and trailing edges of the blade, it can be shown that

$$\frac{c}{s} = \frac{2}{\pi}\left\{\cos\beta \ln\left[\frac{(1/b^4 + 2/b^2\cos^2\beta + 1)^{1/2} + 2/b\cos\beta}{1 - 1/b^2}\right] + \sin\beta \tan^{-1}\left[\frac{2/b \sin\beta}{(1/b^4 + 2/b^2\cos^2\beta + 1)^{1/2}}\right]\right\}. \qquad \text{F2}$$

For any chosen stagger angle β, the solidity $\sigma = c/s$ may be computed for various assumed values of b. By plotting these results, it is possible to determine b graphically for any choice of σ. Table F I gives a set of such corresponding values for a β of 45°.

In the present example the solidity was arbitrarily chosen as unity. The parameters of the cascade geometry are now fixed.

In order to obtain the point to point relation between the ζ' and ζ plane it was necessary to reduce equation F1 to its real and imaginary parts. After a simple but somewhat lengthy calculation there is obtained the form,

$$\zeta' = x' + i y' = s\frac{\cos\beta}{2\pi}\left\{\ln\left[\frac{\left\{(r+a^2/r)\cos\theta + 2a\cosh\gamma\right\} + i\left\{(a^2/r - r)\sin\theta\right\}}{\left\{(r+a^2/r)\cos\theta - 2a\cosh\gamma\right\} + i\left\{(a^2/r - r)\sin\theta\right\}}\right]\right.$$

F1a

$$\left. + i\tan\beta\ \ln\left[\frac{\left\{(r-a^2/r)\cos\theta + 2a\sinh\gamma\right\} + i\left\{(a^2/r + r)\sin\theta\right\}}{\left\{(r-a^2/r)\cos\theta - 2a\sinh\gamma\right\} + i\left\{(a^2/r + r)\sin\theta\right\}}\right]\right\}.$$

Where $\zeta = re^{i\theta}$ and $b = e^{\gamma}$.

THE STRAIGHT THROUGH FLOW

The complex potential function necessary to produce a straight through flow with no circulation is

$$w = \varphi + i\psi = \frac{V_a s}{2\pi}\left[\ln\frac{\zeta + b}{\zeta - b} + \ln\frac{\zeta + a^2/b}{\zeta - a^2/b}\right] \qquad \text{F3}$$

where $V_a s$ represents the strength of the sources and sinks in the ζ plane. In the ζ' plane V_a is the velocity at infinity and s is the cascade spacing. The product $V_a s$, therefore repsents the quantity of flow passing between two adjacent blades.

The deviation of the velocity along any streamline from the value V_a is a measure of the error in locating the bus bars a finite distance from the cascade. If the ratio $\frac{V_a - V_{\zeta'}}{V_a}$ along any streamline, at a position along the streamline corresponding to the location of the bus bars, is negligible then the error due to the bus bars' location is negligible.

The stagnation streamline was chosen for investigation as it has the most radical changes in velocity and direction. Calculations for this streamline in the ζ plane occur where $\theta = 0$, π and $b \geq r \geq a$. Setting $a = 1$ for convenience, and placing $\theta = \pi$, the mapping equation reduces to:

$$x' = s\frac{\cos\beta}{2\pi} \ln\left[\frac{(r+1/r) - 2\cosh\gamma}{2\cosh\gamma + (r+1/r)}\right] ,$$

F1b

$$y' = s\frac{\sin\beta}{2\pi} \ln\left[\frac{(r-1/r) - 2\sinh\gamma}{2\sinh\gamma + (r-1/r)}\right] .$$

In order to facilitate visualization of perpendicular distances from the cascade centerline a simple rotation of axes in the z' plane is introduced,

$$z = x + iy \quad \text{where} \quad x = x'\cos\beta - y'\sin\beta$$
$$\text{and} \quad y = x'\sin\beta + y'\cos\beta . \qquad \text{F4}$$

The complex velocity in the z' plane is,

$$\frac{dw}{dz'} = V_{x'} - i V_{y'} = \frac{\frac{dw}{d\zeta}}{\frac{dz'}{d\zeta}} = \overline{V}_{z'} . \qquad \text{F3a}$$

With the selections of $\theta = \pi$, $a = 1.00$ and $\beta = 45^\circ$ which determines γ for this case,

$$\frac{\overline{V}_{z'}}{V_a} = \frac{1}{\cos\beta}\left[\frac{(r^2-1)^2 + i\tanh\gamma(r^4-1)}{(r^2-1)^2 + \tanh^2\gamma(r^2+1)^2}\right] . \qquad \text{F3b}$$

The magnitude of this ratio does not change under a rotation of the axes.

The value of r in the ζ plane was varied from 1.0 to b. This gave corresponding points in the z' or z plane from

equations F1b and F4 respectively. At the same time the ratio $\frac{V_a - V_x}{V_a}$ was computed through the use of equation F3b.

The values of x/s and corresponding values of $\frac{V_a - V_x}{V_a}$ for the stagnation streamline of the cascade are presented in Table FII with γ as the argument. Fig. F3 provides a graphic display of the results. The cascade in the figure is drawn to scale.

The working surface as finally evolved had bus bars located 16 inches from the cascade centerline. Two sizes of profiles, 6 and 12 inch chord, were used in the investigation. The solidity for the flat plate cascade has been selected as unity thereby limiting the values of the ratio x/s to 16/12 and 16/6. These two cases are shown in Fig. F3.

TABLE FI

CORRESPONDING VALUES OF b and σ at $\beta = 45^\circ$

b	σ at $\beta = 45^\circ$
2.00	.6560
1.95	.6739
1.90	.6930
1.85	.7133
1.80	.7350
1.75	.7586
1.70	.7837
1.65	.8111
1.60	.8413
1.55	.8737
1.50	.9100
1.45	.9506
1.40	.9966
1.35	1.0491
1.30	1.1107
1.25	1.1846
1.20	1.2765
1.15	1.3969
1.10	1.5699
1.05	1.8716
1.00	∞

TABLE FII

CORRESPONDING VALUES OF $\frac{x}{s}$ AND $\frac{V_a - V_x}{V_a}$ at $\sigma = 1.0$ and $\beta = 45^\circ$

r	$\frac{x}{s}$	$\frac{V_a - V_x}{V_a}$	
1.02	±.2959	.9131	
1.04	±.3061	.8289	
1.06	±.3155	.7211	
1.08	±.3274	.6724	
1.10	±.3394	.5993	
1.12	±.3519	.5324	
1.14	±.3650	.4793	← .3535 cascade edges
1.16	±.3794	.4113	
1.18	±.3948	.3537	
1.20	±.4111	.3186	
1.22	±.4345	.2636	
1.24	±.4503	.2227	
1.26	±.4732	.1846	
1.28	±.4994	.1505	
1.30	±.5309	.1189	
1.32	±.5684	.0997	
1.34	±.6190	.0639	
1.36	±.6909	.0494	
1.38	±.8220	.0168	
1.39	+.9743	.0055	

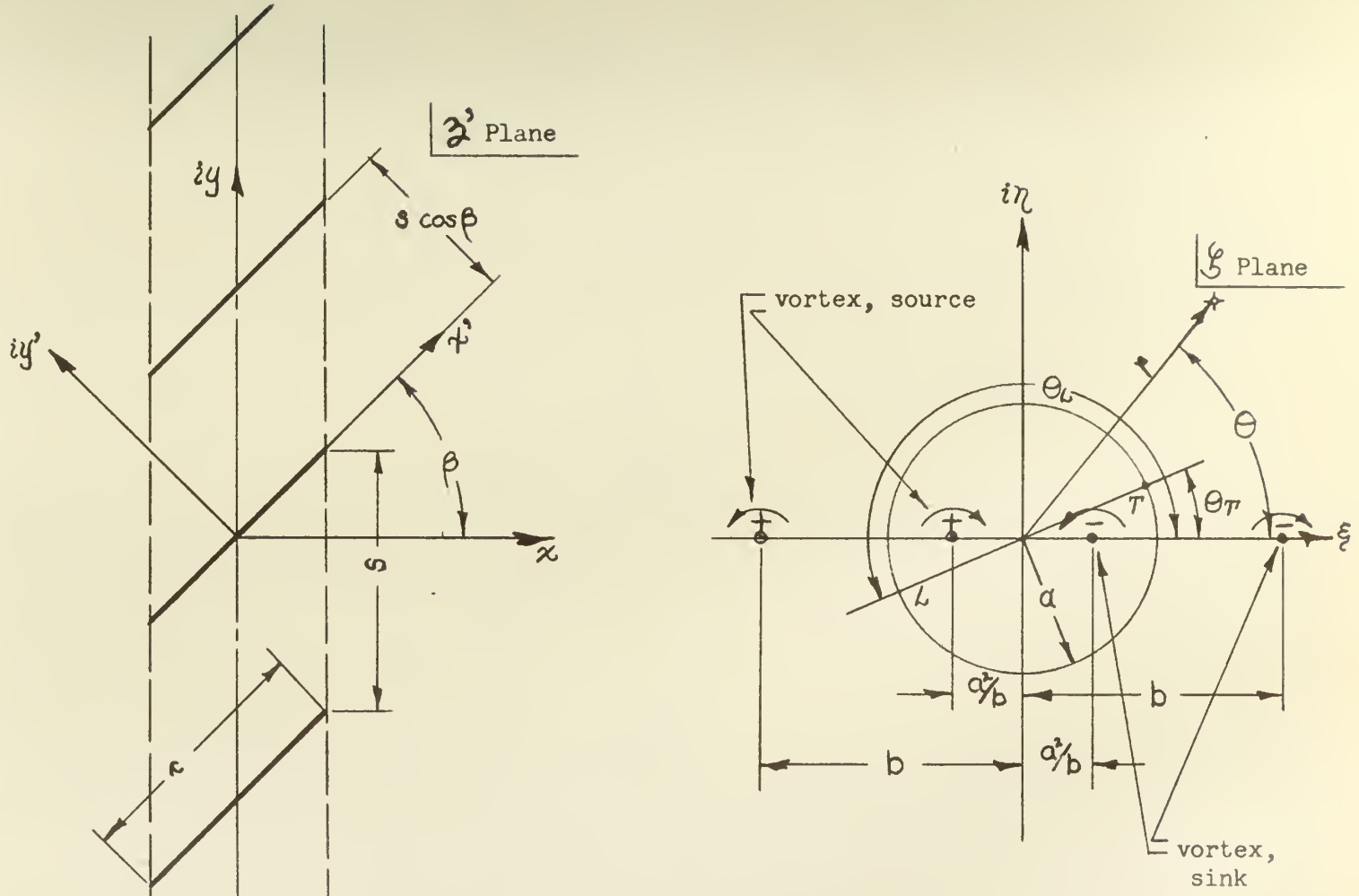
z' Plane
iy
s cosβ
iy'
x'
β
x
s
r
ζ Plane
iη
vortex, source
θL
θ
θT
T
ξ
L
a
a²/b
b
b
a²/b
vortex,
sink

Figure F1

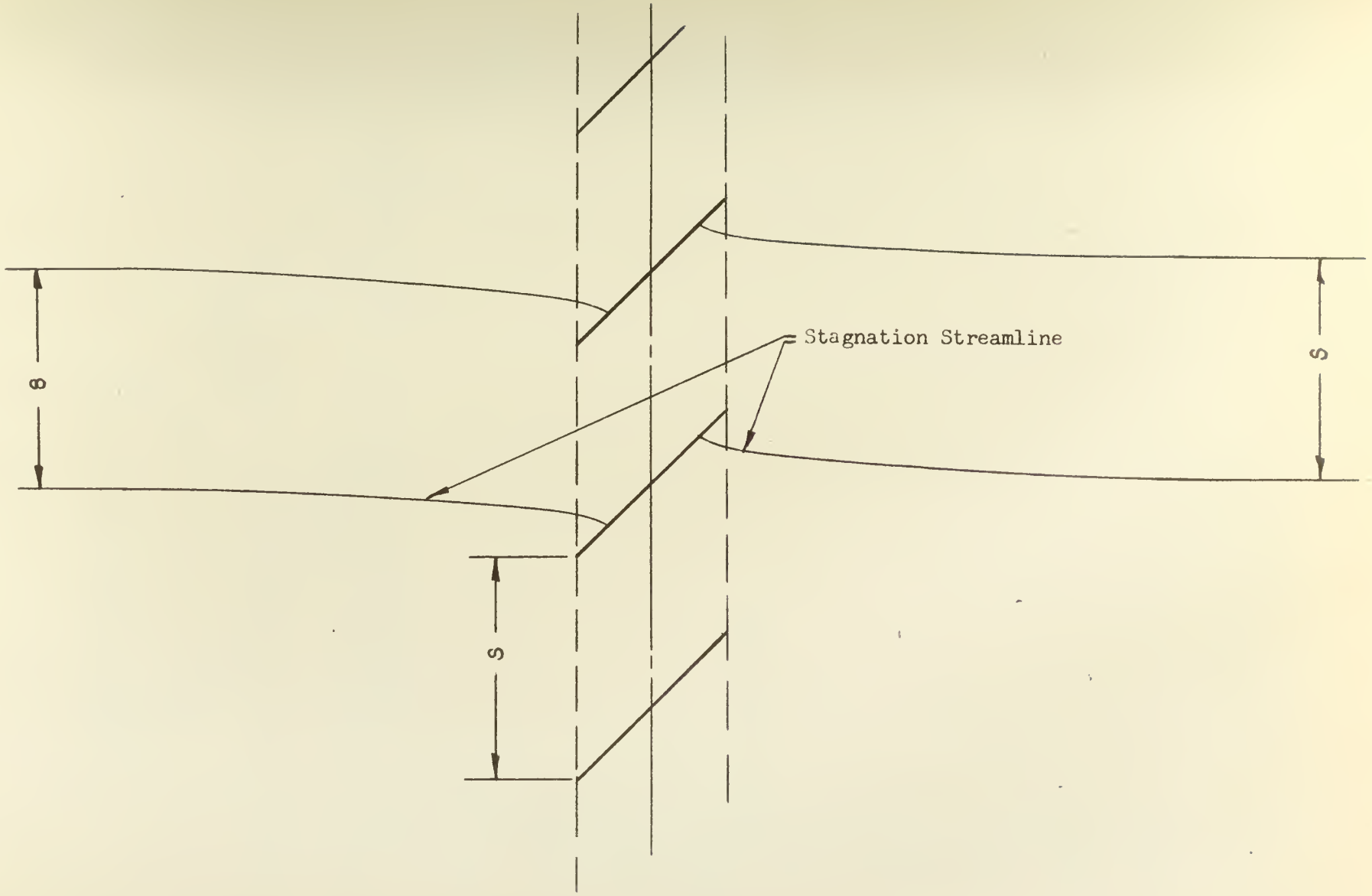

Figure F2

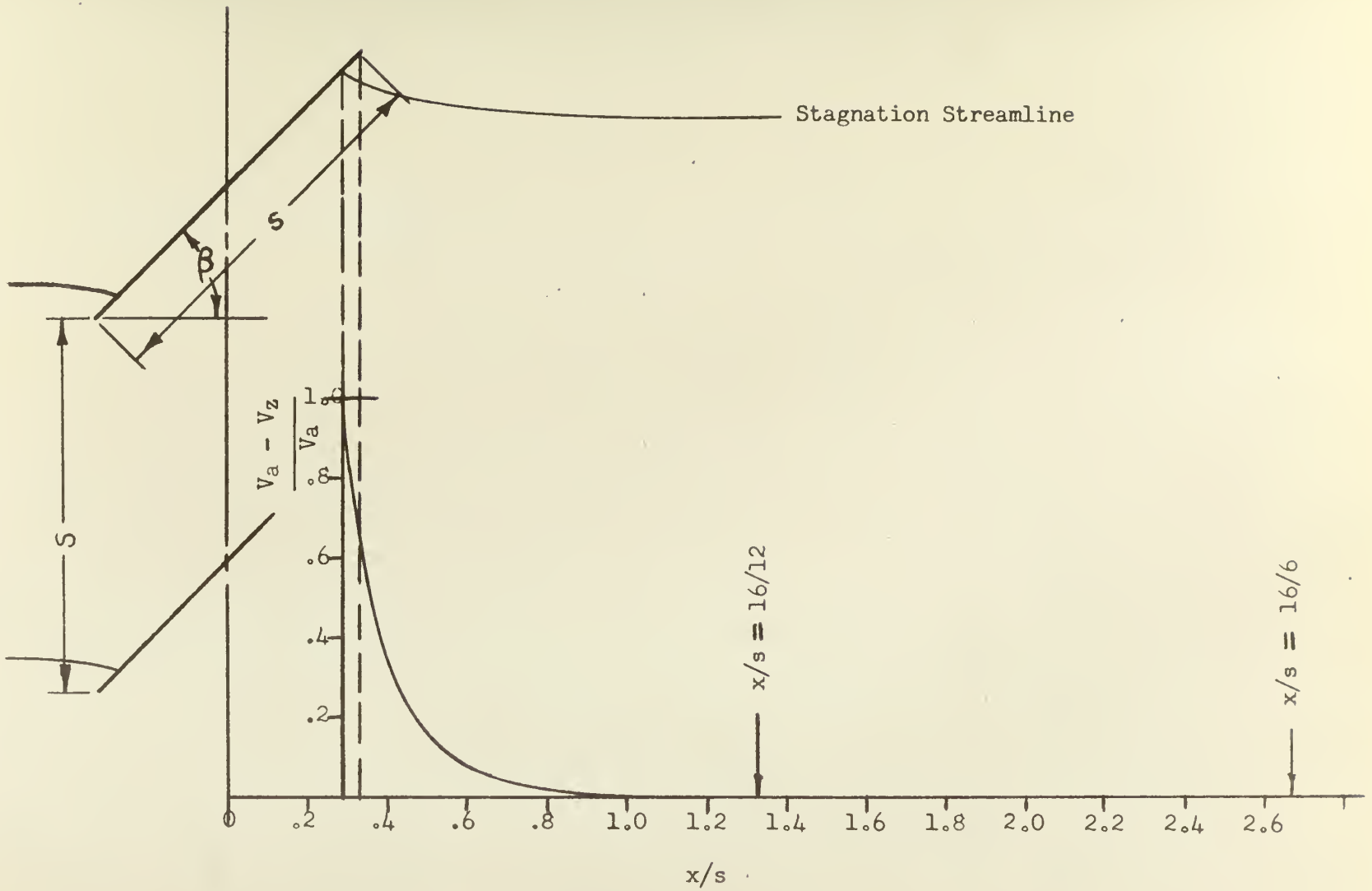
Stagnation Streamline
β
s
S
$\frac{V_a - V_z}{V_a}$
1.0
.8
.6
.4
.2
0
.2
.4
.6
.8
1.0
1.2
1.4
1.6
1.8
2.0
2.2
2.4
2.6
x/s
x/s = 16/12
x/s = 16/6

Figure F3